THE PREFERENTIAL OXIDATION OF CO OVER NICKEL OXIDE CATALYSTS AND THE DOPING EFFECTS OF PLATINUM IN HYDROGEN RICH STREAMS

By

ZIYAAD MOHAMED

BSc (Hons)

Submitted in fulfilment of the academic requirements for the degree of

Master of Science in the

School of Chemistry and Physics

University of KwaZulu-Natal

Durban

South Africa

DECEMBER 2012

As the candidate's supervisor/s I have approved this thesis/dissertation for submission.

Signed: _____ Name: Prof. H.B. Friedrich Date: ____

Signed: _____ Name: Dr. S. Singh Date: ____

ABSTRACT

Hydrogen has now become a suitable candidate for alternative energy generation for small scale applications with the aid of fuel cells. On-board production of hydrogen from methane is the most preferred method via a series of catalytic reactions. However, the carbon monoxide (CO) concentrations following these reforming steps is still too high (±1 %) and is detrimental to the anode of the fuel cell. For maximum output and efficiency of the fuel cell CO concentrations must be reduced to less than 10 ppm. Preferential oxidation (PROX) following the water-gas shift reaction is a promising method that could be employed to reduce the CO content in the reformate gas.

This project entails the synthesis, characterization and testing of nickel based catalysts for the oxidation of CO in H_2 rich streams, and to dope with Pt to determine the effects of the platinum group metal on the catalyst for this reaction. A series of NiO/Al_2O_3, Pt/Al_2O_3 and $Pt/NiO/Al_2O_3$ catalysts were prepared by incipient wetness technique. These catalysts were characterized by TGA, ICP-OES, XRD, BET, TPR, TPD, N_2 adsorption desorption isotherms, CO chemisorptions, SEM-EDX and TEM. The catalysts were then tested for the oxidation of CO in H_2 rich streams.

XRD patterns of the catalysts indicated the presence of NiO and PtO phases on the respective supports and *in situ redox* reactions showed catalysts had reversible phase changes (oxide and metallic) that were stable. N_2 adsorption-desorption isotherms indicated the presence of mesoporous materials for all catalysts studied. Impregnation of Pt on the NiO/Al_2O_3 catalysts promoted the reduction of the catalyst to lower temperatures.

All catalysts were stable for long periods of time in the presence of H_2 at 150 °C. NiO/Al_2O_3 catalysts were not very active for the preferential oxidation of CO within its stipulated temperature ranges giving the highest CO conversion at 290 °C of 11 % with the selectivity towards CO_2 of ± 25 %. The Pt/Al_2O_3 showed much better activity at higher PROX temperatures compared to the NiO/Al_2O_3 with regards to CO conversion and selectivity towards CO_2. The highest CO conversion obtained within the PROX range was ±56 % with a selectivity towards CO_2 of 68 % at 200 °C. The $Pt/NiO/Al_2O_3$ showed a synergistic effect, with much higher CO_2 selectivity and CO conversion within the PROX temperature ranges

compared to both mono-metallic catalysts studied. The highest CO conversion obtained for this catalyst was at 180 °C of 99.9 % with a selectivity towards CO_2 of 74 %.

PREFACE

The experimental work described in this thesis was carried out in the School of Chemistry and Physics, University of KwaZulu-Natal, Westville Campus from March 2010 to November 2012, under the supervision of Prof. Holger B. Friedrich and the co-supervision of Dr. Sooboo Singh.

This study represents original work by the author and has not otherwise been submitted in any form for any degree or diploma to any tertiary institution. Where use has been made of the work of others, it is duly acknowledged in the text.

PLAGIARISM

I, Ziyaad Mohamed, declare that:

1. The research reported in this thesis, except where otherwise indicated, is my original work.
2. This thesis has not been submitted for any degree or examination at any other university.
3. This thesis does not contain any other person's data, pictures, graphs or other information, unless specifically acknowledged as being sourced from other persons.
4. This thesis does not contain other person's writing unless specifically acknowledged as being sourced from other researchers. Where other written sources have been quoted, then:
(a). Their words have been re-written but the general information attributed to them has been referenced.
(b). Where the exact words have been used, then their writing has been placed in italics and inside quotation marks, and referenced.
5. This thesis does not contain text, graphics or tables copied and pasted from the internet, unless specifically acknowledged, and the source being detailed in the thesis and in the Reference sections.

Signed: _____ Date: ____

CONFERENCE CONTRIBUTIONS

Parts of this work have been presented at conferences as detailed below:

1. Poster presentation, Catalysis Society of South Africa (CATSA) conference, Bloemfontein, RSA, November 2010, titled "The Preferential Oxidation (PROX) of CO to CO_2 over metal-supported catalysts".

2. Poster presentation, Catalysis Society of South Africa (CATSA) conference, Krugersdorp, RSA, November 2011, titled "A model approach to a preferential oxidation (PROX) reactor".

3. Poster presentation, 15^{th} International Congress on Catalysis (ICC) conference, Munich, Germany, July 2012, titled "Preferential Oxidation of CO over $Pt/NiO/Al_2O_3$ catalysts".

4. Oral presentation, Catalysis Society of South Africa (CATSA) conference, Langebaan, RSA, November 2012, titled "Preferential oxidation of CO over metal oxide catalysts".

ACKNOWLEDGEMENTS

"Glory be to You, we have no knowledge except what You have taught us. Verily, it is You, the All-Knower, the All-Wise."

(The Quran, 2:32)

Firstly all praises to the Almighty, for guiding me and allowing me to pursue the career I have chosen, and for granting me faith in achieving my goals.

I would like to thank my supervisor, Professor Holger Bernhard Friedrich, for his motivation, guidance and encouragement throughout the project. A word of thanks for my co-supervisor, Dr Sooboo Singh, for his willingness to help at all times.

I also thank Hydrogen South Africa (HySA) for their financial support provided for this study.

I would like to thank all the members of Catalysis Research Group, UKZN for their help, and for creating a friendly and helpful working environment.

Also, the Centre for Catalysis Research UCT, for their efforts and for allowing me to conduct some of my work there. Thanks to Waldo Koorts, Steven Roberts, Euin Cyster (Perkin Elmer) and Jacobus van der Merwe for their help with technical aspects of the GC and the test unit supplied.

A special thanks to a very dear colleague of mine Mr Venkata Dasireddy for his endless support, help, motivation and tireless efforts throughout this entire study. I will always be grateful to him. Also I'd like to thank my friends, Mohamed Islam Fadlalla, Thashini Chetty, Aziz Golandaj and Ebrahim Kadwa for all their support and help throughout the project.

To my dearest wife Sofiah, for her patience, encouragement, support and motivation she has provided throughout this study, and also her family for their support.

Lastly and most importantly, my warmest thanks to my beloved parents and my sister for their inspiration and the rest of my family for all their love, support and guidance throughout my studies. There are really no words good enough to thank all of you.

DEDICATION

To my loving parents Aukbar and Jamila Mohamed

ABBREVIATIONS

Å	: Angstroms
atm	: Atmospheres
BET	: Brunauer-Emmett-Teller
BDDT	: Brunauer-Deming-Deming-Teller
BP	: Back pots
BPR	: Back pressure regulator
EDX	: Energy-dispersive X-ray spectroscopy
GC	: Gas chromatography
GHSV	: Gas hourly space velocity
g	: Gram
h	: Hour
HySA	: Hydrogen South Africa
ICP-OES	: Inductively coupled plasma-optical emission spectroscopy
kPa	: Kilopascal
L	: Litre
MFC	: Mass flow controller
µ	: Micron
mg	: Milligram
mL	: Millilitre
M	: Molar (concentration in mole per litre)
nm	: Nanometre
POX	: Partial oxidation
ppm	: Parts per million
PSD	: Pore size distribution
PGM	: Precious group metals
PROX	: Preferential oxidation
PR	: Pressure regulator
PEMFC	: Proton exchange membrane fuel cell
SEM	: Scanning electron microscopy

SR : Steam reforming

TPD : Temperature programmed desorption

TPR : Temperature programmed reduction

TCD : Thermal conductivity detector

TGA : Thermogravimetric analysis

TOS : Time on Stream

TEM : Transmission electron microscopy

Vol : Volume

WGS : Water-gas shift

wt : Weight

XRD : X-ray diffraction

TABLE OF CONTENTS

LIST OF FIGURES

Page No.

Page No.

Page No.

Page No.

Page No.

LIST OF TABLES

CHAPTER 1

Introduction

1.1. Catalysis

To the non-chemist a catalyst is something that is in a catalytic converter of a vehicle. Indeed, the automotive exhaust converter is a triumphant application with regards to catalysis. Its main function is taking harmful pollutants from exhaust fumes and converting them into less poisonous, environmentally acceptable products. However, not only automotives make use of this important application, catalysis has a much broader scope than just abating pollution. Living matter relies primarily on enzymes which are catalysts by nature. Also the chemical industry would not function without the existence of a catalyst, which is the vital tool in production facilities [1]. For scientists, it is a multidisciplinary and extremely challenging field. What is a catalyst? Although an appropriate universal definition of the term catalyst does not exist, an acceptable definition would be, "a substance increasing the rate of a chemical system that is approaching equilibrium, without being consumed by the reaction itself" [2].

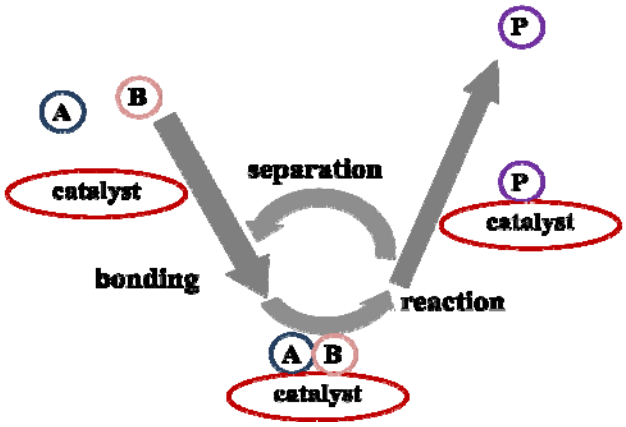

Figure 1.1: Steps of a catalytic reaction adapted from Chorkendorff [1].

Considering the steps of a catalytic reaction between two molecules A and B that give product P (Figure 1.1.) [1], the cycle usually commences with the bonding of A and B to the catalyst. These then react within the complex, generating product P which is also bound to the catalyst. In

the final step, product P separates from the catalyst and leaves the reaction cycle in its original state.

Catalysis lies in the heart the majority of industrial processes such as the production of petrochemicals, pollution abatement and bulk chemicals [3]. At present, the production of green house gases, especially CO_2, has risen drastically due to automobiles, power stations and industrial plant exhaust. Therefore, to reduce the gas emission from these sources, catalysts are mainly employed [4]. Catalysis can be divided into two widespread groups:

i) Heterogeneous catalysis: where the catalyst and the reactants are in different phases
ii) Homogeneous catalysis: where the catalyst and the reactants occur in the same phase

This study focuses only on heterogeneous catalysis.

1.1.1 Heterogeneous catalysis

In a typical catalytic oxidation reaction, taking place at the gas-solid interface, a mixture composed of hydrocarbons and oxygen is passed through the catalyst bed in a fixed-bed reactor at varying temperature conditions [3]. Heterogeneous catalysts are known to be the workhorses of the petrochemical and chemical industry [1]. The five fundamental steps that occur during heterogeneous catalysis are described below [3]:

1) Diffusion of the reactants (boundary layer and pore volume diffusion) to the active site
2) The adsorption of one of the reactants on the catalyst surface
3) Surface reactions
4) Desorption of the products
5) Diffusion away from the active site

Basically, the reactants adsorb onto the surface of the catalyst, followed by the rearrangement of the bonding and desorption of the product(s) [5]. Adsorption of reactants onto the surface of the catalyst can happen in two ways, either by chemisorptions (chemical interaction) or by physisorption (van der Waals interaction), with the former taking place in most cases.

An example of the heterogeneous catalytic oxidation of CO from exhaust gases is given in Figure 1.2 which shows the catalytic cycle with a potential energy diagram. Catalysts based on

noble metals (Pt, Pd and Rd) are employed in this reaction and are located within the catalytic converter. The cycle begins with CO and O_2 molecules adsorbing to the active sites of the metal, where the O_2 dissociates into 2 atoms.

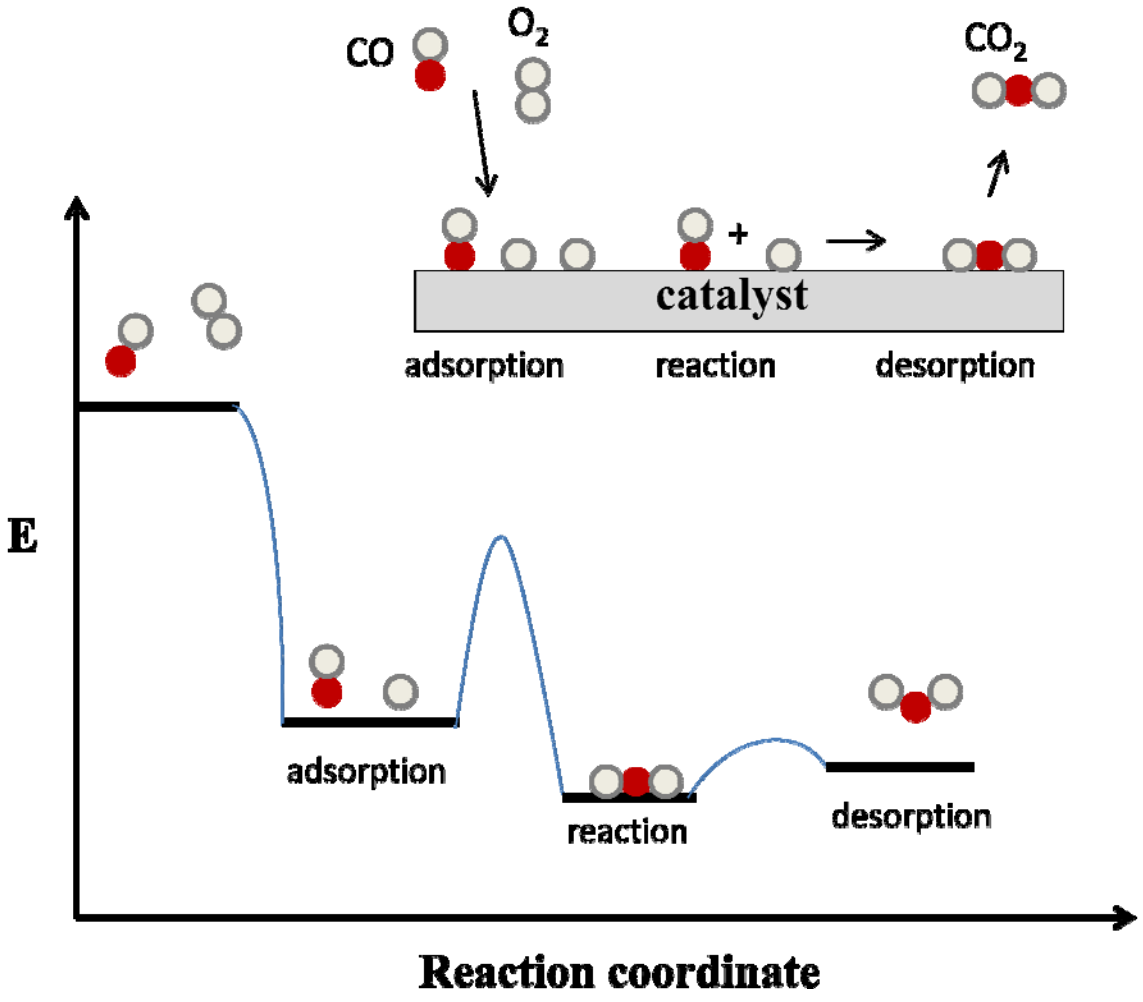

Figure 1.2: Reaction cycle and potential energy diagram for the catalytic oxidation of CO by O_2 adapted from Chorkendorff [1].

The adsorbed CO and one O atom react to form CO_2 which is much more stable and unreactive, interacting weakly with the metal surface it and desorbs almost immediately. Once CO_2 has desorbed, the site becomes available for further reaction cycles to take place. Without the presence of the catalyst, the potential energy that would be required for the total reaction would be much higher.

1.1.2 The heterogeneous supported catalyst

Catalysts employed for heterogeneous catalytic reactions usually consist of a support and an active metal centre [6]. The support is predominantly the main component being a readily cheap, solid material with high surface area and thermal stability. Its main function is to achieve high metal dispersion of the active metal or metal oxide component. Supports most commonly used in heterogeneous catalysis are usually classified into two groups [7]: 1) organic polymers such as polystyrene, polypropylene, polyacrylates and polyvinyl chlorides, and 2) inorganic supports such as alumina, silica, titania, zirconia zinc oxide, glasses, clays and zeolites [1, 7]. The support is generally present in higher amounts with regards to the active metal centre and should be stable under both reaction and regeneration conditions [6].

This study focuses on the inorganic support, γ-alumina which is amphoteric in nature and can be described as oxides that occur as close-packed layers of oxo anions with Al^{3+} cations distributed between tetrahedral and octahedral vacancy positions [8].

Heterogeneous catalysts most commonly utilized are supported metal and metal oxide catalysts. These metals are not inert, especially with regards to the non-noble metals [9]. Between the oxide support and the active metal, the interaction affects metal distribution and accordingly activity, stability and selectivity of the catalyst. Being a transient d-metal, nickel is known to be extensively used as a catalyst in important industrial processes such as reforming, synthesis-gas production and methanation making use of reactions such as hydrogenation, dehydrogenation, oxidation and oxidative dehydrogenation [9]. Factors that are verified for influencing the catalytic properties of supported nickel catalysts include: the preparation methods, nickel loading, reduction temperature and promoters. In addition to these factors, nickel precursors play an important role in catalytic performance [10]. Wang and Lu [11] found that for a methane reforming reaction, the catalyst activity and stability of Ni/Al_2O_3 prepared with a nickel nitrate precursor was better than the Ni/Al_2O_3 prepared using chloride and acetylacetonate precursors. At the same time nickel nitrate and acetate derived catalysts showed higher catalytic activity than the chloride derived catalyst for the oxidative reforming of methane.

The advantages for using supported metal complexes for these types of applications include [7]: (a) easier separation of the catalyst, (b) thermal stability, (c) reduced oxygen and moisture

sensitivity, (d) no solvent dependence and (e) more easily observed corrosion effects and reduced plating. The catalyst should also be highly active for the particular process in which it is utilized, being easily reproducible, show high selectivity and stability for the desired product and process and it should be able to regenerate effectively if any deactivation occurs [7, 12]. Some catalysts are often adjusted by modifiers (additives) to improve the activity and selectivity to the desired products [13]. A modifier is also known as a promoter and may also affect a catalyst's performance in an undesired manner by poisoning the catalyst, in this case it would be regarded as an inhibitor. Promoters can change the binding energy of an active site or its structure and they can be more preferably dispersed on the surface of the catalyst and form alloys with the inactive metal [14].

1.1.3 Oxidation catalysis

Oxidation plays an important role in the majority of industrial processes. It accounts for more than 60 % of all chemicals synthesized through a catalytic pathway. According to Centi et al. [15], processes and products derived from oxidation catalysis account for a net worth of between 20 – 40 billion dollars per annum. Oxidation can be defined as the gain of an oxygen atom, loss of electron(s) or loss of hydrogen [16]. Transition metals are effective candidates for catalyzing these reactions due to their many oxidation states [17]. Oxidation catalysts can be divided into two main categories classified by the method by which the oxygen participates in the reaction. Firstly, the oxides of transition metals containing two or more metal cations where the oxygen is simply transferred from the catalyst bulk. The second consists of supported metals onto which oxygen species can be chemisorbed [18]. For oxidation catalysis, the oxygen source is usually introduced in the feed in the form of air. In the automobile, power and chemical industries, oxidation catalysis plays a vital role by mitigating the concentration of environmentally harmful pollutants that are produced during these reaction processes. These are subsequently converted to eco-friendly emissions. This study focuses on the oxidation of CO, a well known toxic greenhouse gas that contributes to global warming, therefore, making its elimination necessary.

1.2 Hydrogen: The future source of energy

Being the most abundant element on earth and in the universe, hydrogen is widely considered a promising fuel of the future since it exposes high power density, deliverability and cleanliness

[19]. The hydrogen economy typically involves hydrogen production, delivery and distribution, conversion and storage [19]. Accordingly, in the transition to this economy, the first step is to develop a process that produces hydrogen from fossil fuels. This is now of great interest globally and hydrogen is predicted to be the major energy carrier for the future [20, 21]. It poses to being a long-term project in changing the current energy system to one that attempts in combining the cleanliness of hydrogen as a carrier of energy with the aid of fuel cells (FCs) [22], which are the preferred device for harnessing the energy of hydrogen. Fuel cells transform energy into heat and electricity via a potentially renewable and non-polluting route, compared to other technologies that currently have the potential of influencing an energy revolution.

Hydrogen as an energy carrier must be obtained from potential sources of energy such as natural gas, gasoline or alcohols (methanol, ethanol) [23], and these processes should avoid or minimize CO_2 emissions, at least in the long run [22]. For this future energy supply, three requirements must be fulfilled: a) environmental protection, b) security in the energy supply, and c) the utilization of energy sources that promote the economic growth of societies [22]. For hydrogen production, amongst all current technologies, steam reforming is the major source of the world's total hydrogen production, producing 80-85% of the hydrogen from natural gas [24] and it is produced in large scale centralized facilities at present [19].

Hydrogen has been used extensively in the chemical and petroleum industries as raw material in large quantities. It is an essential reactant in oil refineries, and for processes such as methanol and ammonia sysnthesis [25]. While the hydrogen economy is still developing, safe and efficient storage of this gas has been identified as a major technological barrier for small-scale applications, including transportation systems [23, 26]. Therefore, on-board production of hydrogen seems to be the most preferred alternative to overcome the storage problem [23, 27]. Reforming of natural gases composed mainly of methane has been widely used due to its availability, it is cleaner and easily converted to hydrogen [28]. Producing clean hydrogen is usually accomplished by a series of catalytic steps including steam reforming (SR), partial oxidation (POX), autothermal reforming (ATR) and water-gas shift (WGS) [26, 28, 29]. Steam reforming utilizes the reaction between fuel and steam, whereas POX uses the reaction between fuel and oxygen. ATR, also considered as a modified POX process, is defined as the reaction of

hydrocarbons, steam and air [30] and lastly WGS produces hydrogen from the reaction of water and carbon monoxide [25].

1.3 Fuel cell technology

Discovered more than 100 years ago by Sir William Grove and Christian Friedrich Schoenbein, a fuel cell is an electrochemical energy converter that converts the chemical energy of fuel directly into electrical energy and has a large potential for highly efficient power generation [31]. There are many fuel cells classified on the basis of the electrolyte used [32], and amongst these various fuel cell technologies available, the development of the Proton Exchange Membrane (PEM) fuel cell has rapidly accelerated during the last few years, becoming the primary candidate for elevating the commercial possibilities of generating clean and efficient power for portable and mobile applications [29].

1.3.1 Proton exchange membrane fuel cells

Proton exchange membrane fuel cells (PEMFCs) have superior performance over other types of fuel cells and offer high power density, fast start-up, dynamic response times and the ability to vary output quickly with virtually no emissions of harmful pollutants [26]. They generate electricity directly from chemical energy, avoiding the thermodynamic mechanical cycle losses experienced by combustion in conventional power generation [29]. PEMFCs utilize hydrogen as the fuel, which is known for offering maximum energy density (per unit mass) and the maximum cell voltage that can be derived in comparison to other fuels [33].

The fuel cell consists of two electrodes, an anode and a cathode, with a conducting electrolyte (polymer membrane) between them (Figure 1.3). Reactants are transported by diffusion and / or convection to the electrode surfaces (containing catalysts), which act as a barrier between the bulk gas phase and the electrolyte. The electrode surface also provides the sites where oxidation and reduction reactions occur.

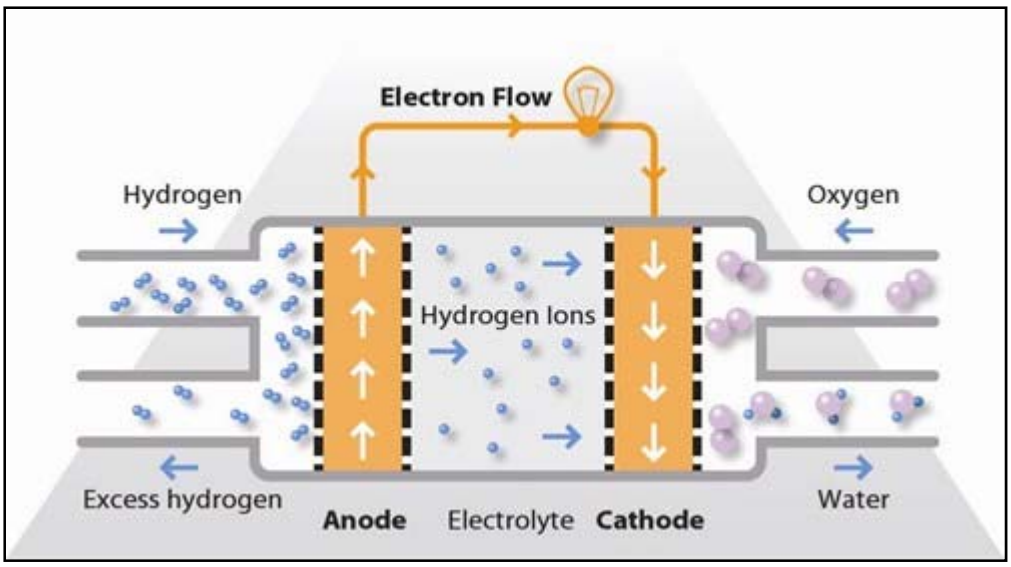

Figure 1.3: A typical fuel cell design [34] (not copyrighted).

Hydrogen is oxidized at the anode to produce hydrogen ions and electrons. The hydrogen ions pass through the proton conducting electrolyte and the electrons through an external circuit. The primary function of the electrolyte is the selective transport of hydrogen ions from anode to cathode. At the cathode, the hydrogen ions, electrons and oxygen combine to produce water, and waste heat is constantly transported away from the cathode. Accordingly, the overall cell reaction in a PEMFC is the combination of hydrogen and oxygen to produce electricity, heat and water [20] (Eqs. 1.1 – 1.3):

Anode: $H_2\ (g) \rightarrow 2\ H^+\ (aq) + 2\ e^-$ (1.1)

Cathode: $\frac{1}{2}\ O_2\ (g) + 2\ H^+\ (aq) + 2\ e^- \rightarrow H_2O\ (l)$ (1.2)

Overall: $H_2\ (g) + \frac{1}{2}\ O_2\ (g) \rightarrow H_2O\ (l)$ + electrical energy + heat (1.3)

There are two major sources for producing hydrogen for PEMFCs, these are fossil fuels through reforming of natural gas or gasoline, coal gasification and partial oxidation of methanol [19] and electrolysis of water [35]. However, at present hydrogen production for PEMFCs is mainly based on reforming of natural gas comprising of: steam reforming, autothermal reforming, partial oxidation followed by the water gas shift reaction. Electrolysis of water for hydrogen production on the other hand offers a totally sustainable energy cycle and a clean source of hydrogen,

however, currently, due to its state of the art technology it is not cost effective [35]. Due to the thermodynamic limitation of the WGS reaction, carbon monoxide (CO) present in the outlet stream is known to adsorb onto the active sites on the platinum anode of the fuel cell catalyst therefore decreasing cell efficiency [36]. This results in significant loss of catalytic activity and power output of the fuel cell [33]. Long term exposure of carbon monoxide leads to electrode degradation which commonly is referred to as CO poisoning [33]. Even trace amounts of CO (ppm levels) have been demonstrated to easily poison the Pt anode, therefore it is necessary to eliminate these traces to sub-ppm levels i.e. less than 10 ppm at the Pt anode in the hydrogen stream with minimal hydrogen loss [37].

1.4 Reforming of hydrogen for the proton exchange membrane fuel cell

The reforming processes that have been or are being reviewed for the production of pure hydrogen from fossil fuels such as natural gas or gasoline (for fuel cell applications), are now an emerging market. The main processes are listed in Table 1.1, adapted from D. Stolten [38].

Table 1.1: Characteristics of processes for hydrogen from fossil fuels

Process	Feedstock	Temperature (°C)	Catalyst
Steam Reforming	Light hydrocarbons	500-900	Ni/ceramic support
Partial Oxidation	Light hydrocarbons	950	Rh/ceramic support
Autothermal Reforming	Light hydrocarbons	1050	Ni/ceramic support
Water-Gas Shift	Syngas	230-350	Fe_3O_4, $Cu/ZnO/Al_2O_3$

1.4.1 Steam reforming

At present, reforming of hydrocarbons by steam reforming is the preferred process for industrial hydrogen production using Ni based catalysts [39]. It involves the conversion of two very stable molecules, water and methane, thus requiring the supply of heat [38] (Eq. 1.4). The reaction is known to generate high H_2/CO ratios, but it comes with a major disadvantage since being an endothermic reaction makes it less viable for the production of hydrogen as a fuel [28].

$$CH_4 + H_2O \rightarrow CO + 3H_2 \quad \Delta H_{298K} = +206 \text{ kJ/mol} \qquad (1.4)$$

Catalysts for these type of reactions are exposed to high temperatures and steam partial pressures. They must therefore be able to show high mechanical stability [38]. Nickel catalysts are usually employed for steam reforming, since they are capable of withstanding these extreme conditions [28].

1.4.2 Partial oxidation

The partial oxidation reaction is known to generate much lower H_2/CO ratios than steam reforming, but does not include the disadvantage of being endothermic [28]. Here, the heat is provided by the partial combustion of the hydrocarbon, eliminating the need for a complex heated reactor [38] (Eq. 1.5).

$$CH_4 + ½O_2 \rightarrow CO + 2H_2 \quad \Delta H_{298K} = -36 \text{ kJ/mol} \qquad (1.5)$$

In this type of system, the hydrocarbon feedstock is mixed together with air (oxygen) and fed to the catalyst, which is usually rhodium [38].

1.4.3 Autothermal reforming

Authothermal reforming (ATR) is an alternative process to generate syngas, and is a hybrid of steam reforming and partial oxidation of methane adiabatically (Eqs. 1.6 and 1.7) to produce suitable H_2/CO ratios, and it does not require externally supplied energy [28]. The design allows for lower temperature ranges, hence a low amount of oxygen is required [38].

$$CH_4 + ½O_2 \rightarrow CO + 2H_2 \quad \Delta H_{298K} = -36 \text{ kJ/mol} \qquad (1.6)$$

$$CH_4 + H_2O \rightarrow CO + 3H_2 \quad \Delta H_{298K} = +206 \text{ kJ/mol} \qquad (1.7)$$

Catalysts employed for this reaction are also nickel based [38]. In a study by Dias and Assaf [28], it was shown that a bimetallic supported nickel catalyst (Ni-Ru) had notably higher activity than a nickel monometallic catalyst for the reforming of methane. The study involved the synthesis of Ni-Al_2O_3 catalysts that were promoted with Pt, Pd and Ir, to enhance the ATR reaction. The results showed that these platinum group metals (PGMs) strongly promoted the conversion of methane in ATR compared to the unpromoted Ni catalyst. Moreover, promoting with Pt was found to be more effective than with the other two PGMs.

1.4.4 Water-gas shift

In the production of hydrogen by the reforming techniques mentioned, these processes are usually followed by the water-gas shift (WGS) reaction to reduce the amount of CO even further [38]. When the reaction (Eq. 1.8) is carried out, activation is usually achieved using Fe-Cr or Cu-Zn based catalysts [19, 38]. These reactions, in association with the former and latter catalysts, are referred to as the high temperature (HT) WGS and low temperature (LT) WGS respectively [19].

$$CO + H_2O \rightarrow CO_2 + H_2 \quad \Delta H_{298K} = -36 \text{ kJ/mol} \qquad (1.8)$$

The WGS process utilizes the reaction between CO and H_2O to produce clean hydrogen that contains much lower levels of CO [1].

Regardless of the reforming techniques employed, unfortunately, significant amounts of CO (0.5 % –1 %) [23] remain together with the products of the subsequent water-gas shift reaction. High levels of this CO can only be tolerated in stacked fuel cells, for short periods of time by bleeding air through the anode passages of the fuel cell [26], however, the overall performance of these stacked PEMFC still suffers. The CO concentration in the hydrogen feed must be kept to sub-ppm levels (less than 10 ppm) for optimum operation of the PEMFC [40]. Since the conversion of CO is thermodynamically limited to levels of about 0.5–1%, further treatment for purifying the hydrogen stream is essential [23]. To achieve this high purification level, various physical and chemical methods have been considered and are now being assessed for application [23].

1.5 Purification of the reformate

Technologies viewed as the final cleaning process step to reduce the CO concentration to sub-ppm levels include: membrane separation, pressure swing adsorption, selective methanation and PReferential OXidation (PROX) [26, 41]. The first three mentioned technologies, pressure swing adsorption, membrane separation and selective methanation are not very promising methods for PEMFC applications.

Pressure swing adsorption is more applicable to stationary fuel processing systems [26], utilizing multiple reactor vessels and pressurization. These require additional compressors to re-humidify H_2 prior to being used in the fuel cell, and a desiccant for adsorbing H_2O from the inlet wet gas stream [41]. Since on-board production of H_2 is the goal of reforming, this method proves to be inefficient. The other option, membrane separation also offers the potential to produce clean H_2, but is coupled with the expense of high operating temperatures and very costly materials [41]. Together with this, it also does not reduce the CO concentration to the desired levels suitable for the PEMFC. Selective methanation has an advantage over the previously mentioned techniques of being simple and the reaction occurs in the presence of H_2, CO_2 and CO which are the products of the water gas shift reaction. The selective methanation reactions are highly exothermic (Eqs. 1.9 and 1.10):

$$CO + 3H_2 \rightarrow CH_4 + H_2O \qquad \Delta H_{298K} = -206 \text{ kJ/mol} \qquad (1.9)$$

$$CO_2 + 4H_2 \rightarrow CH_4 + 2H_2O \qquad \Delta H_{298K} = -165 \text{ kJ/mol} \qquad (1.10)$$

The disadvantage of these reactions is that at 100 % selectivity to CO conversion, 3 moles of H_2 are consumed for every mole of CO removed [26]. Also, the actual selectivity towards CO conversion in this process is lower than 100 % due to the side reaction between CO_2 and H_2 [26]. Considering the limitations in the above mentioned techniques, preferential oxidation appears to be the most promising approach and is more cost effective.

1.6 Preferential oxidation of CO

This technique of removing trace amounts of CO contaminants in H_2 rich streams is effective and offers ease of implementation, due to the reactor's small size and weight, simple design, reliability and safety for on-board fuel processing [42]. For this reaction, the temperature window at which both high selectivity and activity is achieved should essentially be the same [36]. With regards to on-board applications, the preferred operation temperature should ideally be within the range of the water-gas shift exit temperature (± 250 °C) and that of the PEMFC operating temperature (± 80 °C) [36]. The reactions that take place in the preferential oxidation reactor are described below [31] (Eqs. 1.11 – 1.13):

$$CO + ½O_2 \rightarrow CO_2 \quad \Delta H_{298K} = -283 \text{ kJ/mol} \qquad (1.11)$$

$$H_2 + ½O_2 \rightarrow H_2O \quad \Delta H_{298K} = -242 \text{ kJ/mol} \qquad (1.12)$$

$$H_2 + CO_2 \rightarrow H_2O + CO \quad \Delta H_{298K} = +41 \text{ kJ/mol} \qquad (1.13)$$

These reactions should be closely monitored during the process, since only the first reaction (Eq. 1.11), the oxidation of CO to CO_2 is desired [31]. This reaction is usually accomplished at lower temperatures. The undesired H_2 oxidation reaction (Eq. 1.12) is the key competitive reaction that takes place at higher temperatures and must be avoided to minimize the parasitic loss of H_2, while reducing CO to acceptable levels [26]. The formation of H_2O leads to a decrease in the selectivity towards CO_2, and also inhibits the catalyst activity. PROX usually requires minimal amounts of surplus air corresponding to the CO/O ratio or the λ value which is essentially between 1.5 and 2 [31]. Making use of these conditions and achieving full conversion of CO, approximately 0.5 to 1 mole of H_2 is essentially lost for each mole of CO converted [31]. The last reaction that could occur (Eq. 1.13) in the PROX reactor, where low concentrations of CO are found, is the reforming of CO over the catalyst in an O_2 deficient environment by the reverse water-gas shift reaction [31, 36].

1.6.1 Catalysts used for the preferential oxidation of CO

Early studies on PROX were conducted by Oh and Sinkevitch [43], who investigated the performance of a number of noble metals supported on alumina, and some transition metal based catalyst compositions were investigated for their performance in the PROX reaction. Results showed that among all the catalyst types tested Pt, Ru and Rh were the best candidates with regards to selectivity towards CO_2. Following the work of the pioneers, Oh and Sinkevitch, many catalytic formulations have been screened for the PROX reaction and among all, the precious metals Au, Rh, Ru, Pt, Ir and Pd supported on Al_2O_3, MgO, CeO_2, ZnO, TiO_2 and SiO_2 were found applicable [21, 40, 41]. These were found to achieve high CO oxidation rates together with high selectivity [44] within the desired temperature ranges.

Marino et al. [23] reported that Pt catalysts are the most comprehensively studied catalyst. They also reported that Au catalysts, poor catalysts for most reactions due to weak interactions with most adsorbates, when highly dispersed on various metal oxides were active for the CO

oxidation at very low temperatures, even below 0 °C. However, it was also found that metal oxide supported Au catalysts deactivated much faster than the Pt catalyst.

Using precious metal catalysts for the PROX reaction, however, is coupled with high costs and limited durability [27], therefore research has now turned towards alternative catalysts that could be more cost effective and widely available that show similar activity towards the PROX reaction. These could make use of cheaper metals as promoters and also use the noble metals in promotional ways instead of using them independently.

Padilla et al. [21] stated that catalysts for the PROX of CO can be classified into three groups: a) Au catalysts supported on either one or two of the following oxides; SnO_2, Fe_2O_3, $Mg(OH)_2$, TiO_2, CoO_x, NiO_x, CeO_2, MnO_x, Al_2O_3 and ZnO, b) catalysts based on metal oxides, such as Co, Ce, Mn, Cu, and Ni independently or combined with others, and c) noble metal catalysts supported on CeO_2, SiO_2, Al_2O_3, SiO_2-Al_2O_3, MgO, La_2O_3, TiO_2. In the case of type (a) catalysts, these are capable of functioning in the temperature ranges of 50-100 °C fed with CO, O_2, an inert gas and H_2 (5-75 %) with O_2/CO ratios between 1/1 and 20/1. Some studies also reported the addition of H_2O and CO_2. At low temperatures highly dispersed Au particles over the support showed high activity and selectivity, but the catalyst activity was strongly dependant on preparation methods. Type (b) catalysts operate at higher temperatures of ± 160 °C, also fed with CO, O_2, H_2 (40-50 %) and an inert gas with lower O_2/CO ratios of between 1/1 and 10/1 without the addition of CO_2. Finally, type (c) catalysts showed much more intense operation temperatures, almost 300 °C, fed with CO, 1-4 % O_2, 30-70 % H_2, CO_2 and H_2O. Padilla et al. also explained that Pt catalysts were competent candidates for fuel processors, because they can work at high temperatures and have a high resistance towards catalyst deactivation in the presence of CO_2 and H_2O. Many efforts have also been made at improving the selectivity and activity of these Pt/Al_2O_3 catalysts by adding dopants and promoters. These minimize the adsorption of CO, which blocks the adsorption sites of O_2 on the Pt making CO oxidation more difficult. These catalysts indicated ease of CO oxidation favoring O_2 adsorption and CO_2 production.

Ko et al. [37] reported that mono-metallic Pt catalysts usually exhibit noticeable PROX activity only above 150 °C. Therefore, to increase catalytic activity at lower temperatures various

methods were employed in the preparation and pre-treatment of the catalyst. Water vapor treatment increased Pt dispersion and enhanced low temperature catalytic activity. Other authors reported that PROX activity at low temperatures could also be obtained by the addition of a second metal that would enhance CO oxidation. These metals include Fe, Co, Ni, Mn and alkali metals. Ko et al. also studied various promoted Pt catalysts under the same reaction conditions and found that the addition of Ni was the most effective. The effects of synthesis by impregnation and various pretreatment conditions were analyzed on the Ni promoted Pt/Al_2O_3 catalysts and compared with other catalysts. Results obtained indicated that the Ni promoted catalysts were active for the PROX reaction over a wide reaction temperature range. The promoted catalysts showed higher CO conversion and higher selectivity towards CO_2 compared to the non promoted Pt/Al_2O_3 catalyst and other noble metal supported catalysts. The catalyst also showed superior performance when CO_2 and H_2O were introduced into the feed.

Motivation and objectives of this study

Hydrogen as a future source of energy has become a promising alternative to conventional fuel systems. It is widely available, clean and can offer maximum power density as a fuel for fuel cell applications. It is evident that the vital component of the PEMFC's is the platinum based electrode which is poisoned by CO concentrations left in the gas feed after the production of hydrogen. Platinum group metals (PGMs) are also used as catalysts during the cleaning stages of hydrogen, producing a relatively CO free feed for the PEMFC. These metals are known to show high activity and selectivity towards the oxidation of CO.

According to the US Geological Survey [45], South Africa currently possesses more than 75 % of the world's known platinum reserves and also large quantities of other precious metals. Therefore, using these metals for the reforming processes and as electrodes in PEMFC's could have a significant positive effect on the economy, as well as create many socio-economic opportunities for the country. Given these statistics, the South African Government has launched a new programme, Hydrogen South Africa (HySA), which aims at utilizing the country's

valuable reserves to supply at least a quarter of the world's demands for PGM based PEMFC catalysts by 2020.

At this early stage, developing a catalyst that can oxidize CO in the presence of hydrogen for the PROX reaction is of great interest. The catalyst should be highly active and selective for the oxidation of CO, and at the same time be more cost effective and durable compared to the noble metal catalysts already studied. NiO/Al_2O_3 catalysts have shown good activity in the reforming processes that include steam reforming and autothermal reforming of methane to produce hydrogen, and are stable at relatively high temperatures and not easily reducible in the presence of H_2. Since on-board production of H_2 is desirable, maintaining the NiO/Al_2O_3 catalyst for most of the reforming steps could save added time and expense. On the other hand, Pt has demonstrated optimum activity towards the PROX reaction. Research shows that promoting Pt/Al_2O_3 with Ni increases the reaction temperature range, stability and activity of the catalyst. In this project the doping/promotional effects of Pt on the NiO/Al_2O_3 catalysts (in contrast to the reported doping effects of Ni on Pt) will be analyzed and tested for in the CO oxidation and PROX reactions with regards to reaction temperature and varying CO/O_2 ratios between 1/0.5 and 1/2.

The objectives of the study are therefore:

- To synthesize a series of NiO/Al_2O_3 catalysts ranging from 5 weight % to 25 weight %, synthesize a mono-metallic Pt/Al_2O_3 catalyst and dope the most active NiO/Al_2O_3 catalyst with Pt, by using the incipient wet impregnation technique.
- To characterize these catalyst using various physisorption and chemisorption techniques as well as temperature programmed studies, XRD and microscopy.
- To test these catalysts for the oxidation of CO activity in a custom built reactor within the various reaction temperature ranges in H_2 rich streams.

References

[26] R.K. Ahluwalia, Q. Zhang, D.J. Chmielewski, K.C. Lauzze, M.A. Inbody, Catal. Today. 99 (2005) 271-283.

[27] M. Moreno, G.T. Baronetti, M.A. Laborde, F.J. Mariño, Int. J. Hydrogen Energy. 33 (2008) 3538-3542.

[28] J.A.C. Dias, J.M. Assaf, J. Power Sources. 130 (2004) 106-110.

[29] O. Korotkikh, R. Farrauto, Catal. Today. 62 (2000) 249-254.

[30] S. Lim, J. Bae, Int. J. Hydrogen Energy. 35 (2010) 6717-6725.

[31] G. Kolb, Fuel Processing, John Wiley and Sons, New York, 2008.

[32] F. Barbir, Pem Fuel Cells: Theory and Practice, Academic Press, Elsevier, London, 2012.

[33] L.-Y. Sung, B.-J. Hwang, K.-L. Hsueh, F.-H. Tsau, J. Power Sources. 195 (2010) 1630-1639.

[34] Available from: http://www.fuelcelltoday.com/about-fuel-cells/technologies/pemfc. Accessed (29/11/2012).

[35] A. Miltner, W. Wukovits, T. Pröll, A. Friedl, J. Cleaner Prod. 18, Supplement 1 (2010) S51-S62.

[36] M.M. Yung, Z. Zhao, M.P. Woods, U.S. Ozkan, J. Mol. Catal. A: Chem. 279 (2008) 1-9.

[37] E.-Y. Ko, E.D. Park, K.W. Seo, H.C. Lee, D. Lee, S. Kim, Catal. Today. 116 (2006) 377-383.

[38] D. Stolten, Hydrogen and Fuel Cells: Fundamentals, Technologies and Applications, John Wiley & Sons, New York, 2010.

[39] V.P. de Souza, D. Costa, D. dos Santos, A.G. Sato, J.M.C. Bueno, Int. J. Hydrogen Energy. 37 (2012) 9985-9993.

[40] O. Pozdnyakova, D. Teschner, A. Wootsch, J. Kröhnert, B. Steinhauer, H. Sauer, L. Toth, F.C. Jentoft, A. Knop-Gericke, Z. Paál, R. Schlögl, J. Catal. 237 (2006) 1-16.

[41] F. Cipitì, V. Recupero, Chem. Eng. J. 146 (2009) 128-135.

[42] V. Recupero, L. Pino, M. Cordaro, A. Vita, F. Cipitì, M. Laganà, Fuel Process. Technol. 85 (2004) 1445-1452.

[43] S.H. Oh, R.M. Sinkevitch, J. Catal. 142 (1993) 254-262.

[44] E. Moretti, L. Storaro, A. Talon, P. Patrono, F. Pinzari, T. Montanari, G. Ramis, M. Lenarda, Appl. Catal. A: Gen. 344 (2008) 165-174.

[45] Available from: http://minerals. usgs.gov/minerals/pubs/commodity/platinum/mcs-2010-plati.pdfm.u.g.m.p.c.p.m.-.-p.p.a., 2010. Accessed (21/11/2012).

CHAPTER 2

Experimental

2.1. Reagents

All reagents and gases used in this study for catalyst synthesis and catalytic testing are listed in Table 2.1 below:

Table 2.1: Reagents, packing material and gases

Chemicals and Gases	Formula	Purity	Supplier
Nickel nitrate hexahydrate	$Ni(NO_3)_2.6H_2O$	98%	Saarchem
Aluminum oxide (catalyst support)	γ-Al_2O_3		Alfa Aesar
Hexachloroplatanic acid	$H_2PtCl_6.xH_2O$	40% Pt	BDH Chemicals Ltd
Nitric acid	HNO_3	69%	Sigma-Aldrich
Nickel (ICP standard)	Ni	-	Industrial analytical
Platinum (ICP standard)	Pt	-	Fluka
Carborundum (24 grit)		-	Promark chemicals
Hydrogen	H_2	-	Afrox
Argon	Ar	-	Afrox
Nitrogen	N_2	-	Afrox
Synthetic Air	O_2	-	Afrox
Carbon dioxide	CO_2	-	Afrox
Carbon Monoxide	CO		Afrox

2.2. Catalyst Synthesis

A series of NiO/Al_2O_3 catalysts with nickel loadings of 5, 10, 15, 20 and 25 % (w/w) was prepared by the incipient wetness technique adopted from literature [1]. For the various loadings a constant amount of γ-Alumina (20.00 g) was impregnated with an aqueous solution where the

nickel salt content varied according to the desired loadings i.e. 5% (4.95 g), 10% (9.91 g), 15% (14.88 g), 20% (19.82 g), and 25% (29.78 g).

2.2.1 Preparation of NiO/Al_2O_3 catalysts

γ-Al_2O_3 (~20 g, high surface area catalyst support bimodal 18 inch pellets) was crushed to a fine powder using a mortar and pestle. A slurry of Al_2O_3 was made using deionized water. Nickel(II) nitrate hexahydrate was dissolved in a minimum amount of deionized water and added drop-wise to the slurry with vigorous stirring at room temperature for an hour. Water was evaporated on a hot plate at 80 °C until a paste was obtained. The paste was then transferred to a crucible and oven dried overnight at 110 °C. The dry precursor was crushed to a fine powder, and calcined at 500 °C for 8 hours using a LABOFURN furnace (KILN Contractors, South Africa). This method was employed for all NiO/Al_2O_3 catalysts prepared with different nickel loadings.

2.2.2 Preparation of Pt/Al_2O_3 catalysts

To a slurry of deionised water and crushed Al_2O_3 (~10 g), hexachloroplatanicatinic acid (~136 mg) dissolved in a minimal amount of water was added with vigorous stirring at room temperature for twelve hours on a hot plate stirrer. Water was then evaporated at 80 °C until a paste was obtained, which was oven dried overnight at 110 °C. The dry precursor was crushed to a fine powder using a mortar and pestle and calcined at 300 °C for 4 hours using a furnace [2].

2.2.3 Preparation of $Pt/NiO/Al_2O_3$ catalysts

To a slurry of deionised water and crushed 25% NiO/Al_2O_3 (5.0 g), hexachloroplatanicatinic acid (0.066 g) dissolved in a minimal amount of water was added with vigorous stirring at room temperature for twelve hours on a hot plate stirrer. Water was then evaporated at 80 °C to form a paste that was oven dried overnight at 110 °C. The dry precursor was crushed to a fine powder using a mortar and pestle and calcined at 300 °C for 4 hours using a furnace.

2.3. Characterization of NiO/Al_2O_3 catalysts

2.3.1 Thermogravimetric analysis

Thermogravimetric analysis (TGA) and differential scanning calorimetry (DSC) analysis was performed on catalyst samples (~5 mg) contained in an alumina crucible under a static air

environment using a Thermal Analyser SDT Q600 instrument. The temperature was increased from room temperature to 900 °C at a ramp rate of 10 °C/min.

2.3.2 Inductively Coupled Plasma-Optical Emission Spectroscopy (ICP-OES)

Catalyst samples accurately weighed (0.50 g) were dissolved in 5 mL HNO_3 and digested using a Perkin-Elmer Multiwave, microwave sample preparation system at 600 W. Digested catalyst samples were transferred to 100 mL volumetric flasks and homogenized using deionized water. Using commercial stock ICP standards, ICP standards solutions for nickel and platinum were prepared ranging from 0 to 100 ppm. The elemental composition of the catalysts was determined using an Optima 5300 DV PerkinElmer Optical Emission Spectrometer.

2.3.3 Brunauer-Emmett-Teller, Surface area and pore volume measurements

The Brunauer-Emmett-Teller (BET) surface areas of calcined catalysts (~0.05 g) were measured and recorded by nitrogen physisorption isotherms at ± -198 °C using the standard multipoint method (eleven points) on a Micromeritics Gemini instrument. The porosity (pore volume) of the calcined catalysts (~0.05 g) were also measured and recorded with the same instrument using the 14 point method. Prior to BET analyses samples were degassed under a steady stream of nitrogen with a temperature ramp of 2 °C/min to 200 °C and held constant overnight.

2.3.4 Powder X-Ray diffraction

Powder X-ray diffraction (XRD) patterns of calcined catalysts were recorded on a Bruker D8 Advance with Diffracplus XRD Commander Software, and a Bruker VANTEC detector. The radiation source used was Cu Kα (wavelength of 0.1540 nm), operating on a long focus line with a voltage and amperage of 40 kV and 40 mA respectively. The catalysts were scanned in a 2θ range from 2º to 90º at 0.5 degree per minute.

2.3.5 N_2 Adsorption Desorption

The pore size distributions and adsorption, desorption isotherms of the catalysts were calculated using the method of Barrett, Joyner and Helenda (BJH) [3]. Calcined catalyst samples (~0.2 g) were degassed under a steady stream of nitrogen using a Micromeritics Flow Prep 060 Sample degas system, with a temperature ramp of 2°C per min to 200 °C and held constant overnight.

Samples were then analysed using a Micromeritics TriStar II Surface Area and Porosity instrument.

2.3.6 Raman Spectroscopy

Raman spectra of calcined catalysts (~0.05 g) were recorded using an Advantage 532 series spectrometer (NIR spectrometer) utilizing Nuspec software.

2.3.7 Scanning electron microscopy and energy dispersion X-ray spectroscopy

Scanning electron microscopy (SEM) images were obtained using a FEG 1450 Scanning Electron Microscope at 20 kV. Energy dispersion X-ray (EDX) was carried out using a Jeol JSM 6100 Scanning Electron Microscope equipped with a Bruker EDX Detector and analysed with Espirit 1.8.5 software. Samples for EDX were coated with carbon in a Jeol JEE-4C Vacuum Evaporator, whereas samples for SEM images were coated with gold using a Polaron SC Sputter Coater.

2.3.8 Transmission Electron Microscopy

For this technique catalyst samples were diluted with ethanol in an Eppendorf tube and sonicated for 2 minutes, samples were then coated on a formvar copper grid and placed into the microscope. The images were then captured using a Jeol JEM 1010 Transmission Electron Microscope (TEM) operated at a voltage of 100 kV equipped with a MegaView III Soft Imaging System.

2.3.9 Temperature programmed reduction

Temperature programmed reduction (TPR) profiles were obtained using a Micromeritics Autochem II Chemisorption Analyzer. Approximately 0.05 g of fresh calcined catalyst sample was placed on top of quartz wool in a U shaped quartz tube. Prior to reduction, the catalysts were pretreated by heating to 400 ºC under a stream of argon (30 mL/min) for 30 min and then cooled down to 90 ºC under the same stream of argon. The reduction experiments were carried out using 5 vol % H_2 in Ar as the reducing agent with a flow rate of 30 mL/min and the temperature ramped to 1000 ºC at 10 ºC/min.

2.3.10 NH_3-Temperature programmed desorption

Temperature programmed desorption (NH_3-TPD) profiles also involved the use of the Micromeritics Autochem II Chemisorption Analyzer. Fresh calcined catalyst sample (~0.05 g) was placed on top of quartz wool in a U shaped quartz tube and reduced as described for TPR. NH_3-TPD analysis followed once the H_2 consumption was zero by firstly cooling the sample to 100 ºC under a stream of argon, then passing He over the sample for 1 hour. For the next 30 minutes, 4 vol% NH_3 in He was passed over the sample, followed by a 10 °C/min temperature ramp to 1000 ºC under a flow of helium.

2.3.11 CO Chemisorption

Calcined catalyst samples (~0.15 g) were degassed with a flow of N_2 under vacuum at 200 °C using a Micromeritics Flow Prep 060 Sample Degas System, overnight. Samples were analysed using a Micromeritics ASAP 2020 instrument.

2.4 Catalytic Testing

2.4.1 Test unit design

The reactor design is depicted by the schematic drawing in Figure 2.1. This was a custom built PROX reactor and a prototype designed and built by the chemical engineering department (UCT). All tubing and fittings used were supplied by Swagelok. The tubing was stainless steel with ¼ inch (outer diameter) upstream of the reactor tube and ⅛ inch (outer diameter) downstream of the reactor tube (to the Vici valve). All gases were supplied to the system by Tescom pressure regulators (PRs) from Afrox cylinders regulated at 30 bars using Swagelok manifolds and 0.5 μ filters.

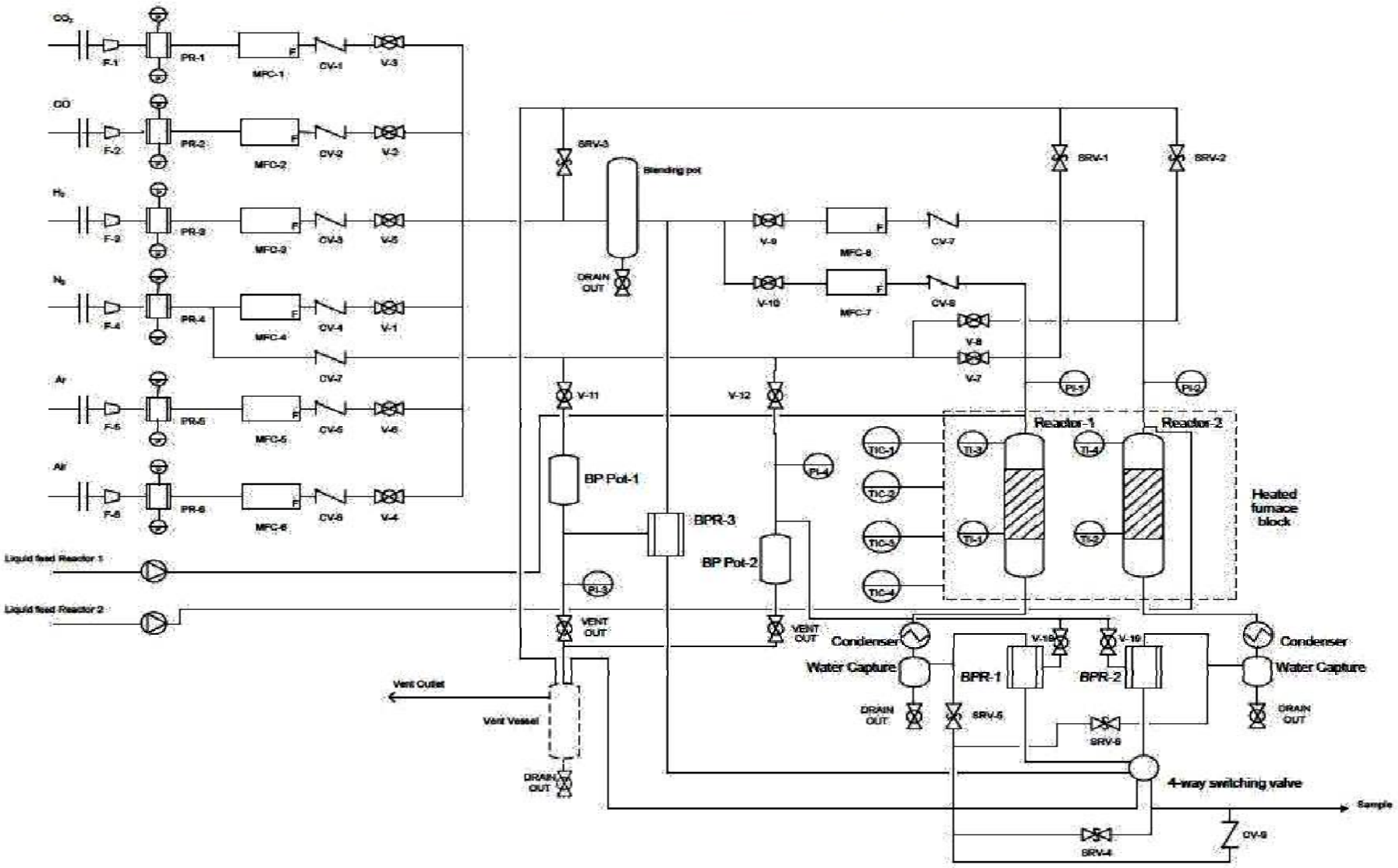

Figure 2.1: Schematic representation of the PROX test unit

The system PRs controlled the inlet pressure to the Brooks Mass Flow Controllers (MFCs) which were fitted with one way valves ensuring flow only towards the reactor tube. Gases exiting the MFCs were allowed to mix in the blending pot from which the mix could be extracted in three ways to: 1) Bypass (control), 2) Reactor-1 or 3) Reactor-2. Each reactor was fitted with a MFC, shut off valve and one way valve. The pressure for the reactors was modulated by the back pressure (BP) pots 1 and 2 which allow larger volumes of gas to be held for much longer periods. These control the Back Pressure Regulators (BPRs) 1, 2 and 3 which were spring regulated allowing the exit of gas only once it exceeded the spring force, therefore maintaining pressure of the reactor as well as the flow rate. Gas exiting the reactors and bypass lead to a 4 way switching valve (Vici valve) which was controlled by an actuator interfaced with a computer. The valve had four inlet ports (Figure.3.2), one for each reactor (ports 2 and 4), one for the bypass (port 3) and the fourth was permanently blocked (port 1). The outlet ports consisted of a sample outlet and a vent where all gases not being sampled exited. From Figure 2.2, when sampling from port 4 which was for reactor 2, ports 1, 2, and 3 were automatically vented. If the sampling position was changed, for example to port 1, the cog of the valve would have rotated clockwise venting ports 2, 3, and 4.

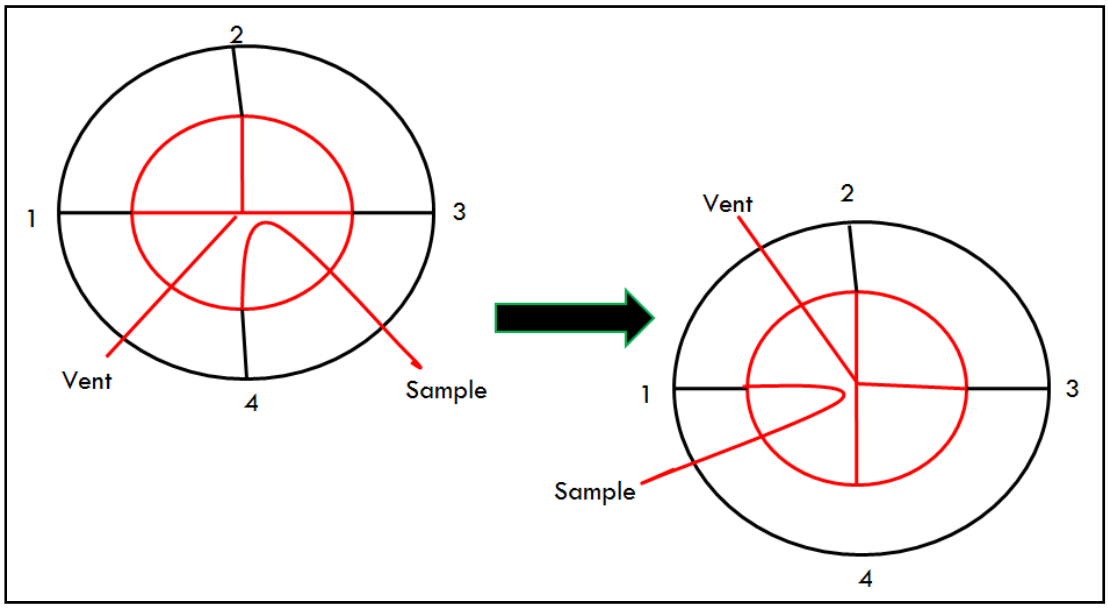

Figure 2.2: Illustration of the Vici valve

2.4.1.1 The reactor tube and catalyst packing

The reactor tube was made of ¾ inch (outer diameter) stainless tubing 49 cm in length. The catalyst was always packed at the isothermal point within zone 3. In order to determine the isothermal point, the reactor tube was packed with carborundum (24 gritt, Promark Chemicals) with glass wool used as a stopper at both ends. The heating modules were switched on and set at a specific temperature and left to equilibrate. A coaxially centred thermocouple was moved at 1 cm intervals within the reactor tube from the bottom to the top and the isothermal point was determined (Appendix A2).

The catalyst (fixed volume diluted with carborundum 1:1 wt/wt) was sandwiched between two layers of glass wool and the remainder of the tube was filled with carborundum and stoppered with glass wool on both ends. An illustration of the packed and actual reactor tube is in the Appendix (Appendix A1). Prior to catalytic testing, leak tests were performed on the reactor tube by flowing N_2 at a pressure of 2 bars. At the end of each experiment, the reactor tube was carefully emptied, washed with water, soaked in an oxalic acid solution, washed again, rinsed with acetone, dried in an oven (110 ºC), and stored for further usage. The used catalyst was carefully removed, sieved, cleaned for separation from the carborundum and characterized.

2.4.1.2 Test unit troubleshooting

The test unit obtained had to be conditioned before any pressure testing, temperature profiling, mass flow controllers and GC calibrations were undertaken.

Firstly, at the onset, installed gas supply lines had major leaks. For health and safety requirements, they were removed and new stainless steel Swagelok ¾ inch lines from the cylinders in a gas bank were installed and fitted to the test unit. An alarm system supplied and installed by Drager was installed in the room for the detection of CO and H_2 gas leaks.

Once the supply lines and detectors were installed and tested for defects, conditioning of the test unit was done. Gases were supplied to the individual MFCs. Some of them were found to have incorrect flow readings. These were purged with the respective gas flowing through them for at least two hours until the readings were stable. Thereafter, each MFC was calibrated at the outlet using a Brooks flow meter, and calibration curves were generated for each individual gas. With

the aid of N_2, the rest of the test unit was pressurized including the reactor tubes. A Restek electronic leak detector and Snoop liquid leak detector (supplied by Swagelok) where used to detect any leaks on the test unit. Once leaks were identified, these were rectified by tightening or replacing some of the fittings. In one case, the reactor tube did not pressurize at all. Since the pressure upstream of the reactor tube was greater than the required pressure of the reactor and no leaks were detected, it was concluded that the BPR of that reactor was malfunctioning. Since the BPRs were spring controlled it could be that the spring had been displaced by the application of pressure in excess of its limit. A new BPR was installed and the reactor tube pressurized perfectly. Once the reactor tubes were pressurized and held the set pressures for more than twelve hours with no indications of any pressure drops, heating lines were installed over the stainless steel tubing below the reactor tubes up to the GC sample injection port.

2.4.2 Gas Chromatograph

The gaseous products were analyzed using an on-line 3 channel Varian CP-4900 Micro Gas Chromatograph equipped with a thermal conductivity detector (TCD). The details and conditions of the GC are shown in Table 2.2.

Table 2.2: Details of Micro GC method

	Channel –I	**Channel -II**	**Channel -III**
Column	Molsieve - 5Å	Molsieve - 5Å	CP-SIL 5 CB
Column length (m)	20 m	10 m	8 m
Carrier gas	Argon	Hydrogen	Hydrogen
Carrier gas pressure	150 kPa	150 kPa	70 kPa
Injector temperature (ºC)	-	40 ºC	40 ºC
Injection time (ms)	40	40	40
Injection volume (nl)	200	200	200
Oven temperature	50 ºC	50 ºC	40 ºC

2.4.2.1 GC troubleshooting

Prior to the GC calibration, many issues regarding the carrier gas and functioning of the GC had to be resolved in order for catalytic activity measurements to be performed. Initially a 2 channel Varian Micro GC was supplied which only had means for using one carrier gas (H_2) which made the detection of hydrogen in the reaction impossible. The GC was modified and a new carrier gas line was installed for argon in Channel 1. Conducting GC runs with individual gases through the test unit, baseline separation of the permanent gas peak in channel two was very unstable, which indicated a leak in that column. After three or four runs on the GC the Drager leak detector fitted in the reactor room picked up an H_2 leak in the laboratory. The GC was opened and it was found that one of the solenoid gaskets was leaking. This problem was rectified with the help of a Perkin-Elmer technician who gave me sufficient training in repairing the GC for minor internal problems. After the leaks on the GC were sorted out and individual gases were sampled, it was found that the Vici valve and the GC software were not "communicating" as expected. A new configuration had to be built in the software for these to "communicate". Once all of these problems were taken care of, the GC was then tested with a mixture of gases and it was found that H_2 and CO did not separate, due to the quantity of gas present in the mixture (50 % H_2 and 1% CO), and they both eluted in the same column. Also the second column was showing a negative peak for water and no clear baseline separation of the permanent gas and CO_2 gas peak. This problem consumed a lot of time and this GC was set aside. The Catalysis Research Centre (Chemical Engineering Department at UCT) offered a loan GC that wasn't being used to carry out the catalytic work of this project. This was a 3 channel Varian Micro GC that had a few minor gas leaks and software problems, which were rectified once it was connected to the test unit. Individual gas retention times were determined and GC calibrations were performed before catalytic experiments were undertaken.

2.4.3 Testing the test unit and GC using a commercial catalyst

A commercial AuTEK® (Au/TiO_2) CO-oxidation catalyst was obtained from Mintek and used to test the performance of the test unit and GC and the results obtained were compared to literature results. Reaction conditions were adopted from Walther et al. [4] and modified to suit the type of set-up available for this project. The simulated reformate feed contained 1 vol. % CO, 0.5 vol. % O_2, 50 vol. % H_2 and N_2 made up the balance. The flow rate was set at 300 mL/min and the

GHSV fixed at 12000 h^{-1}. A catalyst volume of 1.5 mL consisting of mesh sizes between 300-600 microns was used. The catalyst was screened for PROX activity between temperatures ranging from room temperature to 80 °C. A time on stream experiment was also conducted over the catalyst for a 10 hour period to determine the catalysts stability under PROX reaction conditions. GHSV's used for the remainder of the studies were calculated as follows:

$$\text{GHSV} = \frac{\text{total flow rate (mL/min)}}{\text{volume of catalyst (mL)}} \times 60$$

2.4.4 Catalysis of the NiO/Al_2O_3 catalysts

The following equations were used for calculating the amount of CO converted and the selectivity towards the products from the outlet gas:

$$\text{CO conversion (mol \%)} = \frac{CO_{in} - CO_{out}}{CO_{in}} \times 100$$

$$CO_2 \text{ selectivity (mol \%)} = \frac{\text{amount } CO_2 \text{ out}}{\text{amount of total products}} \times 100$$

$$H_2O \text{ selectivity (mol \%)} = \frac{\text{amount } H_2O \text{ out}}{\text{amount of total products}} \times 100$$

2.4.4.1 PROX reactions over NiO/Al_2O_3 catalysts

Catalysts were tested for activity using a simulated reformate feed containing 1 vol. % CO, 0.5 vol. % O_2, 50 vol. % H_2 balanced with N_2 (48.5 vol. %). The flow rate was set at 150 mL/min and the GHSV fixed at 12000 h^{-1}. A catalyst volume of 0.75 mL consisting of mesh sizes between 300-600 microns was used. The catalysts were screened at temperatures ranging from room temperature to 290 °C.

2.4.4.2 CO-oxidation reactions on 25 % NiO/Al_2O_3 catalyst

In order to determine the optimum $CO:O_2$ ratio for the PROX reaction, the 25 % NiO/Al_2O_3 catalyst was tested for CO-oxidation using a simulated feed containing 1 vol. % CO, 0.5,1 and 2 vol. % O_2 and the balance N_2. The flow rate was set at 150 mL/min and the GHSV fixed at 12000 h^{-1}. A catalyst volume of 0.75 mL consisting of mesh sizes between 300-600 microns was used. The catalysts were screened at temperatures ranging from room temperature to 290 °C.

2.4.4.3 PROX reactions on 25 % NiO/Al_2O_3 catalyst with optimum $CO:O_2$ ratio

PROX activity was studied on the 25 % NiO/Al_2O_3 catalyst using a simulated reformate feed containing 1 vol. % CO, 2 vol. % O_2, 50 vol. % H_2 and the balance N_2. The flow rate was set at 150 mL/min and the GHSV fixed at 12000 h^{-1}. A catalyst volume of 0.75 ml consisting of mesh sizes between 300-600 microns was used. The catalyst was tested at temperatures ranging from room temperature to 290 °C. A time on stream experiment was conducted using a fresh catalyst and the same feed for 30 hours. The catalyst was also screened at GHSVs ranging from 6000 - 18000 h^{-1} for effects on conversion and selectivities. A regeneration study of the catalyst after the CO oxidation and PROX reactions was performed by calcining the used catalyst in-situ at 300 °C under a positive air flow.

2.4.5 Catalysis over Pt/Al_2O_3

2.4.5.1 CO-oxidation reactions on Pt/Al_2O_3 catalyst

In order to determine the optimum $CO:O_2$ ratio for the PROX reaction over the Pt/Al_2O_3 catalyst, the catalyst was first tested for CO-oxidation using a simulated feed containing 1 vol. % CO, 0.5 and 2 vol. % O_2 and the balance N_2. The flow rate was set at 150 mL/min and the GHSV fixed at 12000 h^{-1}. A catalyst volume of 0.75 mL consisting of mesh sizes between 300-600 microns was used. The catalysts were screened at temperatures ranging from room temperature to 250 °C.

2.4.5.2 PROX reactions on Pt/Al_2O_3 catalyst with optimum $CO:O_2$ ratio.

PROX activity was studied on the Pt/Al_2O_3 catalyst using a simulated reformate feed containing 1 vol. % CO, 0.5, 1 and 2 vol. % O_2, 50 vol. % H_2 and the balance N_2. The catalyst volume used was 0.75 mL consisting of mesh sizes between 300-600 microns with a flow rate of 150 mL/min and a GHSV of 12000 h^{-1}. The catalyst was screened within at temperatures ranging from room temperature to 200 °C. A time on stream experiment was conducted using a fresh catalyst and the same feed for 24 hours to determine the catalyst's stability.

2.4.6 Investigations on $Pt/NiO/Al_2O_3$ catalyst

2.4.6.1 PROX reactions on $Pt/NiO/Al_2O_3$ catalyst with optimum $CO:O_2$ ratio

The PROX reaction was studied over the $Pt/NiO/Al_2O_3$ catalyst using a simulated reformate feed containing 1 vol. % CO, 0.5-2 vol. % O_2, 50 vol. % H_2 and the balance N_2. The catalyst volume used was 0.75 mL consisting of mesh sizes between 300-600 microns with a flow rate of 150 mL/min and a GHSV of 12000 h^{-1}. The catalyst was screened within a temperature window of room temperature to 200 °C. A time on stream experiment was conducted using fresh catalyst and the same feed for 24 hours to determine the catalyst's stability.

2.4.6.2 Iso-conversions

Selectivity of the products for the catalysts were analysed at a set iso-conversion point in order to determine the effect of the catalysts with regards to the conversion of CO and selectivity of CO_2. In order to obtain iso-conversion, the GHSVs were varied at constant temperature.

2.5 Used catalyst characterization

Catalysts used for CO oxidation and PROX reactions were characterized by BET and powder XRD as described previously (Section 2.3.3 and 2.3.4).

References

[1] K. Opoku-Gyamfi, A.A. Adesina, Appl. Catal. A: Gen. 180 (1999) 113-122.

[2] E.-Y. Ko, E.D. Park, K.W. Seo, H.C. Lee, D. Lee, S. Kim, Catal. Today. 116 (2006) 377-383.

[3] P. Salagre, J.L.G. Fierro, F. Medina, J.E. Sueiras, J. Mol. Catal. A: Chem. 106 (1996) 125-134.

[4] G. Walther, D.J. Mowbray, T. Jiang, G. Jones, S. Jensen, U.J. Quaade, S. Horch, J. Catal. 260 (2008) 86-92.

CHAPTER 3

Characterization of the NiO/Al_2O_3 Systems

3.1 Thermogravimetric analysis

Thermogravimetric analysis of the lower loaded nickel 5 % (Ni5) and higher loaded nickel 25 % (Ni25) loaded catalysts was carried out in order to determine the calcination temperature of the freshly prepared uncalcined NiO supported catalysts.

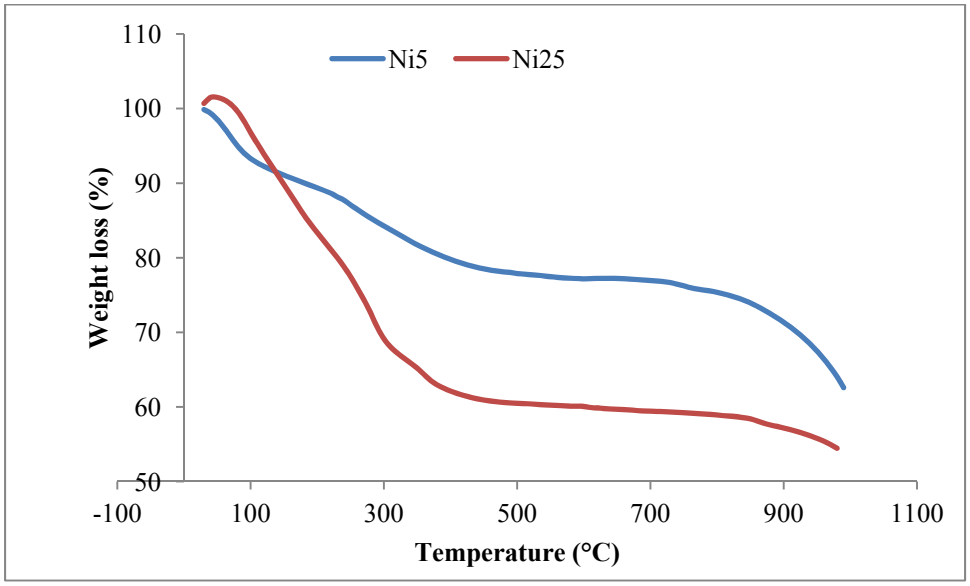

Figure 3.1: Thermogravimetric analysis of the uncalcined Ni5 and Ni25 catalysts

Figure 3.1 indicates that both the uncalcined samples show slight weight losses in the temperature region of 100-200 °C. This can be attributed to the desorption of water from the material. Furthermore, the percentage weight loss in the temperature region of 200-400 °C can be attributed to the decomposition of the $Ni(NO_3)_2$ to NiO;

$$Ni(NO_3)_2 \rightarrow NiO + 2NO_2 + O_2$$

Ni25 shows a higher percentage weight loss in both temperature regions compared to Ni5, which corresponds to the concentration of the nickel nitrate used in the synthesis of the two catalysts.

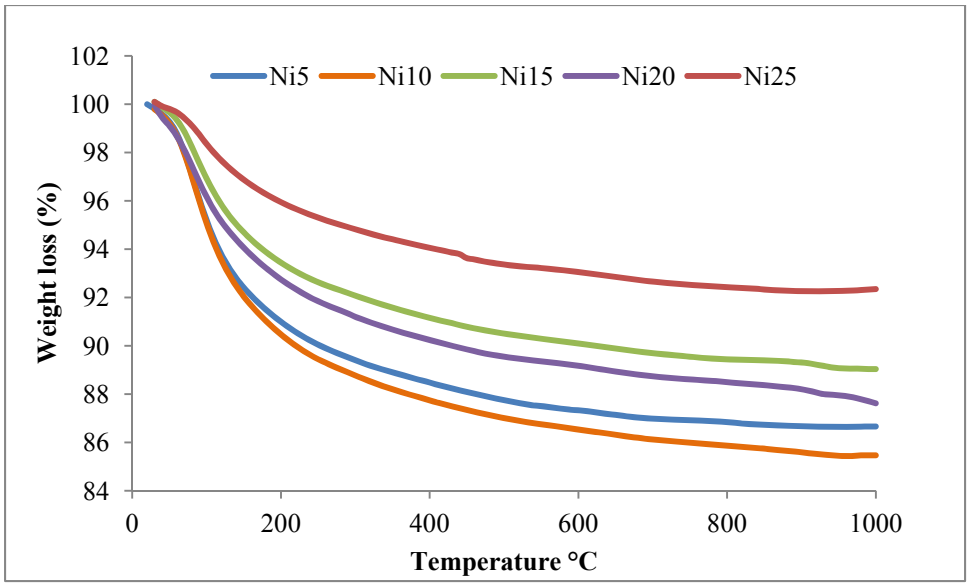

Figure 3.2: Thermogravimetric analysis of the calcined NiO/Al_2O_3 catalysts

All calcined catalysts indicated a similar percentage weight loss below 200 °C which can be seen in Figure 3.2. This is due to the desorption of water from the catalyst surface during heating. None of the calcined catalysts, however, showed any substantial weight loss between 200-400 °C, which would be characteristic for the decomposition of metal nitrates. Therefore, nickel present on the surface of the alumina is in an oxide form and not as the nitrate. Following the calcination in a positive air flow environment at 500 °C for 4 hrs, the nitrates were removed from the nickel salt resulting in the formation of a NiO layer on the surface of the alumina.

3.2 Inductively coupled plasma – optical emission spectroscopy

The presence of nickel on the surface of the alumina support was quantitatively determined by ICP-OES (Table 3.1). This technique is a bulk technique, and provides useful information about the total metal present in the catalyst. All the catalysts showed Ni loadings similar to the nominal weight loadings.

Table 3.1: ICP-OES results for the NiO/Al_2O_3 catalysts

Catalyst	Nominal Ni content (wt %)	Ni from ICP (wt %)
Ni5	5	4.8
Ni10	10	9.0
Ni15	15	12.5
Ni20	20	19.1
Ni25	25	24.6

3.3 Physisorption methods

Nitrogen adsorption-desorption isotherms for the series of NiO/Al_2O_3 catalysts with various Ni loadings are shown in Figure 3.3.

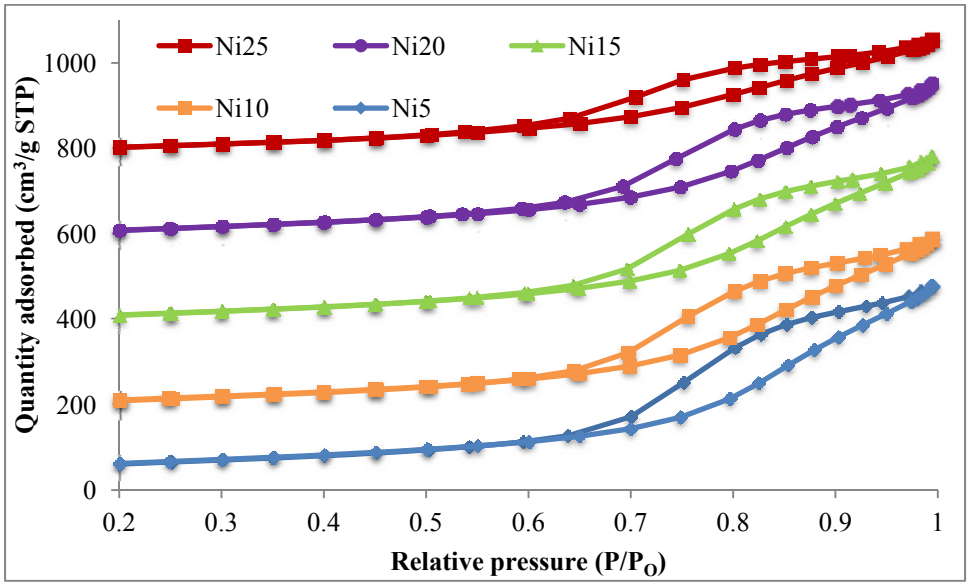

Figure 3.3: Adsorption isotherms of the NiO/Al_2O_3 samples

All samples show isotherms of the type IV in the classification of Brunauer, Deming, Deming and Teller (BDDT) [1] with H1 hysteresis loops characteristic for mesoporous materials [2]. As can be seen from Figure 3.3, the steepness of the capillary condensation steps clearly indicates

uniformity of mesopores. The condensation step for all isotherms are within the same relative pressure range and no drastic decrease in the steepness of the capillary condensation is observed with increasing molar fractions of NiO that would also indicate the presence of larger primary mesopores [2]. Isotherms displayed are all indicative of a large volume of primary mesopores from the steepness of the capillary condensation steps generated [2].

According to Morris et al. [2], adsorption isotherms that have steep condensation steps will represent narrow distributions for the corresponding pore size distribution (PSD) curves generated. However, isotherms with broader condensation steps also generate broader pore size distributions.

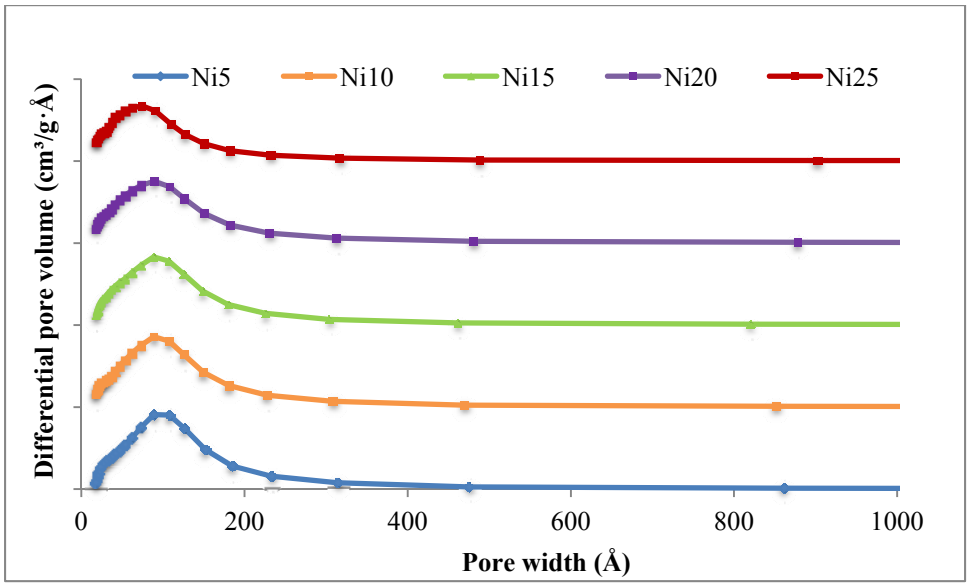

Figure 3.4: Pore size distributions of the NiO/Al_2O_3 samples

Figure 3.4 shows the PSDs according to the BJH method for the NiO/Al_2O_3 samples studied. From this, it is clearly visible that due to the steepness of the capillary condensation steps representing broad isotherms, the corresponding PSDs generated are indeed broader. From these PSD curves it is evident that as the weight percent of nickel increases, the number of pores generating high pore widths decrease, which is also attributed to the decrease of the average pore size. From the hysteresis loops generated, the steepness of the capillary condensation steps clearly indicates that the catalyst do not lose their mesoporosity with an increase in the nickel weight percent.

Table 3.2: Surface characterization of the NiO/Al_2O_3 catalysts

Catalyst	Surface area (m^2/g)	Pore volume (cm^3/g)	Pore diameter (Å)
Alumina	225	0.78	127.6
Ni5	216	0.72	125
Ni10	204	0.64	117
Ni15	185	0.63	116
Ni20	178	0.54	111
Ni25	189	0.47	94

Therefore it can be concluded that the nickel oxide particles are not disturbing the pore structure of the alumina support, but are blocking the pore mouth of the support [1]. The blocking of the pores of the alumina, results in the decrease of the surface area, pore volume and pore size as shown in Table 3.2.

3.4 CO Chemisorption

In order to estimate the metal dispersion and crystallite sizes of the NiO on the surface of the alumina support, chemisorption using CO as the adsorbate was conducted on all Ni/Al_2O_3 catalysts. The metal dispersions were calculated from the CO adsorption data using a stoichiometric ratio of 1 for Ni:CO. The CO adsorption plots generated are shown in Figure 3.5. From the figure it can be seen that with an increase in pressure, the amount of CO chemisorbed on the surface of the catalysts increases. Also, the total quantity of CO adsorbed on the surface of the catalysts increases with an increase in the NiO loading on the surface of the support. Thus the total CO chemisorbed on the surface of the NiO/Al_2O_3 catalysts is the mostly chemisorbed on the NiO particles present on the catalysts.

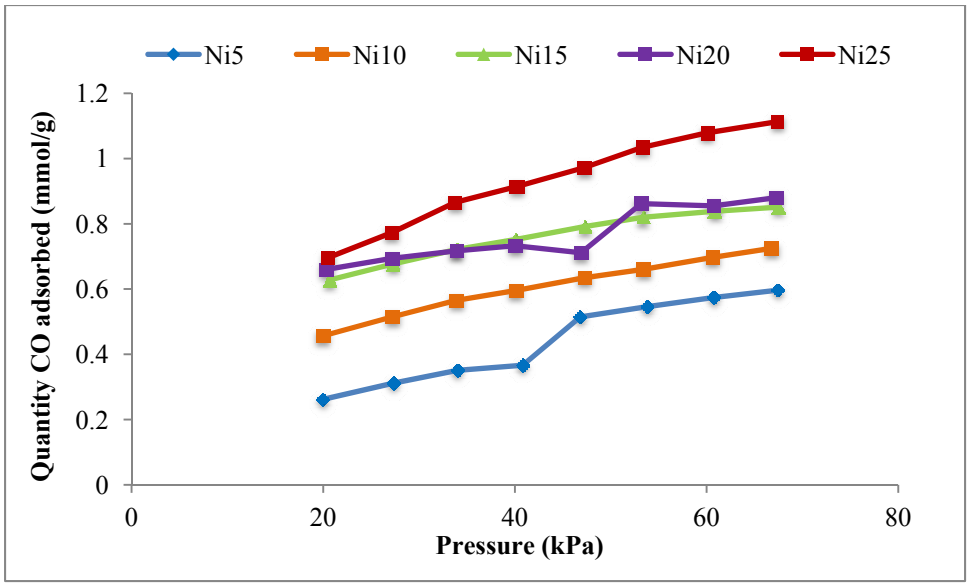

Figure 3.5: CO Chemisorption profiles of the NiO/Al_2O_3 catalysts

The metal dispersions determined for the NiO/Al_2O_3 catalysts are shown in Table 3.3.

Table 3.3: Metal dispersions and crystallite sizes of the NiO/Al_2O_3 catalysts

Catalyst	Metal Dispersion (%)	Crystallite Size (nm)
Ni5	15.1	7
Ni10	15.8	6
Ni15	15.3	7
Ni20	16.9	6
Ni25	19.0	5

From this it can be seen that for the lower NiO loadings, Ni5, Ni10 and Ni15, the metal dispersions are within the same range, differing by ±1 %, hence the crystallite sizes of these NiO/Al_2O_3 catalysts are also similar. It is evident that the NiO particles are agglomerated on the surface of the alumina, indicated by the rough surface morphologies for the catalysts in the SEM images (Section 3.8.1). The higher loaded NiO catalyst Ni25, showed the highest metal

dispersion of 19 %, indicating that higher metal loadings generate particles that are smaller in size.

3.5 Powder XRD of the NiO/Al_2O_3 catalysts

The stacked X-ray diffractograms of alumina (a) and all NiO/Al_2O_3 materials (b-f) are shown in Figure 3.6. The characteristic peaks for γ-Al_2O_3 are observed at 2θ values of 37.18°, 45.36° and 66.71° with the corresponding d spacing's of 2.39, 1.97 and 1.52 respectively, for all the catalysts. These d spacings correspond to those listed in the JCPDS file no: 10-425.

With regards to the NiO samples (b-f), determining the d spacings at the lower loadings for the NiO was more difficult due to the NiO having shoulder peaks which generally overlap with those of alumina. All the NiO phases are compared with the ICDD files obtained by using Peak Match Software and the JCPDS file no: 4-0835 [JCPDS].

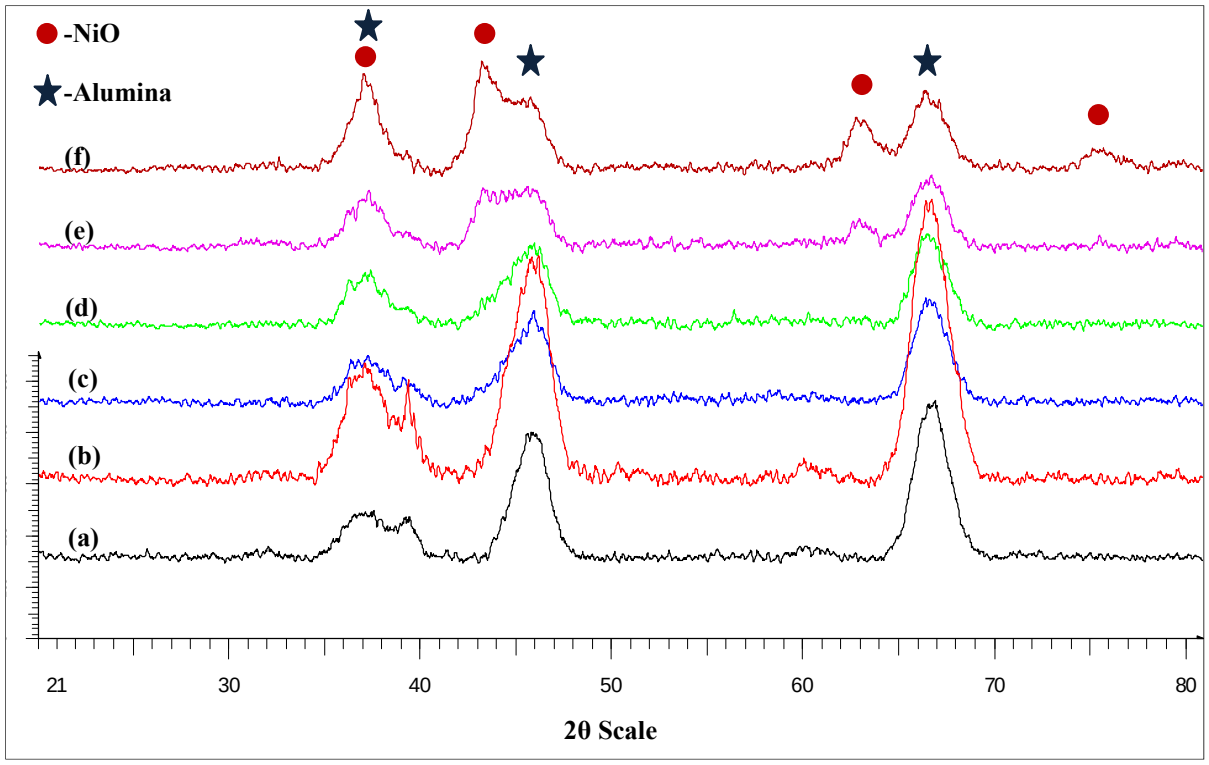

Figure 3.6: XRD diffractograms of (a) Alumina, (b) Ni5, (c) Ni10, (d) Ni15, (e) Ni20 and (f) Ni25

All NiO loaded catalysts show characteristic peaks at 2θ values of 37.18°, 45.36° and 66.71° with the corresponding d spacings of 2.41, 1.25 and 1.47, respectively, which clearly indicates the presence of NiO. For the higher NiO loaded catalysts (Ni20 and Ni25), the presence of NiO was shown by the peaks at 2θ values of 43.26° and 62.5°, with the corresponding d spacings of 2.08 and 1.48 respectively.

3.6 Temperature programmed studies

3.6.1 Reduction

Figure 3.7 shows the TPR profiles of the NiO/Al_2O_3 catalysts. All catalysts showed a slight negative peak in the temperature region of 100-200 °C which is attributed to physisorbed moisture on the surface of the catalysts. The onset reduction temperature for all catalysts is within the temperature region of 300-400 °C, whilst NiO catalysts with higher loadings of NiO show a decrease with regards to the onset reduction temperature. Also an increase in NiO loading shows a peak shift in the TPR towards lower temperatures.

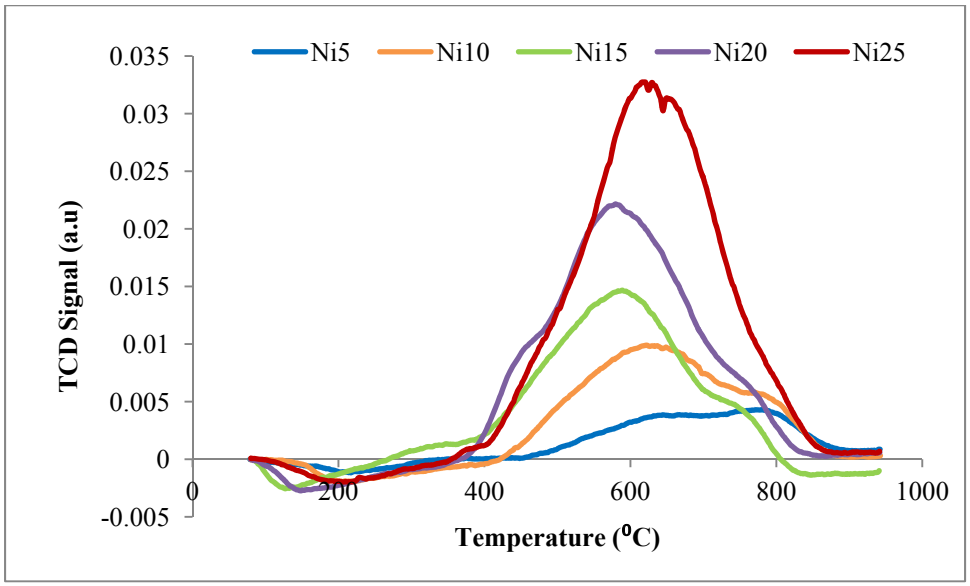

Figure 3.7: TPR profiles of the NiO/Al_2O_3 samples

The H_2 consumption peaks of NiO/Al_2O_3 samples with low NiO loadings are known to shift to higher temperatures, which suggest that the supported Ni^{2+} ions are well dispersed on the support, hence making them more difficult to reduce due to the strong interaction between the NiO and the Al_2O_3 [3, 4]. With regards to Ni25, the reduction peak present is at a higher

temperature compared to the reduction peak of the Ni20. According to S. Ren et al, [3], these high temperature reductions of high NiO loadings can be attributed to the reduction of Ni^{2+} ions incorporated into tetrahedral and octahedral vacancies on the surface of the Al_2O_3 support. The increase in the broadness and peak shoulder at 670 °C could be an indication of NiO particles that are loosely bound on the support, and these particles saturate the surface of the support forming bulk NiO [5]. From Table 3.4 it can be seen that the hydrogen consumption and degree of reducibility increases with an increase in the NiO weight percent of the catalysts. This indicates that the higher loading of Ni is more easily reduced than the lower loadings. The Al_2O_3 support did not generate any reduction peaks [3], therefore the reduction peaks shown on the NiO/Al_2O_3 catalysts attribute to the reduction of NiO only.

Table 3.4: TPR data obtained for the NiO/Al_2O_3 catalysts

Catalyst	Temperature (°C)	H_2 consumption (cm^3/g)	Degree of reducibility (%)
Ni5	641	5.2	28.6
	787	3.1	16.8
Ni10	616	22.0	61.8
	796	2.7	7.4
Ni15	312	1.2	2.6
	585	35.0	72.9
	754	3.2	6.5
Ni20	444	2.6	3.5
	582	37.7	51.2
	757	3.4	4.6
Ni25	624	65.3	69.1

From the deconvolution of the TPR peaks generated (Fig.3.7), hydrogen consumption and the degree of reducibility (Table 3.4), it is clear that the reduction of NiO follows the pathway shown below;

$$Ni^{2+} \rightarrow Ni^{1+} \rightarrow Ni^{0}$$

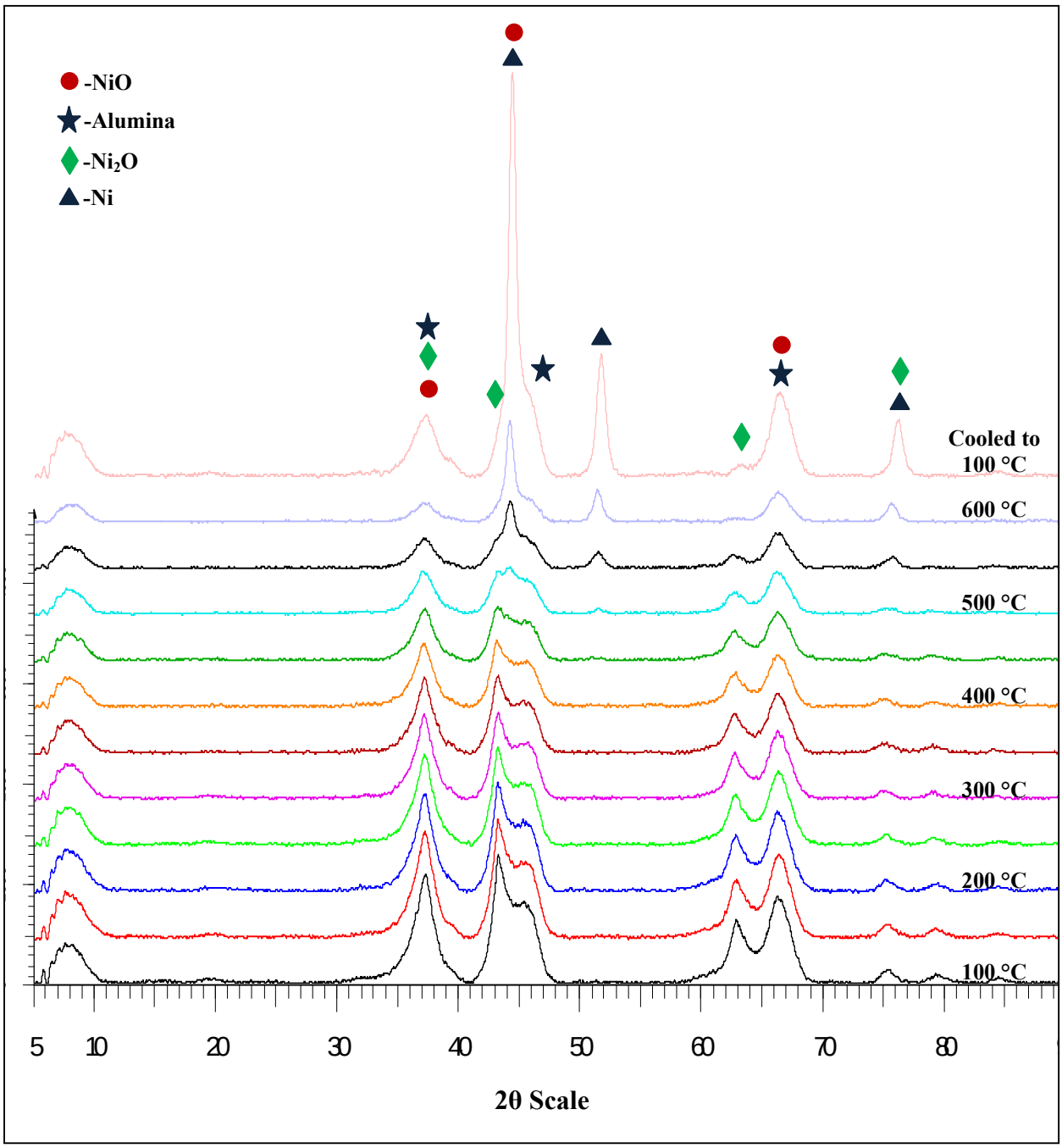

Figure 3.8: *In situ* XRD diffractogram of Ni25 under a reducing atmosphere

To investigate the phase changes in the NiO under a reducing atmosphere, *in situ* XRD was carried out for Ni25 by flowing 5 % hydrogen in Ar (30 ml/min) over the sample from room temperature to 600 °C in temperature increments of 50 °C. Figure 3.8 shows the *in situ* diffractogram of Ni25 under the reducing atmosphere. The diffractogram indicates no phase change in the NiO until 450 °C, which also corresponds to the results obtained from the TPR profile. No observable change is seen with regards to the crystallite size or crystallinity of the catalyst within the temperature region of 100-400 °C, indicating that the catalyst is stable up to 400 °C under this reducing environment. The desorbed species from the catalyst within the temperature region of 100-250 °C, which was shown by the negative peak in TPR profile, are the physisorbed species, most likely moisture from the atmosphere and they are not evident to any species from the NiO structure. From the *in situ* XRD diffractogram, the phases of NiO, Ni_2O and Ni metal are observed within the temperature region 450-600 °C, which shows the reduction pathway of NiO. These phases are confirmed with the ICDD file nos: 010870712 (Ni), 010721464 (Ni_2O) and 010780429 (NiO) with peaks at 2θ values of 44.53°, 51.83°, 62.79° and 76.73°, with the corresponding d spacings of 2.03, 1.76, 1.47 and 1.24 respectively. The complete reduction of NiO to Ni occurred at a temperature of 600 °C, where the Ni remained in its metallic form when cooled to 100 °C.

3.6.2 Oxidation

In order to investigate the oxidizing capacity of the Ni in its metallic form following its reduction after *in situ* XRD under H_2, an *in situ* XRD oxidation experiment was conducted. Nitrogen was passed through the sample at 100 °C in order to remove the 5 % H_2 in Ar gas that was physisorbed on the surface of the catalyst. After this, air was passed through the sample at a flow rate of 30 ml/min and the temperature was increased from room temperature to 600 °C in increments of 50 °C. Figure 3.9 shows the *in situ* XRD diffractograms of the initially reduced Ni25 under an oxidizing atomosphere. From the *in situ* XRD diffractograms it is evident that Ni remains in its metallic form until 300 °C. The transformation of the Ni metal back to the NiO phase takes place within the temperature range of 100-300 °C. This transformation follows the inverse path way to the reduction which is shown below;

$$Ni^0 \rightarrow Ni^{1+} \rightarrow Ni^{2+}$$

This transformation of the Ni metal to the NiO phase via the intermediate Ni_2O phase is evident from the following ICDD file nos: 010870712 (Ni), 010721464 (Ni_2O) and 010780429 (NiO). The characteristic peaks of Ni, NiO and its intermediate Ni_2O phase are now seen within the temperature region of 100-300 °C.

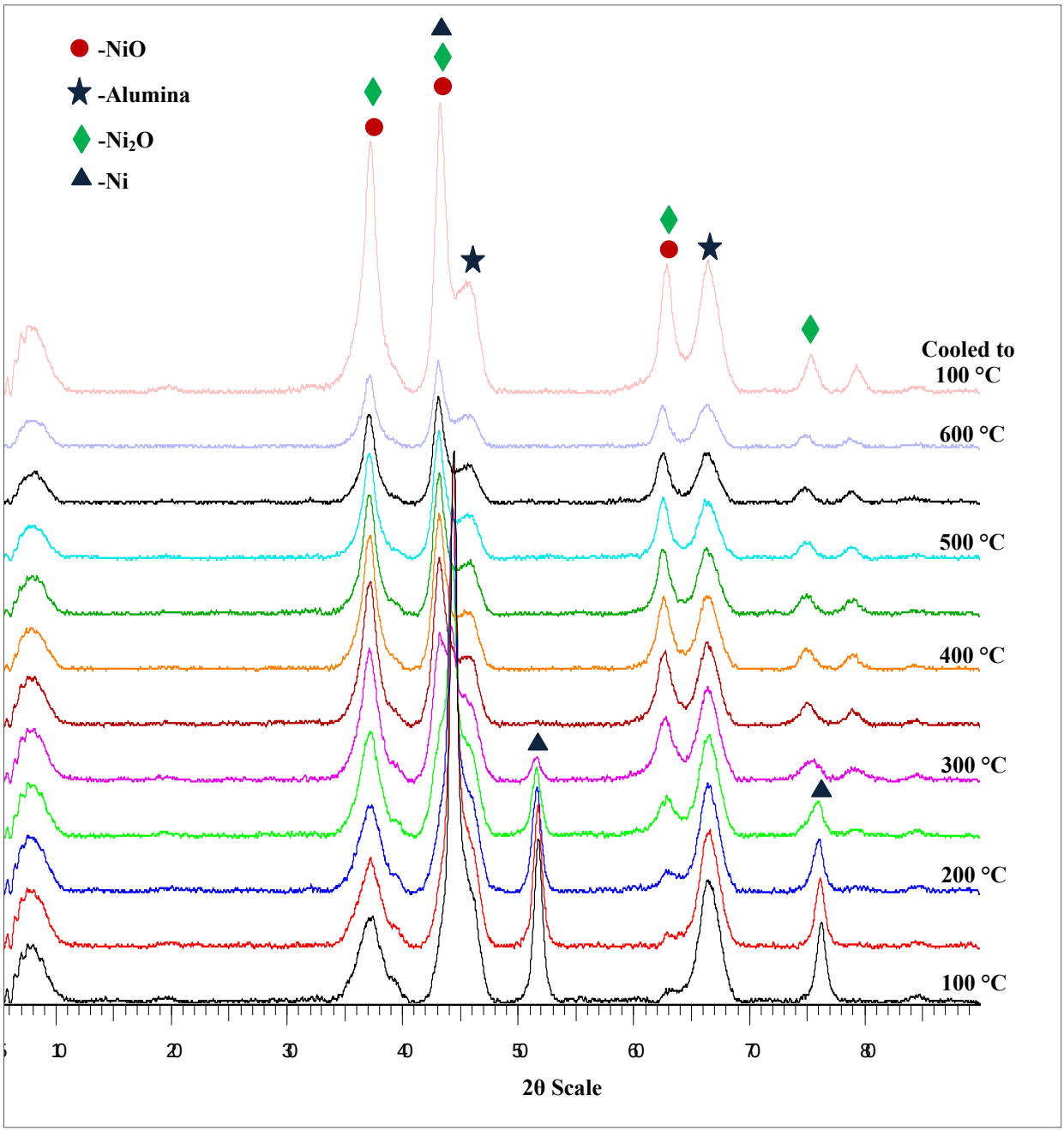

Figure 3.9: *In situ* XRD diffractogram of reduced Ni25 under an oxidizing atmosphere

The complete oxidation of Ni metal to NiO had occurred at about 400 °C and the Ni remained in its oxide form when cooled to the 100 °C. This *in situ* reduction and re-oxidation indicates that the Ni present on the catalyst can be reduced to its metallic form and be re-oxidized to form its oxide phase again, suggesting that the catalyst is stable under *redox* conditions and has reversible phase changes.

3.6.3 Temperature programmed NH_3 desorption

The TPD profiles of the NiO/Al_2O_3 catalysts are shown in Figure 3.10. Overall, the catalysts exhibit three types of acidic sites (Table 3.5), peaks from 350 °C to 450 °C are attributed to weak acidic sites, those from 450 °C to 550 °C are attributed to moderate acidic sites and those above 550 °C to strong acidic sites [6].

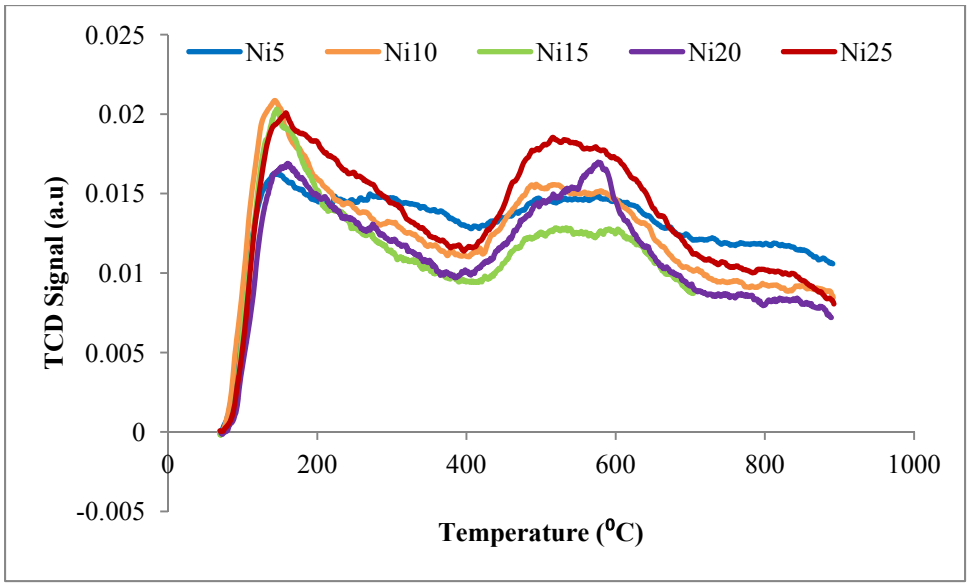

Figure 3.10: TPD profiles of the NiO/Al_2O_3 samples with different molar ratios of NiO

TPD results showed that NH_3 desorbed from Lewis acid sites when heated at 200 °C and from Brønsted acid sites of adsorbed NiO in the temperature range of 450-700 °C (Table 3.5). At higher NiO loadings, Lewis acidity of the catalyst remains unaffected with an increase in the Brønsted acidity. The various types of surface acidic sites were quantified by analysing the desorbed NH_3 and classified according to their desorption temperature. Weak, strong and some moderate acidic sites are attributed to the three peaks present in the TPD profile of the NiO/Al_2O_3 catalysts and the acidic sites on the catalyst increase as the NiO loading increases

(Table 3.5). Weak acidic sites are dominant in all catalysts. As NiO loadings increase the specific acidity of the catalyst also increases.

Table 3.5: Surface characterization of the NiO/Al_2O_3 catalysts

Catalyst	No. of acidic sites (mmol NH_3/g)			Total acidic sites (mmol NH_3/g)	Specific acidity (mmol/m^{-2})
	Weak	Moderate	Strong		
Al_2O_3	0.41	0.38	1.10	1.89	0.0084
Ni5	0.72	0.37	0.08	1.17	0.005
Ni10	1.45	1.17	0.56	3.18	0.015
Ni15	1.07	0.55	0.65	2.27	0.012
Ni20	1.48	0.82	0.23	2.53	0.014
Ni25	1.88	0.68	-	2.56	0.027

3.7 Raman Spectroscopic studies

Figure 3.11 depicts the Raman spectra of the NiO/Al_2O_3 catalysts which indicates that all the catalysts showed a fluorescence background giving rise to bands at 480 cm^{-1} and 810 cm^{-1} which are characteristic for pure γ-Al_2O_3 [7]. As the NiO loading increases there is no shift or evidence of new bands being formed. This is due to the overlapping of the characteristic NiO band with Al_2O_3 [7]. Raman bands at other wavelengths are difficult to observe due to the strong fluorescence radiation exhibited by the samples. The characteristic bands for the NiO could be observed at 510 cm^{-1} if the samples were exposed for longer time periods (4 h) under the laser.

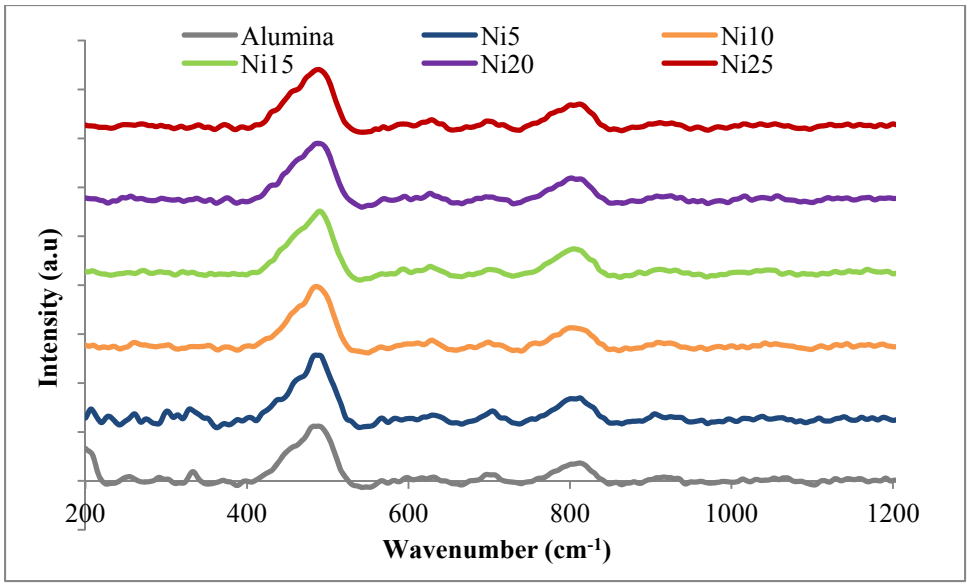

Figure 3.11: Raman spectra of the NiO/Al_2O_3

3.8 Microscopic studies

3.8.1 Scanning electron microscopy-energy dispersive X-ray

SEM images were used to study the surface morphology of the catalysts. Figure 3.12 shows the SEM images of the Ni/Al_2O_3 catalyst. From the figure it can be observed that Al_2O_3 particles (a) combine with each other and tend to form globules which were also mentioned by Kiss et al. [8]. These globules tend to comprise many primary particles with their dimensions being a few micrometers [8]. With regards to the NiO loaded samples (b-f), the surface morphologies of the catalysts tend to be a little rougher and particles are irregular and wrinkled. However, not much of a change in morphology can be observed with the impregnation of NiO of different molar ratios. According to Kiss et al. [8], for impregnated NiO/Al_2O_3 catalysts, the presense of the Al_2O_3 phase becomes invisible due to the NiO phase forming thin or thick shell-like formations around the Al_2O_3 particles. This "shell" catalyst can ensure maximum use of the active component and gives greater thermal stability of the catalyst sample [8].

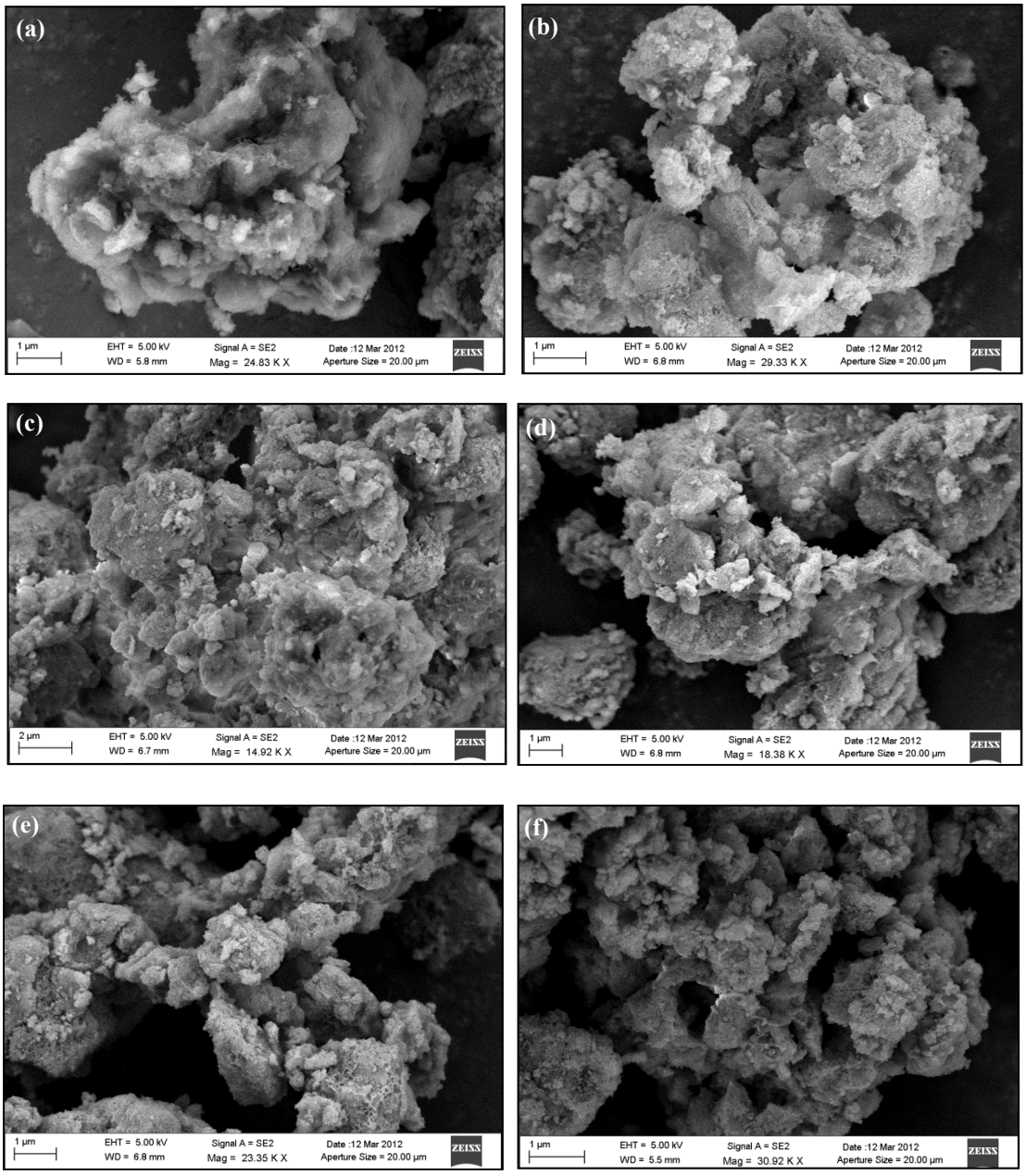

Figure 3.12: Scanning electron micrographs of the NiO/Al_2O_3 catalysts. (a) Al_2O_3, (b) Ni5 (c) Ni10 (d) Ni15 and (e) Ni20 and (f) Ni25

Samples of NiO on alumina with increasing weight percentages of NiO show an increase in crystalline nature and the growth of the particles is observed. This is also evidenced by the crystallite size determined in chemisorption experiments and the increase in the crystallinity was also observed by powder XRD. SEM-EDX mappings (Appendix C) show that NiO is well dispersed on the surface of the Al_2O_3 and the presence of the metals are also shown in the elemental mapping graphs.

3.8.2 Transmission electron microscopy

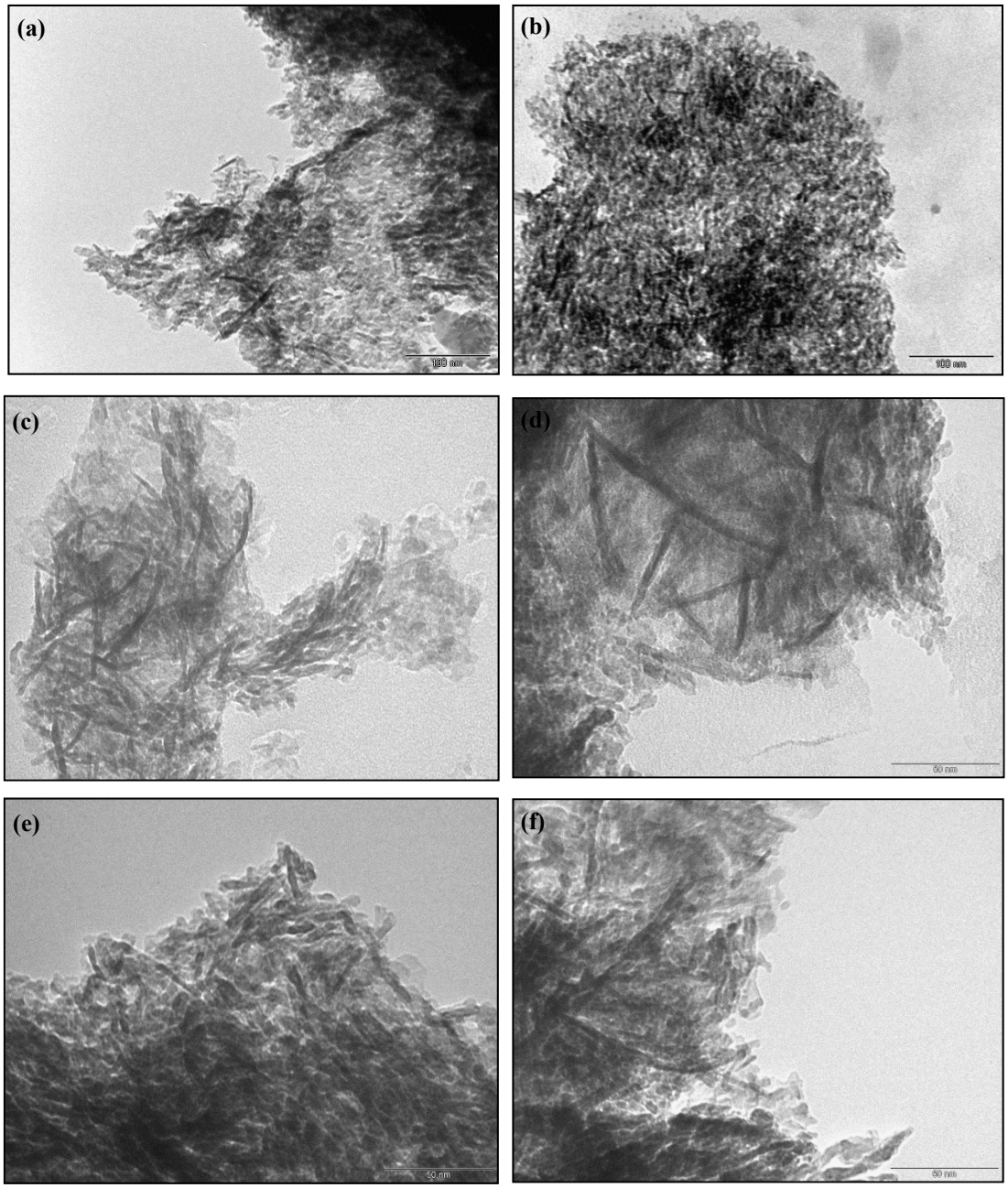

Figure 3.13: Transmission electron micrographs of the NiO/Al_2O_3 catalysts. (a) Al_2O_3, (b) Ni5 (c) Ni10 (d) Ni15 and (e) Ni20 and (f) Ni25

Figure 3.13 shows the TEM images of the NiO/Al_2O_3 catalyst samples. From these images it can be observed that the interface between the nickel particles (dark spots) and alumina support is

not well defined, however, it can be seen that the dispersion of nickel across the support was uniform. The morphology of the particles appears to be spherical and rod-shaped with minimum aggregation, which also relates closely to data obtained by Ghule et al. [9]. Figure 3.12 indicates that at low or no NiO loadings (a and b) almost no difference is seen between the Al_2O_3 and Ni5 samples, which may be attributed to the quasi-amorphous nature being displayed, due to NiO being well dispersed over the support. For catalyst samples (c- f) NiO particles are more distinctly pronounced and visible which can be attributed to the samples being more crystalline in nature, which corresponds to XRD and SEM data. The measured nickel particle sizes (diameter of the particle) had a range of 2-12 nm. These particle sizes are in agreement with the crystallite sizes calculated from the chemisorption experiments (Section 3.4). Particle size measurements are shown for the Ni5 and Ni25 in Appendix C.

References

[1] P. Salagre, J.L.G. Fierro, F. Medina, J.E. Sueiras, J. Mol. Catal. A: Chem. 106 (1996) 125-134.

[2] S.M. Morris, P.F. Fulvio, M. Jaroniec, J. Am. Chem. Soc. 130 (2008) 15210-15216.

[3] S. Ren, J. Qiu, C. Wang, B. Xu, Y. Fan, Y. Chen, Chin. J. Catal. 28 (2007) 651-656.

[4] B. Li, S. Kado, Y. Mukainakano, T. Miyazawa, T. Miyao, S. Naito, K. Okumura, K. Kunimori, K. Tomishige, J. Catal. 245 (2007) 144-155.

[5] C. Li, Y.-W. Chen, Thermochimica Acta. 256 (1995) 457-465.

[6] M.M. Khader, J. Mol. Catal. A: Chem. 104 (1995) 87-94.

[7] A. Aminzadeh, H. Sarikhani-fard, Spectrochimica Acta Part A: Mol. Biomol. Spectros. 55 (1999) 1421-1425.

[8] E. Kiss, G. Bošković, M. Lazić, G. Lomić, R. Marinković-Nedučin, Scanning. 28 (2006) 236-241.

[9] A.V. Ghule, K. Ghule, T. Punde, J.-Y. Liu, S.-H. Tzing, J.-Y. Chang, H. Chang, Y.-C. Ling, Mater. Chem. Phys. 119 (2010) 86-92.

CHAPTER 4

NiO/Al_2O_3 Catalytic testing

4.1 Testing of the test unit with a commercial catalyst

The test unit used for the catalytic reactions of this study was initially loaded with a commercial catalyst supplied by MINTEK. The AuTEK® catalyst (Au supported on TiO_2) was screened for PROX activity by adapting the methods from Galletti et al. [1], Walther et al. [2] and Yu et al. [3]. Galletti et al. [1] studied similar catalysts and reported maximum conversions in the temperature region below 80 °C. In contrast, the results obtained in this study, Figure 4.1, showed that at room temperature, the catalyst showed maximum CO conversion in the presence of H_2 and moderate selectivity towards the formation of CO_2. CO conversion of the catalyst was temperature dependant and decreased as temperature increased, which corresponds to literature [3], where maximum conversions reported were achieved at low temperatures.

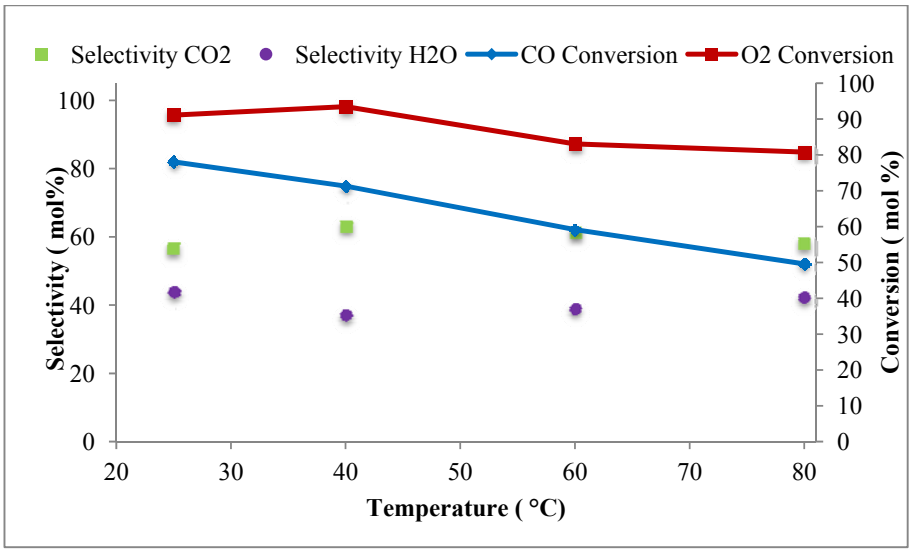

Figure 4.1: PROX reaction over the AuTEK® catalyst with a $C:O_2$ ratio of 1:0.5

The selectivity towards water at room temperature was lower than that to CO_2 and the selectivities remained fairly constant over the temperature range screened. This catalyst was thus found to be effective for the oxidation of CO in the presence of H_2 and didn't favour the undesired oxidation of H_2.

Thereafter the catalyst was pretreated under a stream of H_2 for 4 hours, and then subjected to a time on stream (TOS) experiment (Figure 4.2). Results indicated constant activity, for the PROX reaction, with regards to the conversion of CO. However, the selectivity towards CO_2 is considerably higher for this reaction. For the time on stream reaction the selectivity towards H_2O is lower than that of the initial PROX testing, showing that pre-reducing the catalyst was beneficial.

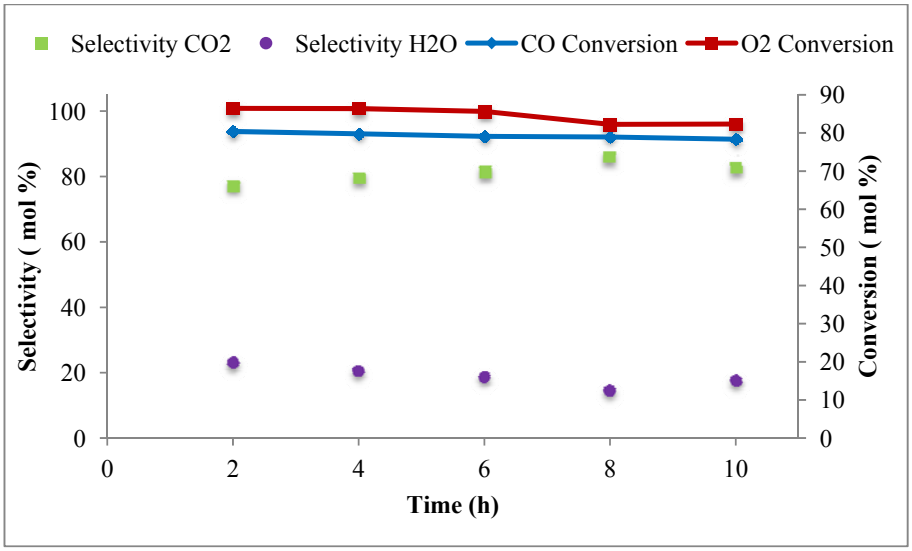

Figure 4.2: TOS PROX reaction over the AuTEK® catalyst at room temperature

From the results obtained from the AuTEK® catalyst, Figures 4.1 and 4.2, which also correspond closely to the literature reported on similar catalysts used in different system setups[1, 2], it was concluded that the reactor setup available was ideal and functioning for the catalytic testing of the catalysts prepared for this study.

4.2 Preliminary PROX reactions over Ni-Al_2O_3 catalysts

Preliminary testing of the mono-metallic NiO catalysts (Ni5 and Ni25) for PROX activity was then carried out. However, the catalysts were screened up to 290 °C, which is beyond the PROX range of room temperature to 250 °C. This was to determine if activity would increase for these catalysts at higher temperatures, since initial results showed low and constant conversion. This activity at higher temperatures would also give an indication if these catalysts are active for the CO oxidation reaction.

CO conversion and selectivity towards CO_2 for the catalysts tested under PROX conditions were attributed to the presence of the NiO metal particles on the surface of the alumina, since

the support alone showed no conversion and selectivity towards CO_2 in the temperature ranges screened.

Figure 4.3 shows the results from the PROX reaction using the mono-metallic Ni5 catalyst. From this it can be seen that from room temperature to 100 °C the catalyst is not active for the oxidation of CO. At 150 °C the selectivity towards H_2O dominates over the selectivity to CO_2. This result indicates that the catalyst favours the oxidation of H_2 rather than the oxidation of CO at low temperatures. CO conversion for this catalyst is only observed after 150 °C, where an increase in the selectivity towards CO_2 is also evident. CO conversion and selectivity towards the formation of CO_2 is temperature dependant for this reaction as both tend to increase with temperature after 150 °C. The selectivity towards H_2O decreases as temperature and CO conversion over the catalyst increase.

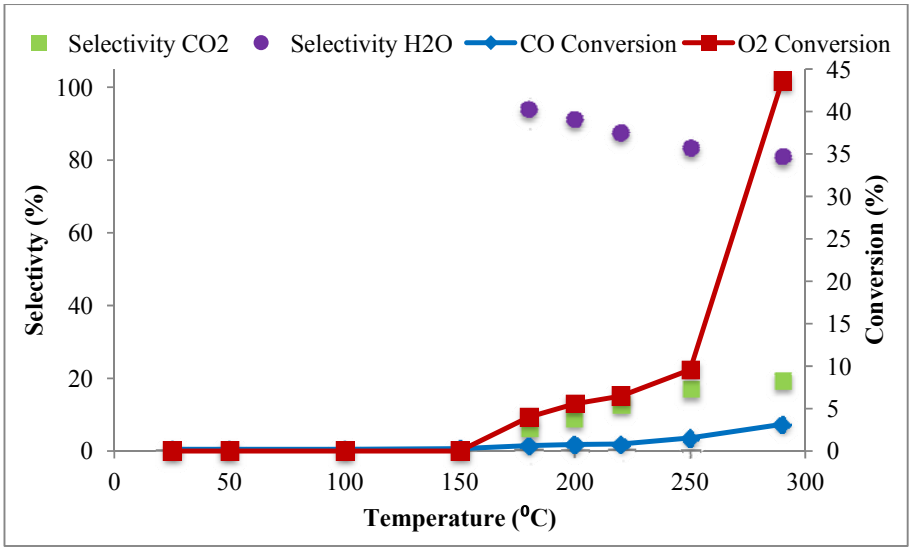

Figure 4.3: PROX reaction over the Ni5 catalyst with a C:O_2 ratio of 1:0.5

Selectivity towards CO_2 and the CO conversion over this catalyst was highest at 290 °C, with selectivity towards CO_2 of ± 20 % and a CO conversion of ± 3.5 %. Results obtained for the Ni5 thus showed poor activity towards the oxidation of CO in the presence of H_2 within the temperature range screened. This low CO conversion over this catalyst may be due to the low number of acidic sites (Section 3.6.3) and may also be due to the low metal dispersion (Section 3.4) observed. Accordingly, the surface area obtained for this catalyst was higher than those of the other NiO/Al_2O_3 catalysts, indicating that the amount of Ni active sites present on this catalyst could be very low and therefore this catalyst would not show good activity towards the oxidation of CO in the PROX range. CO chemisorption results for this

catalyst showed that the quantity of CO chemisorbed is much lower than found for the higher loaded catalysts (Section 3.4) and therefore it could be a possibility that in the presence of excess H_2 this catalyst is not chemisorbing CO efficiently, resulting in lower conversion of CO in the reaction, since this catalyst was also tested in its oxide form and not reduced prior to the reaction.

The tests showed that the catalyst indicated an increase in selectivity towards CO_2 and CO conversion may have been obtained at higher temperatures (above 290 °C), but that is far beyond the PROX temperature range. From the CO conversion results and chemisorption results (Section 3.4) obtained for this catalyst, it is clear that the conversion of CO is dependent on the metal dispersed and also the quantity of CO that can be chemisorbed on the support. Therefore, catalysts that had low metal dispersions and showed similar properties to the Ni5 catalyst, such as Ni10 and Ni15, were not considered for catalytic testing under PROX reaction conditions. With regards to the Ni20 and Ni25 materials, the Ni25 showed higher metal dispersions and quantities of CO chemisorbed (Section 3.4) and the reduction temperature of the catalyst was much higher compared to all the other catalysts (Section 3.6.1) characterized. Therefore, the Ni25 catalyst was tested instead of the intermediate Ni loaded catalysts.

Figure 4.4 shows the results for the PROX reaction using the mono-metallic Ni25 catalyst. The same trend is observed from room temperature to 100 °C as for the Ni5 catalyst, where the catalyst is not active for the oxidation of CO. At 150 °C the selectivity towards H_2O is at its highest, relative to the selectivity towards CO_2. This result of the selectivity towards H_2O dominating over the selectivity to CO_2 at very low CO conversions may be a result of the oxidation of H_2 being more favorable than the oxidation of CO at low temperatures for this catalyst.

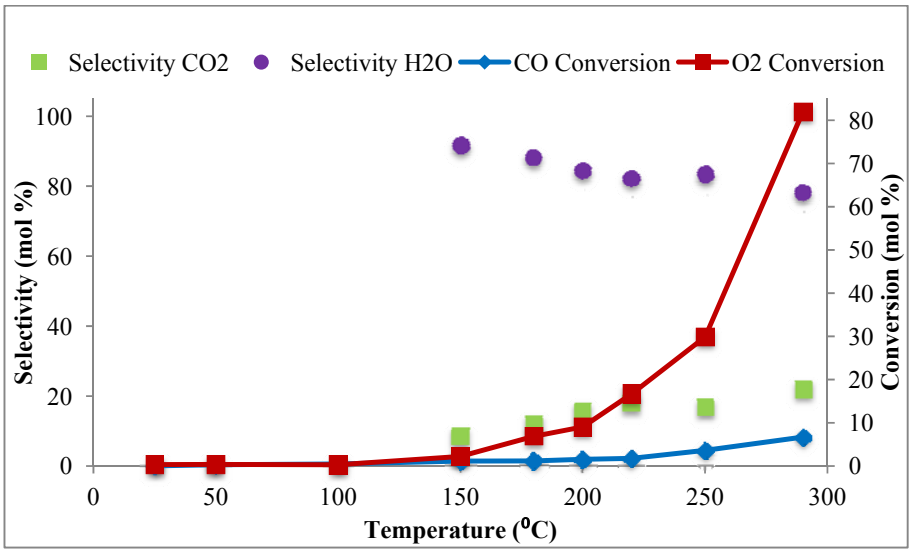

Figure 4.4: PROX reaction over the Ni25 catalyst with a C:O_2 ratio of 1:0.5

The selectivity towards H_2O for this catalyst decreases as CO conversion and temperature increase. CO conversion and selectivity for this catalyst was at its highest at 290 °C with a conversion of ± 6 % and selectivity towards CO_2 of ± 22 %. The reason for the slightly higher CO conversions over this catalyst when compared to Ni5 is likely due to the higher number of acidic sites (Section 3.6.3) present on the surface of the support and may also be due to higher metal dispersions (Section 3.4) obtained compared to all lower loaded Ni catalysts. The surface area obtained for this catalyst was much lower than that of the support and all of the other NiO/Al_2O_3 catalysts (Section 3.3), indicating that the amount of Ni active sites present on this catalyst was higher, therefore allowing more surface interactions to take place. CO chemisorption results for this catalyst indicated that the quantity of CO chemisorbed is much higher than on the other catalysts (Section 3.4), and therefore this catalyst showed slightly better activity for the CO oxidation reaction than the other catalyst (Ni5) synthesized.

Compared to the Ni5 catalyst, this catalyst also shows signs of improved selectivity towards CO_2 and CO conversions at temperatures beyond the PROX range. These results are also explained by the TPR (Section 3.6.1) where the reduction of the catalyst takes place at high temperatures (± 600 °C). This reduction of the catalysts could be evidence that the catalysts reduce to their metallic form and become more active at higher temperatures. This was confirmed by the XRD patterns of the spent catalyst. With regards to the Ni25, the degree of reducibility (Table 3.4) is much higher than for the Ni5 catalyst, and the amount of active

sites on the Ni25 catalyst, compared to the Ni5 catalyst, is higher. Also the metal dispersion is higher (Section 3.4) for the Ni25 catalyst, and these could be the reasons for the Ni25 showing slightly better activity. The Ni25 catalyst was therefore used for the remainder of catalytic testing on the NiO/Al_2O_3 mono-metallic systems.

4.3 CO oxidation reactions over the Ni25 catalyst

CO oxidation studies were performed using the Ni25 catalyst to determine the effects of O_2 in the reaction with regards to CO conversion. These studies were conducted under the same conditions as the PROX reaction but in the absence of H_2. Similar temperature ranges were investigated for the CO oxidation reactions as for the PROX reaction, from room temperature to 290 °C. Also, according to Wang and Lu [4], NiO catalysts are known to be more active for oxidation reactions at higher temperatures. Figures 4.5-4.7 show the results for the CO oxidation reactions over the Ni25 catalysts with varying $C:O_2$ ratios. From Figure 4.5, using a $C:O_2$ ratio of 1:0.5, it can be observed that the Ni25 catalyst is more active for the oxidation of CO in the absence of H_2. The activation temperature is similar to that for the PROX reactions, where the catalyst starts showing activity towards CO oxidation at 150 °C.

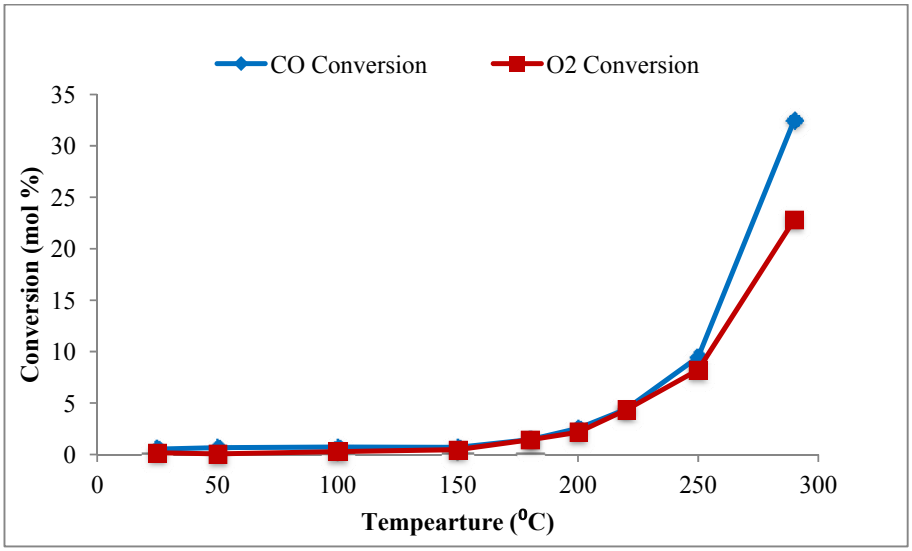

Figure 4.5: CO oxidation reaction over the Ni25 catalyst with a $C:O_2$ ratio of 1:0.5

However, compared to the PROX reaction (Figure 4.4) using the same $C:O_2$ ratio, the catalyst in the absence of H_2 shows much better activity and this is due to CO being a milder reducing agent than H_2. As the temperature increases from 150 °C, the CO conversion also increases. Maximum CO conversion obtained was ± 34 % at 290 °C and an O_2 conversion of 25 %.

Figure 4.6 shows the CO oxidation reaction using a C:O_2 ratio of 1:1. Similar to the previous reaction using a C:O_2 ratio of 1:0.5 (Figure 4.5), the increase of the O_2 content also indicates that the catalyst starts showing activity towards the oxidation of CO from around 150 °C. CO conversion increases as temperature increases and is similar to the 1:0.5 CO to O_2 oxidation reaction until 200 °C. After 200°C, the conversion of CO obtained is higher than observed for the reaction with a C:O_2 ratio of 1:0.5, with a maximum CO conversion of ± 39 % at 290 °C. The O_2 conversion for this reaction also increases as temperature and CO conversion increases, but is only about 20 % at maximum CO conversion.

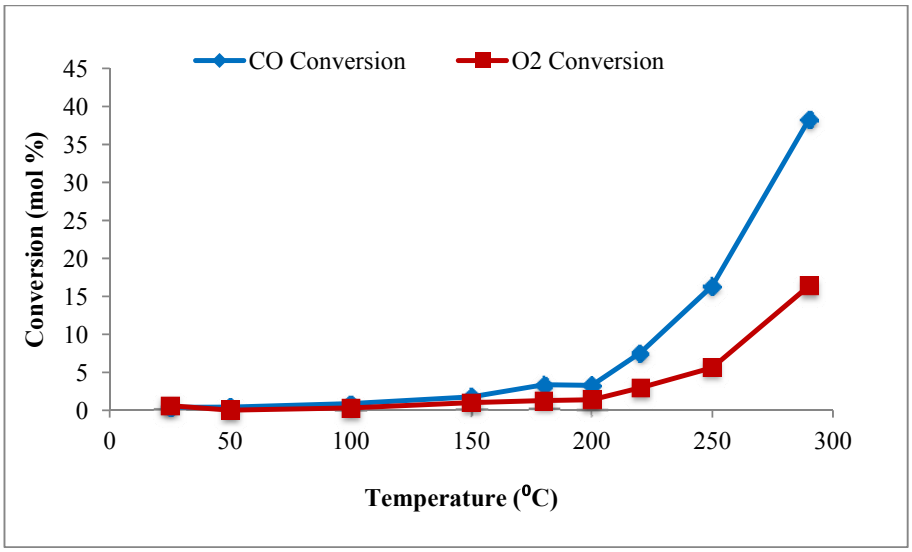

Figure 4.6: CO oxidation reaction over the Ni25 catalyst with a C:O_2 ratio of 1:1

Figure 4.7 shows the results of the CO oxidation reaction over the catalyst using a C:O_2 ratio of 1:2. The catalyst is also active from 150 °C, similar as found for the 1:0.5 and 1:1 C:O_2 ratios. CO conversion increases with temperature and the maximum conversion is obtained at 290 °C of ± 48 %. This increase in CO conversion is not very much higher than that seen for the other C:O_2 ratios investigated, but this catalyst could give higher conversions at temperatures beyond 290 °C, which is mentioned in literature by Wang and Lu [4], however, higher temperatures are not suitable for this study.

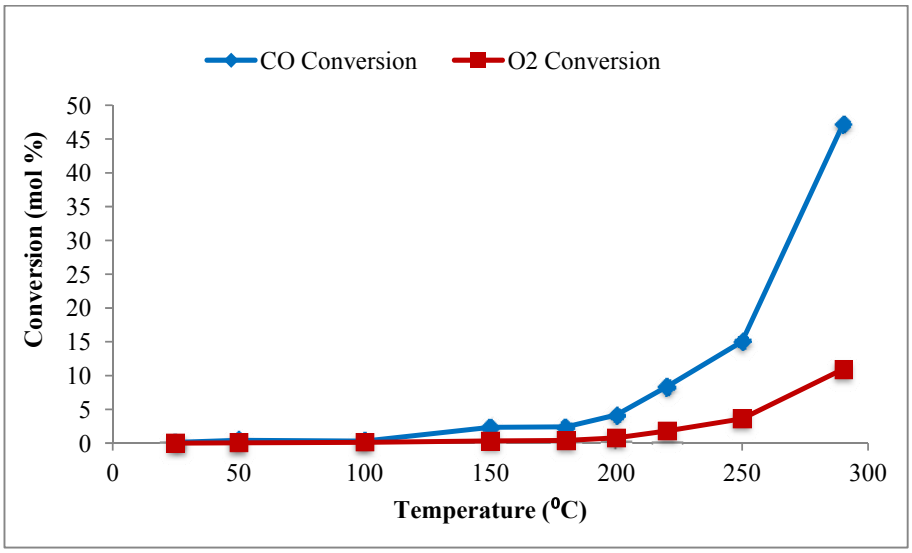

Figure 4.7: CO oxidation reaction over the Ni25 catalyst with a C:O_2 ratio of 1:2

O_2 conversions are much lower than found for the previous reactions (Figure 4.5 and 4.6), since the amount of O_2 present is now in excess to the stoichiometric carbon ratio, implying that the reaction is not O_2 limited. From the reaction (Eq. 4.1) it is observed that one mole of CO uses half a mole of O to produce CO_2.

$$CO + ½O_2 \rightarrow CO_2 \qquad (4.1)$$

Therefore using the stoichiometric ratio of C:O_2 could be a limiting factor during the PROX reaction, if the catalyst at higher temperatures is reducing to its metallic form and requires additional O_2 to re-oxidize. The CO oxidation reactions carried out confirm that this catalyst is active for the oxidation of CO in the absence of H_2 and further testing of the catalyst using different C:O_2 ratios in the PROX reaction were examined to determine the effect on CO conversion.

4.4 PROX Reactions using Ni25

The activity of the catalyst was investigated over 30 hours using a C:O_2 ratio of 1:0.5 at 150 °C. From Figure 4.8 it is observed that CO conversion and selectivity towards CO_2 are stable over this period. Slight fluctuations can be observed for the conversion of CO and the selectivity towards CO_2, but these are less than 2%. No decrease in the conversion and selectivity towards of CO_2 was observed during the time on stream (TOS) experiment.

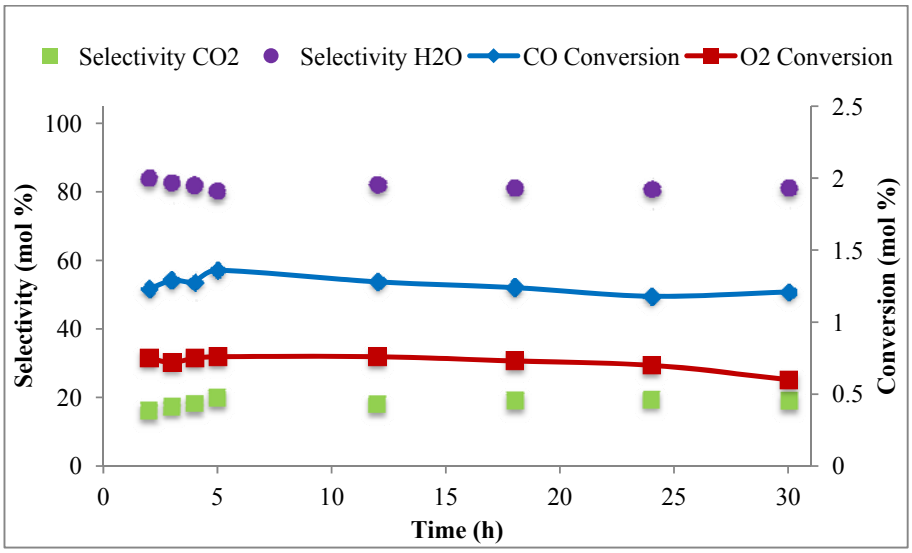

Figure 4.8: TOS PROX reaction over the Ni25 catalyst at 150 °C

Following the time on stream experiment, and from the CO oxidation reactions depicted in Figures 4.5-4.7, it is observed that Ni25 shows good activity for the oxidation of CO in the absence of H_2, where the highest conversion of CO was obtained using a C:O_2 ratio of 1:2. Therefore, it was decided to carry out a PROX reaction using the same ratio of 1:2.

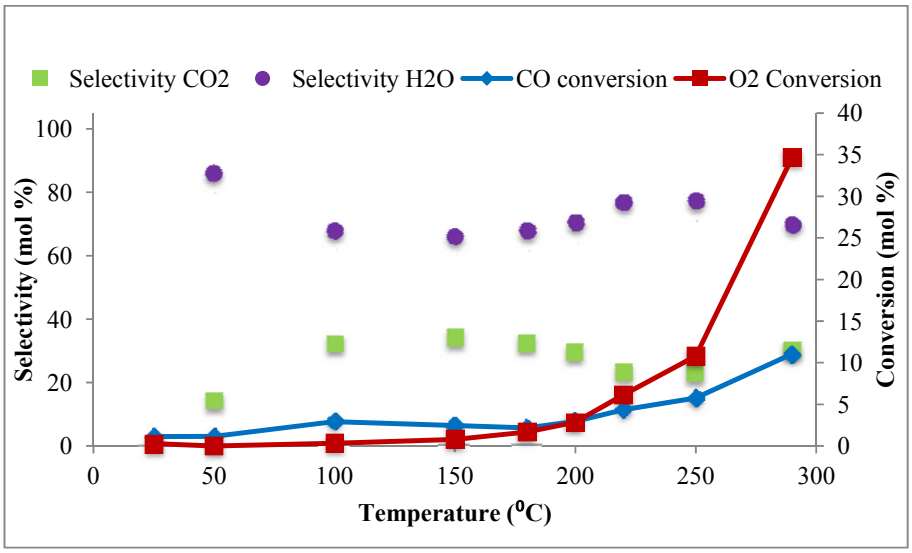

Figure 4.9: PROX reaction over the Ni25 catalyst with a C:O_2 ratio of 1:2

Figure 4.9 shows the results of the PROX reaction of the Ni25 catalyst using the C:O_2 ratio of 1:2, and from this it can be seen that the CO and O_2 conversion followed a similar general trend as for the CO oxidation reactions. As the temperature increases the conversion of CO

increases and the O_2 conversion also increases with increasing CO conversion. However, compared to the PROX reaction (Figure 4.4) using an O_2 ratio of 0.5, here the O_2 conversion is much lower and clearly the reaction is not O_2 limited. This result also shows slightly higher CO conversions at most of the temperatures investigated. The conversion of CO and the selectivity towards CO_2 are greater than the conversion and selectivities obtained for the PROX reaction (Figure 4.4) using an O_2 ratio of 0.5. Therefore it is evident that the Ni25 catalyst was slightly more active in the PROX reaction using the C:O_2 ratio of 1:2. Compared to the CO oxidation reactions, the CO conversion in the presence of H_2 is much lower, with maximum conversion being obtained at 290 °C of ± 11 %. This also is beyond the PROX temperature range and therefore a PGM metal that is active for the PROX reaction could supplement this catalyst in terms of activity and selectivity. This will be discussed in the chapter that follows.

Following all reactions carried out over the catalysts, conversion and selectivity measurements were also taken whilst the reactor was cooling, at two temperatures. All catalysts showed similar conversions at similar temperatures (e.g. heating to 150 °C and cooling to 150 °C) with an error difference of ± 5 %.

All catalysts were calcined in-situ at 300 °C for 4 hours prior to the next reaction under a positive flow of air. Upon heating for the next reaction, catalysts were screened at a temperature of 150 °C to determine if catalyst was active with a similar CO conversion and selectivity towards CO_2. The majority of the reactions carried out in this section were done with the Ni25 catalyst, which showed very good stability and reproducibility, and it was re-used for all the reactions.

4.5 Used NiO/Al_2O_3 catalyst characterization

From Table 4.1 it can be observed that with regards to the surface properties of the catalyst, the surface areas, pore volumes and pore diameters of the used Ni5 and Ni25 catalysts removed from the reactor tubes show decreases compared to those shown in Table 3.2 (Section 3.3). Results shown are consistent, where decreases in the surface areas are accompanied by decreases in the pore volumes and, with regards to the pore diameter, the catalysts lose porosity when the surface areas decrease [5].

Table 4.1: Surface characterization of the used NiO/Al_2O_3 catalysts

Catalyst	Surface area (m^2/g)	Pore volume (cm^3/g)	Pore diameter (Å)
Ni5	195	0.50	108
Ni25	164	0.42	91

XRD patterns of the used catalysts are depicted in Figure 4.10 where no new phase changes can be observed for the catalysts compared to the fresh catalysts discussed in Section 3.5. During catalytic reactions, the catalysts showed no signs of reduction, since O_2 balances were constant (± 95-101 %) and showed no decreases.

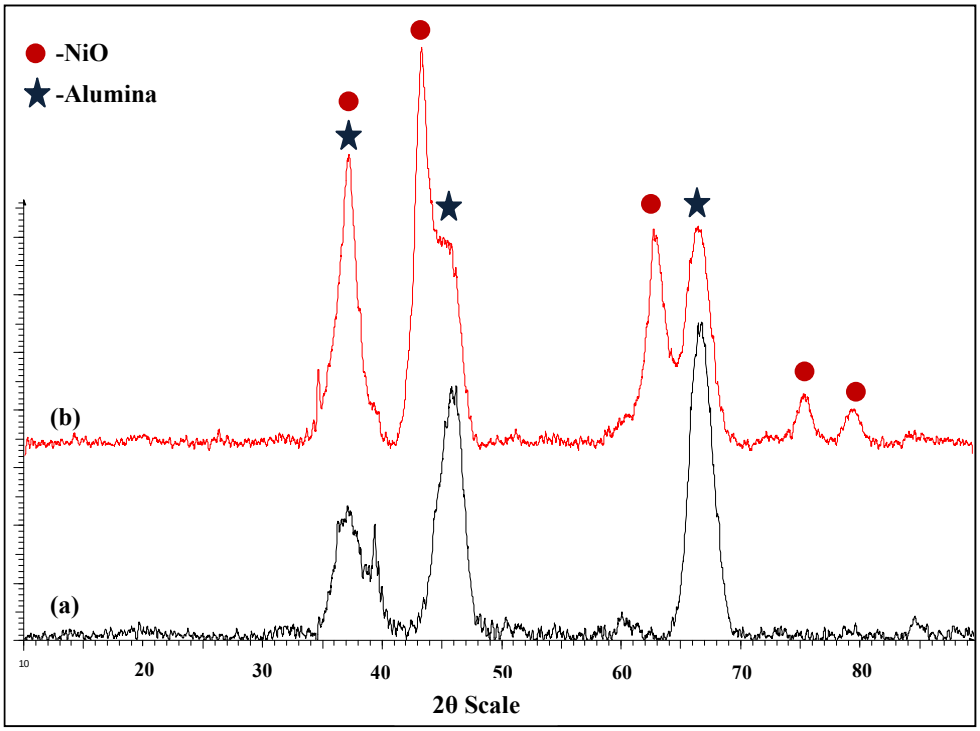

Figure 4.10: XRD diffractograms of used (a) Ni5 and (b) Ni25

Also the Mars and van Krevelan mechanism (Figure 4.11) proposes that the reactant, in this case CO, extracts lattice O_2 from the surface layers of the catalysts, thereby reducing them [6]. This lattice O_2 is then replenished by O_2 from the feed during the re-oxidation process [6]. This reaction could also be coupled with the Eley-Rideal mechanism (Figure 4.11),

which explains that CO not residing on the catalyst surface long enough to define the physisorbed state, can interact with an adsorbed O_2 species to form CO_2 [6].

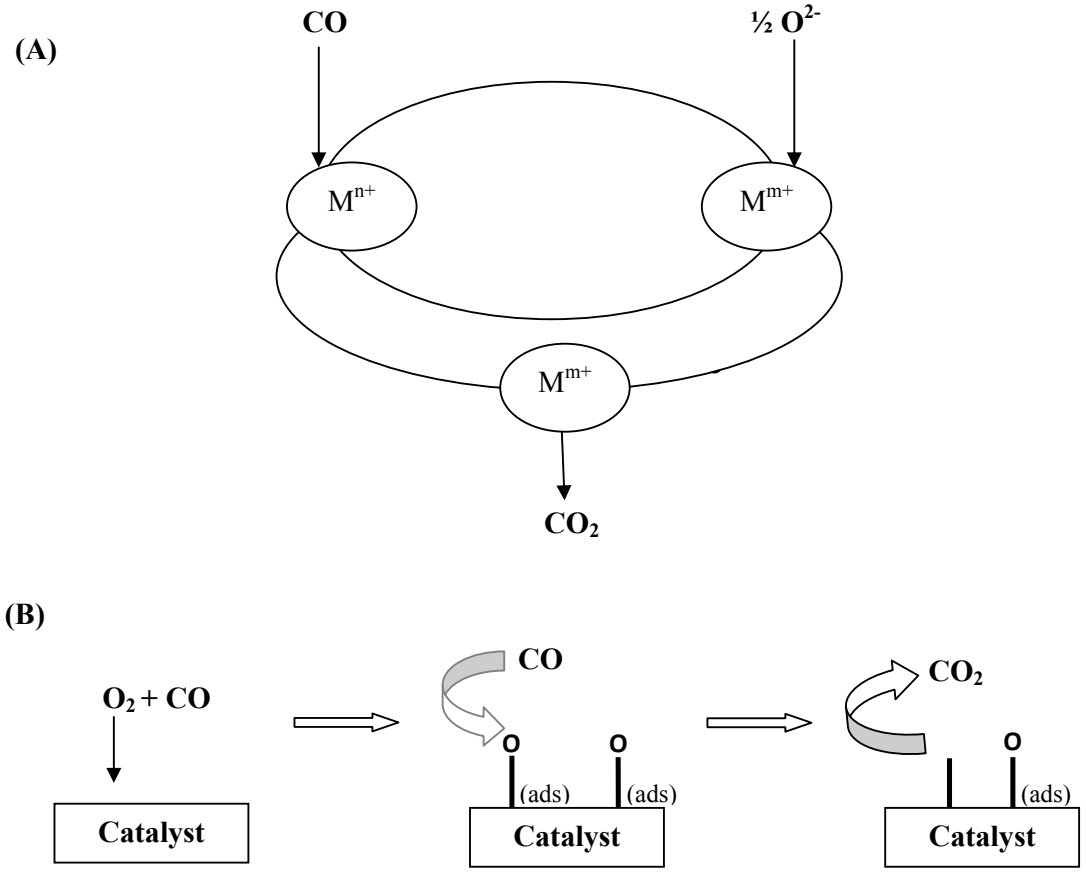

Figure 4.11: Schematic diagram of (A) Mars and van Krevelan oxidation-reduction mechanism (n, m = oxidation states and M = metal) and (B) the Eley-Rideal mechanism

References

[1] C. Galletti, S. Fiorot, S. Specchia, G. Saracco, V. Specchia, Chem. Eng. J. 134 (2007) 45-50.

[2] G. Walther, D.J. Mowbray, T. Jiang, G. Jones, S. Jensen, U.J. Quaade, S. Horch, J. Catal. 260 (2008) 86-92.

[3] W.-Y. Yu, W.-S. Lee, C.-P. Yang, B.-Z. Wan, J. Chin. Inst. of Chem. Eng. 38 (2007) 151-160.

[4] S. Wang, G.Q. Lu, Appl. Catal. A: Gen. 169 (1998) 271-280.

[5] E. Elkhalifa, H. Friedrich, Catal. Lett. 141 (2011) 554-564.

[6] B.K. Hodnett, Heterogeneous catalytic oxidation: fundamental and technological aspects of the selective and total oxidation of organic compounds, John Wiley and Sons, New York, 2000.

CHAPTER 5

Supported Pt Systems

5.1 Inductively coupled plasma – Optical emission spectroscopy

The presence of platinum on the alumina support and the NiO/Al_2O_3 material was quantitatively determined by ICP-OES. From Table 5.1 it can be observed that the weight percentages of metal obtained were similar to the nominal weight loadings. However, with the $Pt/NiO/Al_2O_3$ (Pt-Ni-Al) catalyst a slightly lower percentage of Ni was obtained.

Table 5.1: ICP-OES results for the supported Pt catalysts

Catalyst	Nominal weight (%)		Weight (%) (From ICP)	
	Pt	Ni	Pt	Ni
Pt-Al	0.5	-	0.45	-
Pt-Ni-Al	0.5	25	0.56	21

5.2 Physisorption methods

Nitrogen adsorption-desorption isotherms for the supported Pt catalysts are shown in Figure 5.1. Both catalysts show typical type IV isotherms in the classification of Brunauer, Deming, Deming and Teller (BDDT) [1], with H1 hysteresis loops which are characteristic for mesoporous materials [2]. From the figure it can be seen that the steepness of the capillary condensation steps clearly indicate uniformity of mesopores. The condensation steps for both isotherms are within the same relative pressure ranges and no drastic decrease in the steepness of the capillary condensation is observed. For the mono-metallic Pt/Al_2O_3 (Pt-Al) material, however, the adsorption isotherm has a steep condensation step, and according to Morris et al. [2] these will represent narrow distributions for the corresponding PSD curves generated.

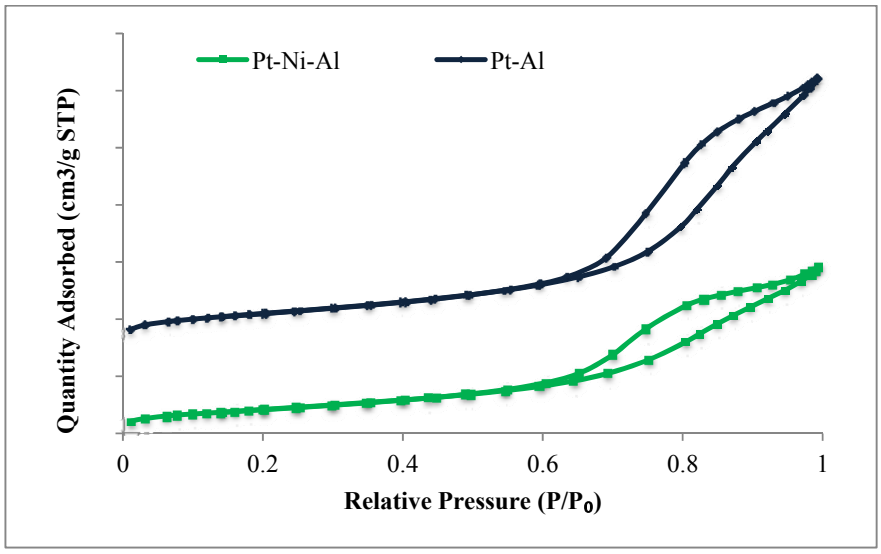

Figure 5.1: Adsorption isotherms of the supported Pt catalysts

This is evident from the PSD graphs generated in Figure 5.2. With regards to the bi-metallic Pt-Ni-Al material, however, isotherms generated indicate broader condensation steps which will therefore generate broader PSD's. This is evident from the PSD graphs plotted in Figure 5.2.

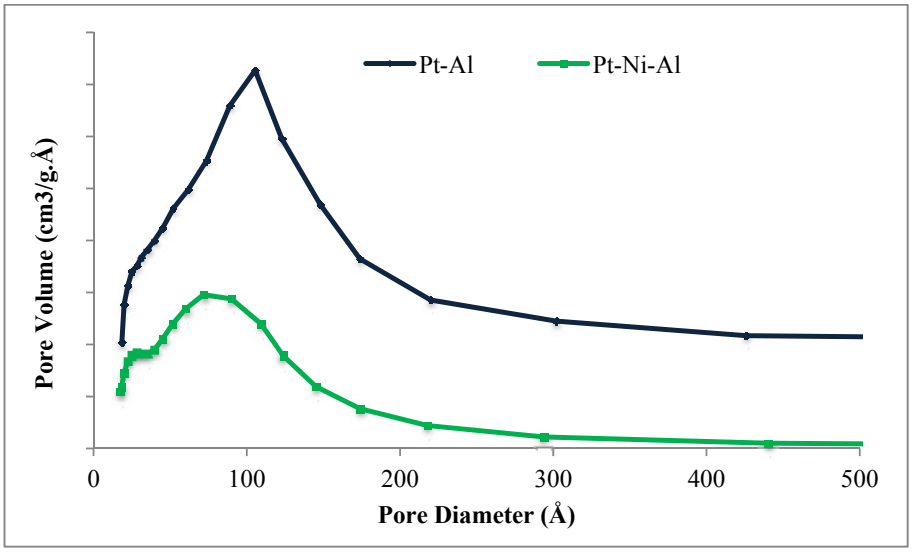

Figure 5.2: Pore size distributions of the supported Pt samples

From Table 5.2 it can be observed that after the impregnation of Pt onto the support as well as onto the mono-metallic Ni25 catalyst, the surface areas and the pore volumes decrease compared to the Al_2O_3 support and the mono metallic Ni25 catalyst. Pore diameters, however, tend to show a slight increase, which may be due to the additive effect of Pt by the

impregnation method. According to Li et al. [3] this increase of pore diameter is due to the tendency of the Pt atoms to be more preferably located on the surface of the supports and Pt-Ni alloys may form.

Table 5.2: Surface characterization of the supported Pt catalysts

Catalyst	Surface Area (m^2/g)	Pore Volume (cm^3/g)	Pore Diameter (Å)
Alumina	225	0.78	127.6
Pt-Al	207	0.70	128.1
Pt-Ni-Al	156	0.43	110.3

5.3 CO Chemisorption

The metal dispersions and crystallite sizes of the Pt on the surfaces of the alumina support and the mono-metallic Ni25 catalyst were determined by chemisorption using CO as the adsorbate. Metal dispersions were calculated from the CO adsorption data using a stoichiometric ratio of 1 for Pt:CO. The CO adsorption plots generated are shown in Figure 5.3, where it can be seen that with an increase in pressure, the amount of CO chemisorbed on the surface of the Pt-Ni-Al catalysts increases. However, the amount of CO chemisorbed on the mono-metallic Pt-Al catalyst seems to be constant with no evident increase. Zhi-Min et al. [4] compared the amount of CO adsorbed on two 5% Pt/Al_2O_3 catalysts, both reduced by different reducing agents. Results indicated that the catalysts that reduced almost completely showed better CO adsorption; also the dispersion of the Pt particles was effected by degree of reduction for the uniform dispersion of the metal. In this study (this dissertation) 0.5 % Pt was employed and reduced for a short period of time prior to the experiment. Since the Pt particles present in the material were well dispersed for this catalyst, it therefore showed a lower CO adsorption. The Pt-Ni-Al material, however, showed better CO adsorption to the mono-metallic Pt-Al, but this was relatively similar compared to the mono-metallic Ni25 (Section 3.4) which was highest in the Ni series. This suggests that the amount of metal content on the surface of the support provides better CO adsorption for the catalyst.

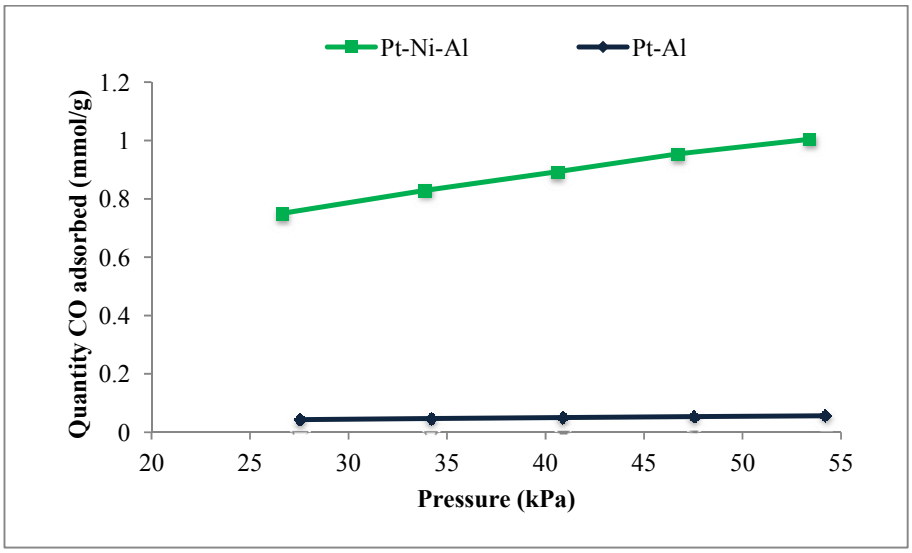

Figure 5.3: CO chemisorption profiles of the supported Pt catalyst

The metal dispersions determined for both supported Pt catalysts are shown in Table 5.3. From this it can be seen that the mono-metallic Pt-Al catalyst has a higher metal dispersion of 39 % as compared to the Pt-Ni-Al catalyst with a metal dispersion of 14 %. This result of the Pt-Ni-Al catalyst which showed a lower percentage dispersion, could be due to the Pt atoms alloying with the Ni particles present on the support following the impregnation [3]. Also, surface characterization results obtained, shown in Table 5.2 for the Pt-Ni-Al catalyst, compared to the mono-metallic Ni25 catalyst, shown in Table 3.2 (Section 3.3), indicates that after Pt impregnation the pore volume and pore diameter for the catalyst increases slightly, while only the surface area decreases. This is evidence that the Pt atoms are not occupying the pores in the support but are preferably located on the surface instead.

Table 5.3: Metal dispersions and crystallite sizes of the supported Pt catalysts

Catalyst	Metal Dispersion (%)	Crystallite Size (nm)
Pt-Al	39	3
Pt-Ni-Al	14	7

Crystallite sizes for the catalyst depicted in Table 5.3 show that for the mono-metallic Pt catalyst the size is 3 nm and that for the Pt-Ni-Al catalyst is 7 nm. Mono-metallic Ni25 had a crystallite size of 5 nm (Section 3.4) and after impregnation of Pt on this catalyst, the

crystallite size increased to 7 nm. This result could be due to Pt-Ni alloys forming that give rise to slightly larger crystallites [3].

5.4 Powder XRD diffraction

The stacked X-ray diffractograms of the supported Pt catalysts are presented in Figure 5.4. The diffraction pattern of Pt-Ni-Al (a) indicates the existence of both NiO and Al_2O_3 (γ-Al_2O_3) phases. The Al_2O_3 characteristic peaks are observed at 2θ values of 37.18°, 45.36° and 66.71° with the corresponding d spacings of 2.39, 1.97 and 1.52, respectively, for both catalysts. These d spacings correspond to those of the JCPDS file no: 10-425. For the NiO phases, peaks at 2θ values of 37.18°, 45.36° and 66.71° with the corresponding d spacings, corresponding to JCPDS file no: 4-0835, of 2.41, 1.25 and 1.47 respectively.

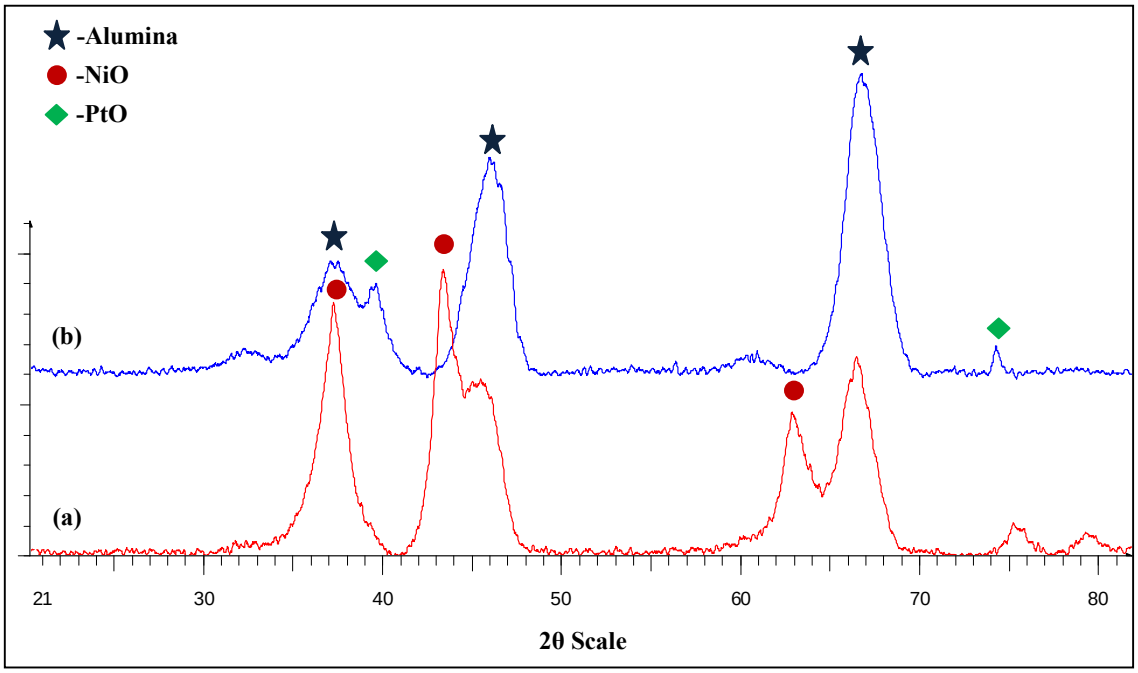

Figure 5.4: XRD diffractograms of the (a) Pt-Ni-Al and (b) Pt-Al catalysts

For both samples containing Pt, peaks are at 2θ values of 39.3° and 74.27° with the corresponding d spacings of 2.28, and 1.27 respectively. These are characteristic of the PtO phases that correspond to ICDD file no's: 010841439 and 010732359.

5.5 Temperature programmed studies

5.5.1 Reduction

Figure 5.5 shows the temperature programmed reduction profiles of the supported Pt samples. For the mono-metallic Pt-Al catalyst a broad reduction peak is observed at around 330 °C, which can be assigned to the reduction of platinum oxide to its metallic form [5]. As can be seen from the figure there is a pronounced influence following Pt addition on the NiO reduction temperature for the Pt-Ni-Al sample. This reduction temperature shifting to lower temperatures is attributed mainly to the change in mechanism of the NiO reduction [3, 5, 6].

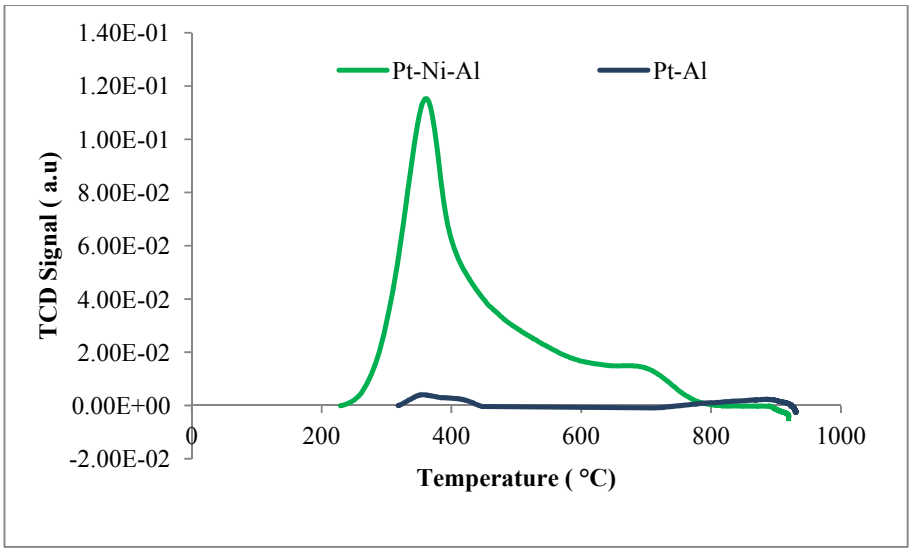

Figure 5.5: TPR profiles of the supported Pt catalysts

De Souza et al. [6] mentioned that the reduction of Pt oxide previous to reduction of the Ni oxides results in the formation of Pt^0 sites that are essentially available to activate H_2 to atomic $H^{\bullet}$ at much lower temperatures compared to that required for H_2 activation on NiO. The surface of the NiO then receives this transferred $H^{\bullet}$ through a spillover mechanism, reducing the NiO to Ni^0 at lower temperatures. This mechanism suggests that the nucleation of the Ni^0 is controlled by the activation of H_2. The shoulder peak observed in the TPR of Pt-Ni-Al at higher temperatures is attributed to the NiO species that are still interacting strongly with the support [6, 7]. From Table 5.4 it can be seen that the hydrogen consumption and degree of reducibility is higher for the Pt-Ni-Al catalyst compared to the mono-metallic Pt-Al catalyst. Also this higher consumption of H_2 is attributed to the presence of the NiO also present in the Pt-Ni-Al catalyst, which now reduces at lower temperatures due to the

association of strong metal-metal oxide interactions between the Pt and Ni particles on the surface of the support [8].

Table 5.4: TPR data obtained for the supported Pt catalysts

Catalyst	Temperature (°C)	H_2 consumption (cm^3/g)	Degree of reducibility (%)
Pt-Al	330	6.0	3.9
Pt-Ni-Al	330	64.1	71.0
	587	19.0	13.0

To investigate the phase changes occurring on the Pt-Ni-Al catalyst under a reducing atmosphere, *in situ* XRD was carried out under similar conditions to those used for the mono-metallic Ni25 catalyst (Section 3.6.1). Figure 5.6 shows the *in situ* diffractograms under a reducing atmosphere.

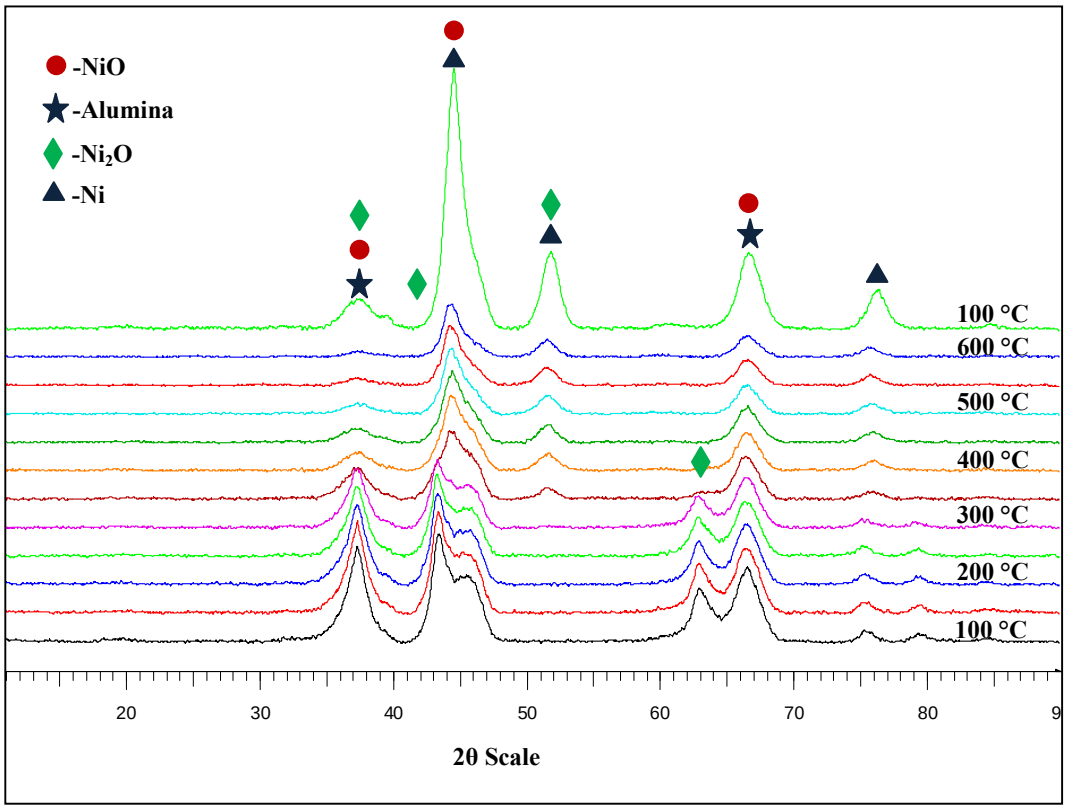

Figure 5.6: *In situ* XRD diffractograms of the Pt-Ni-Al catalyst under a reducing atmosphere

No observable change is seen with regards to the crystallite size or crystallinity of the catalyst within the temperature region of 100-300 °C, indicating that the catalyst is stable up to 300 °C under this reducing environment. However, compared to the mono-metallic Ni25 catalyst, this catalyst starts reducing now from ±350 °C, suggesting that the impregnation of Pt promotes NiO reduction which was also evident from the TPR profile of the catalyst. From the *in situ* XRD diffractograms, the phases of NiO, Ni_2O and Ni metal are observed within the temperature region 350-600 °C, which shows the reduction pathway of NiO similar to that of the mono-metallic Ni25 catalyst. These phases are confirmed with the ICDD file nos: 010870712 (Ni), 010721464 (Ni_2O) and 010780429 (NiO) with peaks at 2θ values of 44.53°, 51.83° 62.79° and 76.73°, with the corresponding d spacings of 2.03, 1.76, 1.47 and 1.24 respectively. The complete reduction of NiO to Ni occurred at a temperature of 600 °C and the Ni remained in its metallic form when cooled to 100 °C. The presence of the Pt phases on the Pt-Ni-Al catalyst cannot be clearly seen due to the loading of Pt being so low, and according to Li et al. [3], Pt binds to the Ni particles present on the support and forms alloys and therefore will not be clearly identified by XRD. Also the metal dispersions from the chemisorption results obtained show that mono-metallic Pt-Al has a higher metal dispersion on the support, whereas the dispersion of the Pt-Ni-Al is slightly lower compared to that of the mono-metallic Ni25 catalyst (Section 3.4). If Pt had interacted with the surface of the support of the mono-metallic Ni25 catalyst it would show an increase in the metal dispersion, which is clearly not the case.

5.5.2 Oxidation

In order to investigate the oxidizing capacity of the Pt-Ni-Al catalyst in its metallic form following its reduction after *in situ* XRD under H_2, an *in situ* XRD oxidation experiment was conducted similarly as for the mono-metallic Ni25 catalyst as described in Section 3.6.2. Figure 5.7 shows the *in situ* XRD diffractograms of the initially reduced Pt-Ni-Al catalyst under an oxidizing atomosphere. From the *in situ* XRD diffractograms it is evident that Ni remains in its metallic form until 200 °C. The transformation of the Ni metal back to the NiO phase takes place within the temperature range of 100-250 °C suggesting that the impregnation of Pt on the mono-metallic Ni25 catalyst also promotes its oxidation, lowering the temperature for this by 100 °C. The transformation also follows the inverse path way to the reduction which is shown below:

$$Ni^0 \rightarrow Ni^{1+} \rightarrow Ni^{2+}$$

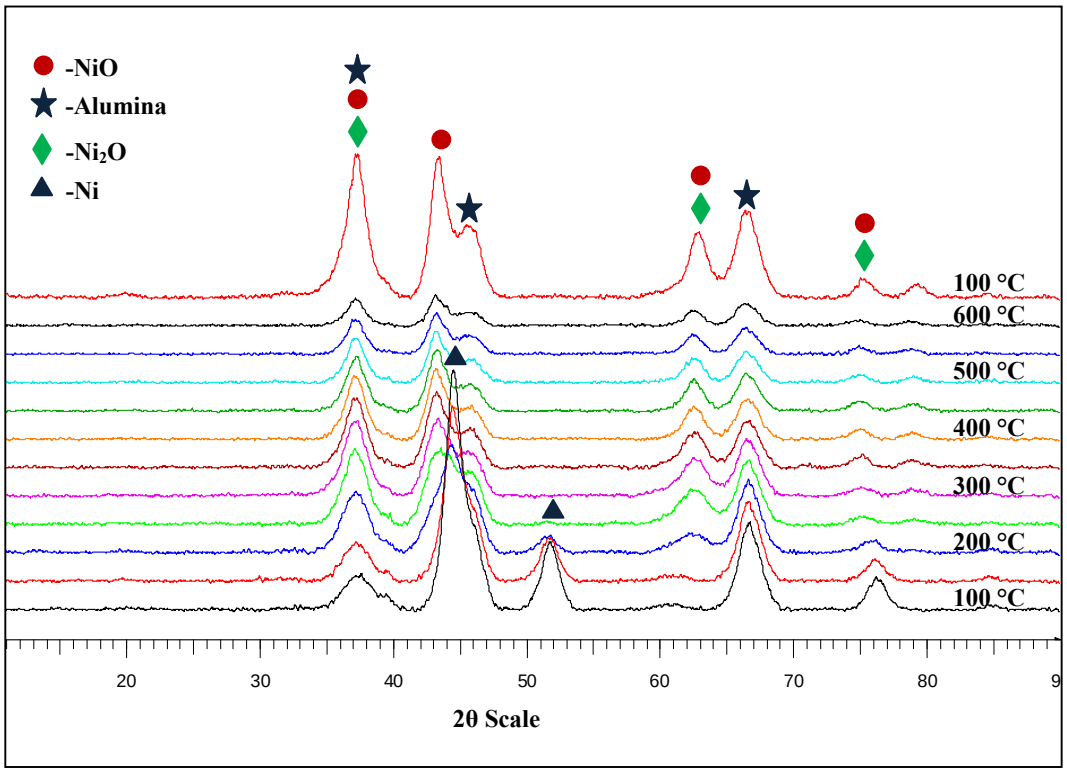

Figure 5.7: *In situ* XRD diffractograms of the reduced Pt-Ni-Al catalyst under an oxidizing atmosphere

This transformation of the Ni metal to the NiO phase via the intermediate Ni_2O phase is evident from the following ICDD file nos: 010870712 (Ni), 010721464 (Ni_2O) and 010780429 (NiO). The characteristic peaks of Ni, NiO and its intermediate Ni_2O phases are now within the temperature region of 100-200 °C. The complete oxidation of Ni metal to NiO occurs at about 250 °C and the Ni remained in its oxide form when cooled back to 100 °C. This *in situ* reduction and re-oxidation indicates that the catalyst can be reduced to its metallic form and then be re-oxidized to form its oxide phase at lower temperatures compared to the mono-metallic Ni25 catalyst, suggesting that this catalyst is also stable under *redox* conditions and undergoes reversible phase changes.

5.5.3 Temperature programmed NH_3 desorption

The TPD profiles of the supported Pt catalysts are shown in Figure 5.8. Both Pt containing catalysts exhibit three types of acidic sites (Table 5.5), peaks from 350 °C to 450 °C are attributed to weak acidic sites, those from 450 °C to 550 °C are attributed to moderate acidic sites and those above 550 °C to strong acidic sites [9]. TPD results showed that NH_3 desorbed

from Lewis acid sites when heated at around 200 °C and from Brønsted acid sites of NiO in the Pt-Ni-Al catalyst within the temperature range of 450-700 °C (Table 3.5).

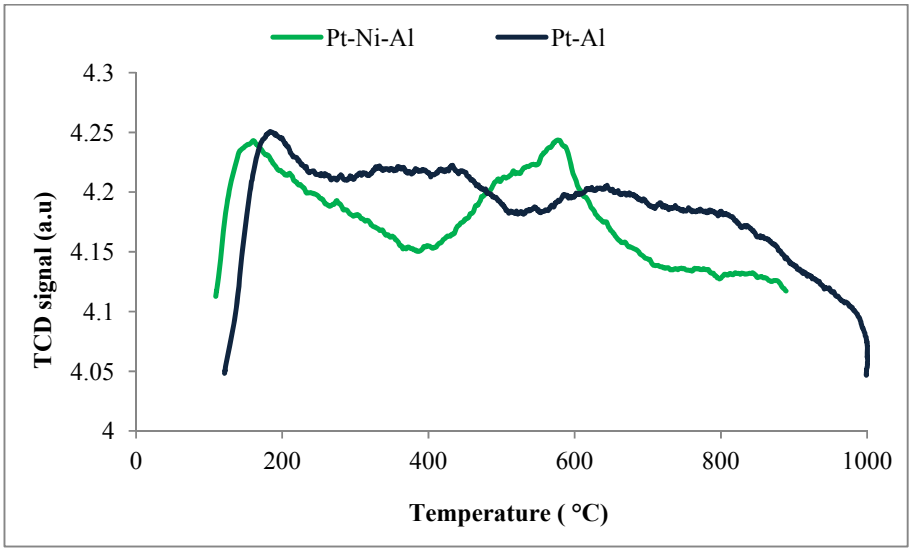

Figure 5.8: TPD profiles of the supported Pt catalysts

The various types of surface acidic sites were quantified by analysing the desorbed NH_3 and classified according to their desorption temperatures. Weak, moderate and strong acidic sites are attributed to the three peaks present in the TPD profile of the supported Pt catalysts, and the number of acidic sites on the bi-metallic Pt-Ni-Al catalyst is higher (Table 3.5). This is due to the presence of the NiO particles which contribute to the acidic sites present in the material. Therefore, the specific acidity of the Pt-Ni-Al catalysts is higher than the mono-metallic Pt-Al and the mono-metallic Ni25 catalyst (Section 3.6.3).

Table 5.5: Surface characterization of the supported Pt catalysts

Catalyst	No. of acidic sites (mmol NH_3/g)			Total acidic sites (mmol NH_3/g)	Specific acidity (mmol/m^{-2})
	Weak	Moderate	Strong		
Pt-Al	0.68	0.38	1.14	2.2	0.0106
Pt-Ni-Al	1.97	0.72	0.41	3.1	0.0199

5.6 Microscopic studies

5.6.1 Scanning electron microscopy-energy dispersive X-ray

The surface morphology of the Pt catalysts are shown in Figure 5.9. As mentioned before in Section 3.8.1, the Al_2O_3 particles tend to combine with each other forming globules.

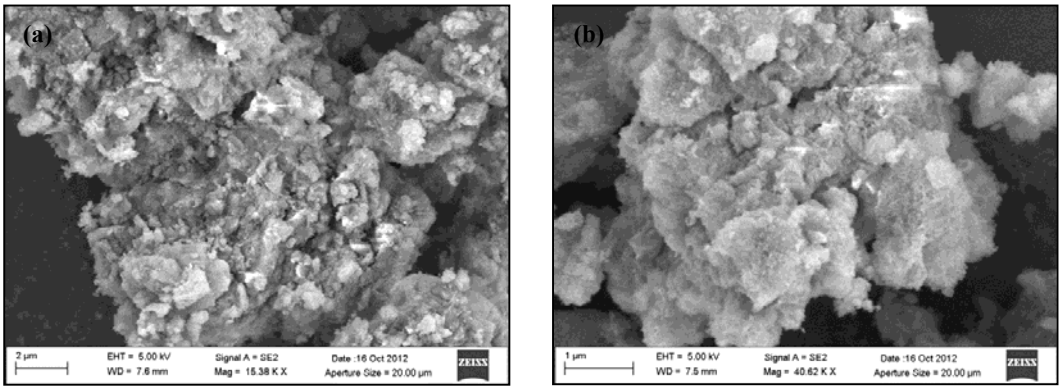

Figure 5.9: Scanning electron micrographs of the (a) Pt-Al and (b) Pt-Ni-Al catalysts

After the impregnation of NiO onto the Al_2O_3 support not much of a morphological change can be observed. However, for the NiO loaded catalyst described in Section 3.8.1, the surface morphology of the catalyst was a little rougher and contained particles that were irregular and wrinkly. After the impregnation of Pt on the support and on the mono-metallic Ni25 catalysts, no change in morphology could be observed. This could also be due to the Pt content being so low. According to Kiss et al. [10], for impregnated NiO/Al_2O_3 catalysts the presence of the Al_2O_3 phase becomes invisible due to the NiO phase causing thin or thick shell-like formations around the Al_2O_3 particles. Due to the higher amounts of NiO present compared to Pt, the morphology of the catalyst remained the same. SEM-EDX mappings of both Pt containing samples are shown in Appendix C, where an even distribution of metal particles on the supports was observed. Also, the elemental mapping of the catalysts in Appendix C confirms the presence of the metals on the surface of the supports, which was in agreement with the ICP and XRD results, thus confirming the presence of Pt in both samples.

5.6.2 Transmission electron microscopy

The TEM micrographs of the supported Pt catalysts are shown in Figure 5.10. The rod-shaped spheres marked with a dashed box in both micrographs (a) and (b) are attributed to the alumina support.

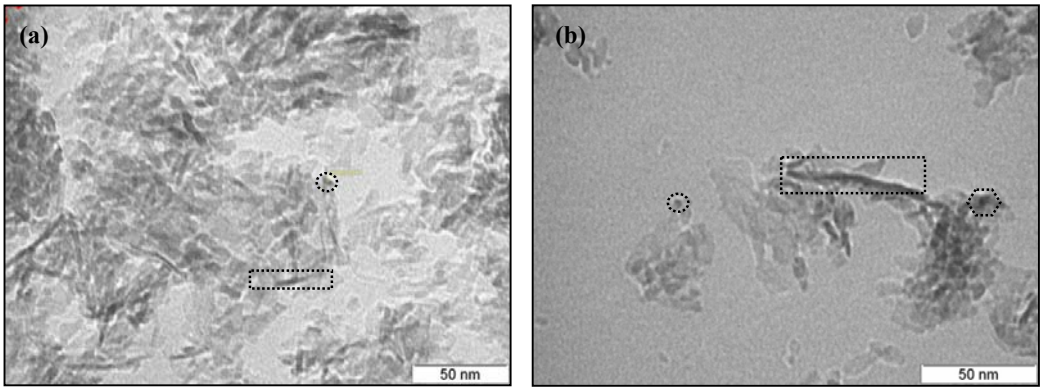

Figure 5.10: Transmission electron micrographs of the (a) Pt-Al and (b) Pt-Ni-Al catalysts

For the mono-metallic Pt- Al and the Pt-Ni-Al catalyst it is clear that the Pt particles are uniformly distributed across the surfaces of the supports, these are marked with a dashed line (circle) in both micrographs. This uniform distribution was also reported in literature by Liu et al. [4]. From (b) the presence of larger particles is attributed to the Ni species also present on the support this is marked with a dashed hexagonal line. Particle size measurements from TEM indicate Pt particles between 2 and 3 nm and those for Ni between 5 and 12 nm (minimum of 10 images and 20 particles per catalyst). This is in agreement with the crystallite sizes measured from CO chemisorption experiments. Particle measurements are indicated for both the supported Pt catalysts in Appendix C.

5.7 Catalytic testing of Pt supported catalysts

Prior to catalytic testing of the catalysts under PROX conditions the mono-metallic Pt-Al catalyst was screened for CO oxidation activity in the absence of H_2, in order to determine the effects of O_2 in the reaction with regards to CO conversion.

5.7.1 CO oxidation reactions

Similar temperature ranges were screened for the CO oxidation reactions as for the mono-metallic Ni25 catalyst (Section 4.2). Figures 5.11 and 5.12 show the results for the CO oxidation reactions over the Pt-Al catalysts with varying C:O_2 ratios. From Figure 5.11, using a C:O_2 ratio of 1:0.5, it can be observed that the catalyst is active for the oxidation of CO in the absence of H_2 and shows higher CO conversions compared to the mono-metallic Ni25 (Section 4.3). The active temperature is also similar to the mono-metallic Ni25 catalyst where the catalyst starts showing activity towards CO oxidation at 150 °C. As the temperature increases from 150 °C, the CO conversion and O_2 conversion increase and they are at their highest at 250 °C with a CO conversion of ± 55 % and a similar O_2 conversion of 55 %.

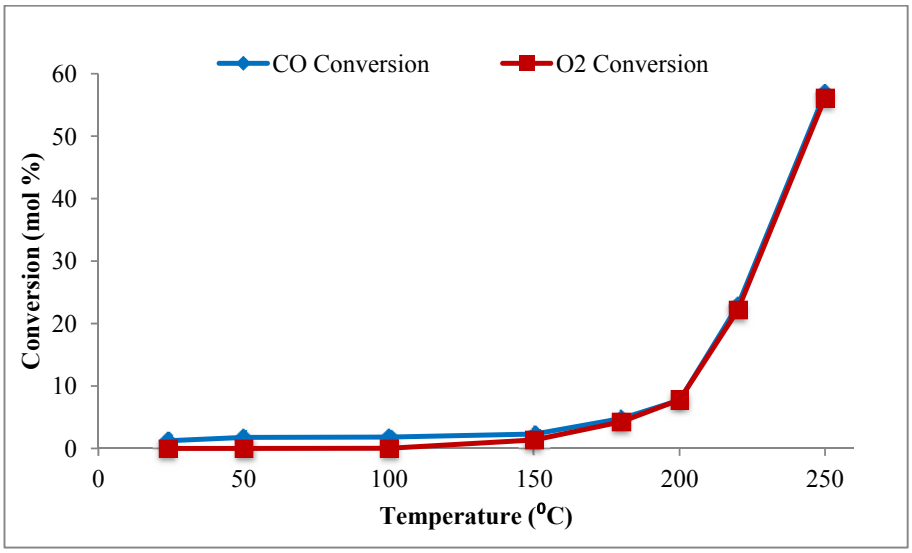

Figure 5.11: CO oxidation over the Pt-Al catalyst employing a C:O_2 ratio of 1:0.5

Figure 5.12 shows the CO oxidation reaction over the catalyst using a C:O_2 ratio of 1:2. The catalyst is also active from 150 °C, similar to the previous reaction using a C:O_2 ratio of 1:0.5. CO conversion increases with temperature and the maximum conversion is obtained at 220 °C, of ± 99.9 %, and then remains constant even at 250 °C. O_2 conversion for this catalyst is also temperature dependant as well as CO conversion dependent and increases as both increase, but unlike the previous reaction, the O_2 conversion is significantly lower at a maximum CO conversion of about 23 % (as expected). These results clearly indicate that supplementing the reaction with excess O_2 enhances the CO conversion of the catalyst dramatically, since the catalyst is not being starved of O_2.

$$CO + ½O_2 \rightarrow CO_2 \qquad (5.1)$$

From the reaction (Eq. 5.1), using the stoichiometric ratio of C:O_2 could be a limiting factor during the PROX reactions, if the catalysts at higher temperatures are reducing to their metallic form and require additional O_2 to re-oxidize them, which is evident from the *in situ redox* reactions of the catalyst. The CO oxidation reactions carried out confirm that the Pt-Al catalyst is active for the oxidation of CO in the absence of H_2 and further testing of the catalyst using different C:O_2 ratios in the PROX reaction was carried out to determine their effect on CO conversion.

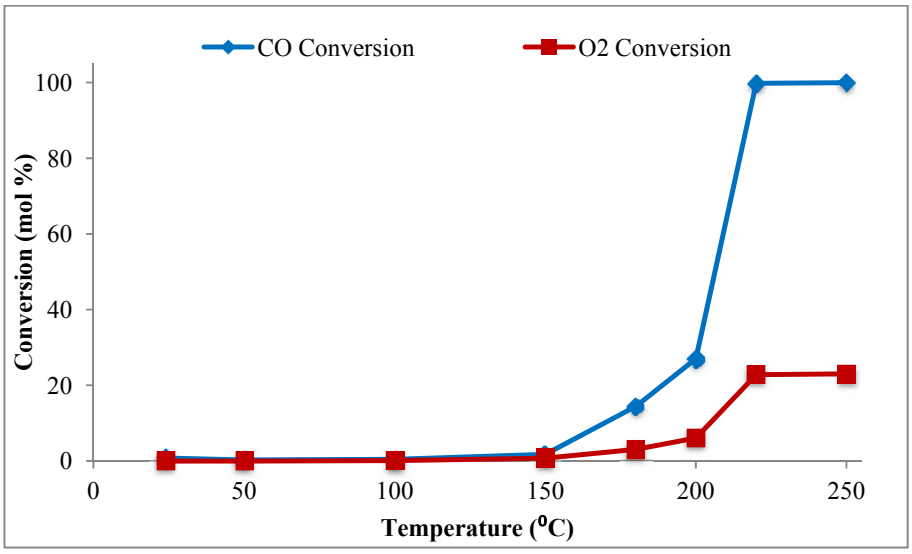

Figure 5.12: CO oxidation over the Pt-Al catalyst employing a C:O_2 of 1:2

5.7.2 PROX Reactions over Pt-Al catalyst

The activity of the Pt-Al catalyst was examined over a period of 24 hours using a C:O_2 ratio of 1:0.5 at 150 °C. From Figure 5.13 it is observed that CO conversion and selectivity towards CO_2 are stable over a period of 24 hours.

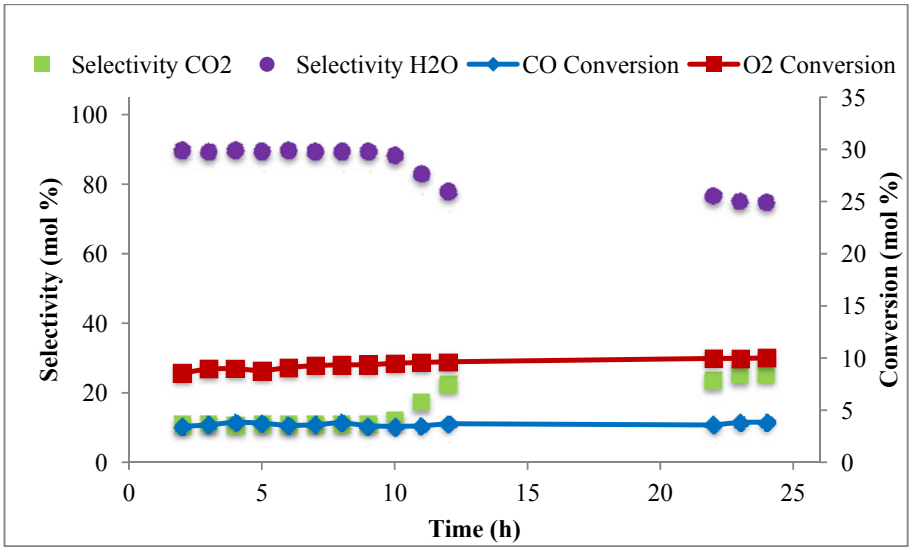

Figure 5.13: TOS study of the PROX reaction over the Pt-Al catalyst at 150 °C

A slight increase can be observed for the selectivity towards CO_2 after 10 hours with an increase of about 4 % over this period, and this remains constant for the remainder of the

reaction period at 22 %. A CO conversion of ± 4 % is observed which remained constant over the 24 hour period.

Following the time on stream experiment, the catalyst was subjected to a PROX reaction using a $C:O_2$ ratio of 1:0.5 with varying temperature. Since the PROX reaction takes place within the temperature range of room temperature to 250 °C [11], and Pt catalysts are known to be stable below 200 °C, this reaction was only screened up to 200 °C [12] to avoid any inhibition of the Pt catalyst that could occur during the reaction at temperatures too high for the precious metal [13].

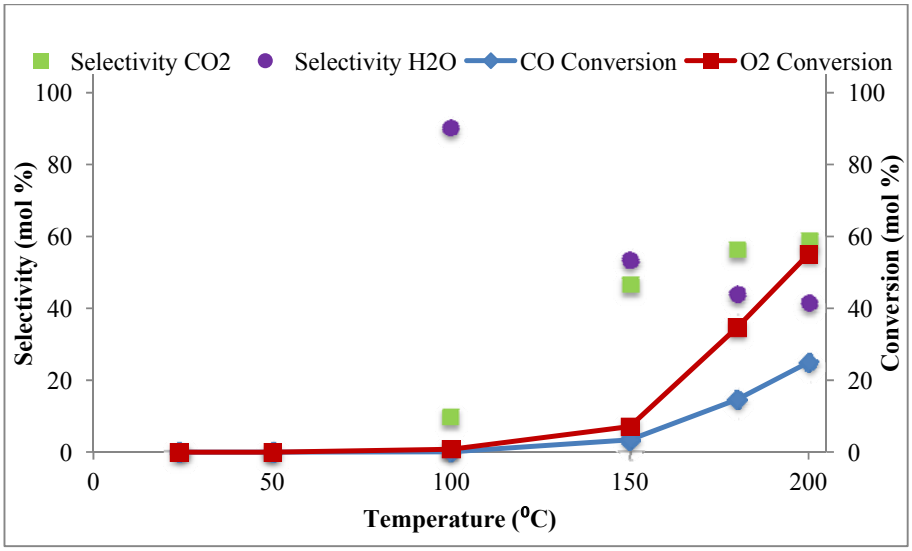

Figure 5.14: PROX reaction over the Pt-Al catalyst employing a $C:O_2$ ratio of 1:0.5

Figure 5.14 shows the catalyst activity in the PROX reaction, which unlike the mono-metallic Ni25 (Section 4.2) starts showing activity towards the oxidation of CO from 100 °C onwards. As the temperature increases for this reaction, CO conversion, O_2 conversion and selectivity towards CO_2 also increases. With regards to the selectivity towards CO_2, after 100 °C, there is a drastic increase from 15 % to 55 % at 150 °C and it reaches its highest of 60 % when conversion is at its highest at 200 °C with the CO conversion at ± 25 %. H_2O selectivity for this catalyst decreases with temperature and is at its lowest when the CO conversion was at its highest.

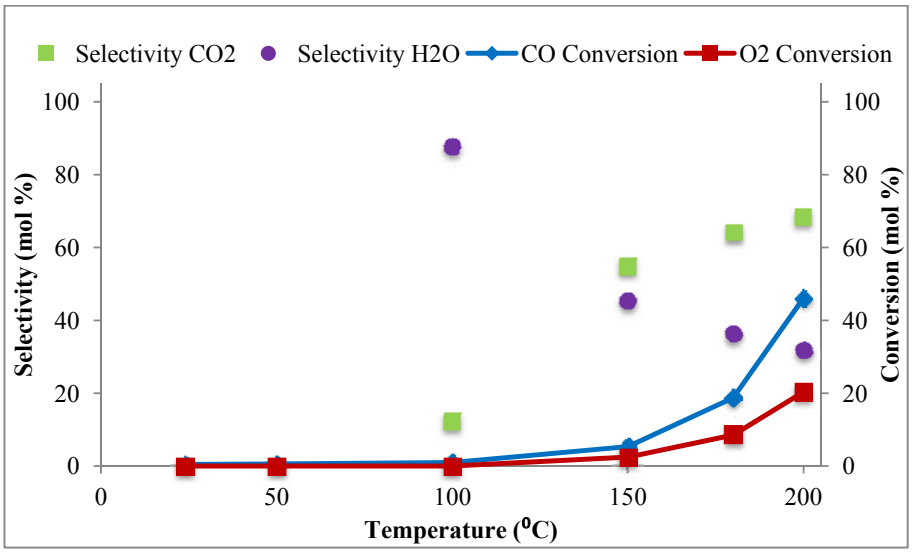

Figure 5.15: PROX reaction over the Pt-Al catalyst employing a C:O_2 ratio of 1:1

Following the results obtained using a C:O_2 ratio of 1:0.5, which showed moderate activity towards the oxidation of CO in the presence of H_2, the Pt-Al catalysts was tested under PROX conditions using C:O_2 ratios of 1:1 and 1:2.

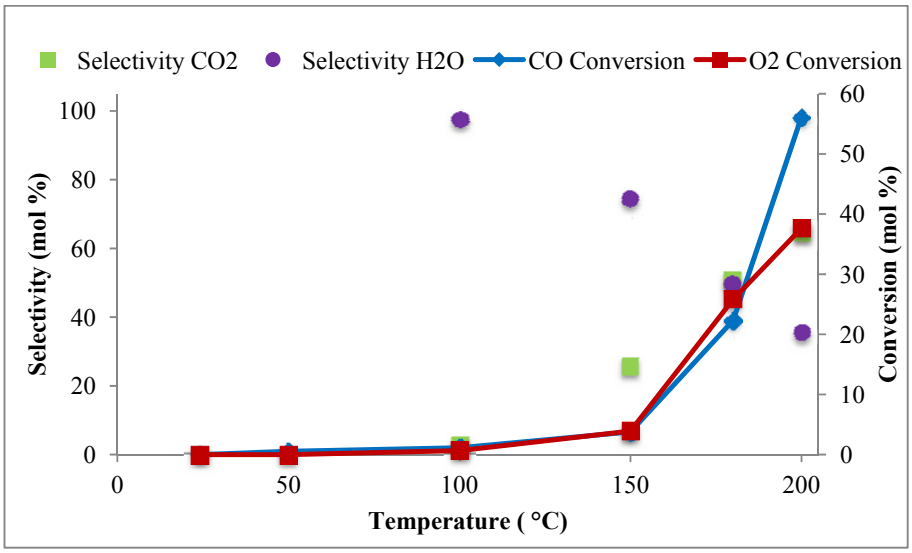

Figure 5.16: PROX reaction over Pt-Al catalyst employing a C:O_2 ratio of 1:2

Figures 5.15 and 5.16 show the PROX reactions of the Pt-Al catalysts and similar trends are seen for catalytic activity compared to the CO oxidation reactions and the PROX reactions using the different C:O_2 ratios. From Figure 5.14, the maximum CO conversion using a 1:1 C:O_2 ratio obtained is ± 47 % with a selectivity towards CO_2 of 68 %. The maximum CO conversion obtained with the 1:2 C:O_2 ratio, in Figure 5.16, is ± 56 % with a similar

selectivity, towards CO_2 of 68 %. Therefore increasing the O_2 content in the feed increases CO conversion and decreases the O_2 conversion.

The Pt-Al catalyst showed better activity than the mono-metallic Ni25 catalyst under PROX conditions and it is clear that the PGM catalyst is much more effective than the nickel catalyst for the oxidation of CO in H_2 rich streams. Also the increase of O_2 in the reaction feed enhances the catalytic activity with regards to CO conversion.

5.7.3 PROX Reactions over Pt-Ni-Al catalyst

CO oxidation reactions were not conducted over the Pt-Ni-Al catalysts since the traits that the reactions showed for both the mono-metallic catalysts were similar with regards to the CO conversion. Increasing the O_2 content for both mono-metallic catalysts increased the CO conversion and (obviously) decreased O_2 conversions.

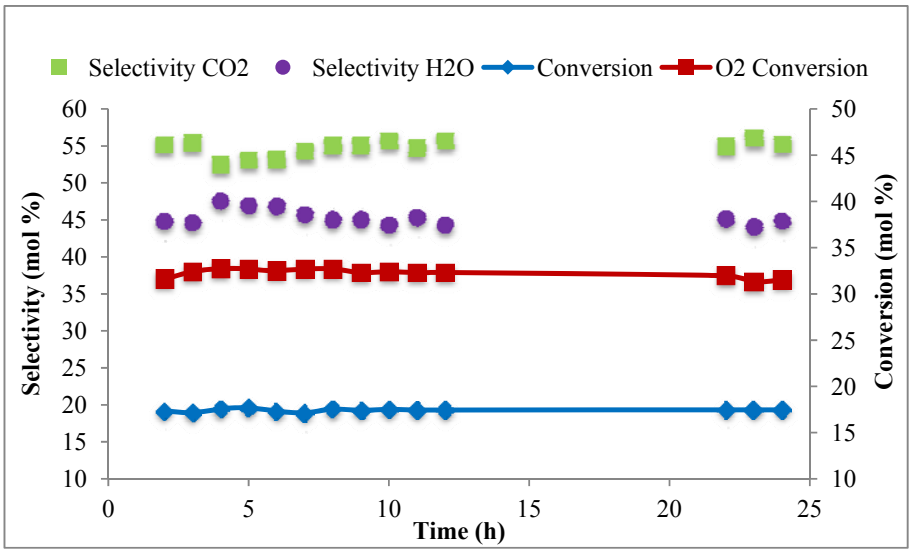

Figure 5.17: TOS study of the PROX reaction over the Pt-Ni-Al catalyst at 150 °C

The activity of the Pt-Ni-Al catalyst was tested in the PROX reaction over a period of 24 hours using a C:O_2 ratio of 1:0.5 at 150 °C, conditions similar to those used for both mono-metallic catalysts. From Figure 5.17 it is observed that CO conversion and selectivity towards CO_2 are stable over a period of 24 hours. Compared to the mono-metallic catalysts, however, under these reaction conditions the Pt-Ni-Al shows better activity. A CO conversion of ± 18 % is observed with selectivity towards CO_2 in the region of ± 55%. Following the TOS reaction, the catalyst was subjected to a PROX reaction using a C:O_2 ratio of 1:0.5, where the temperature was now varied.

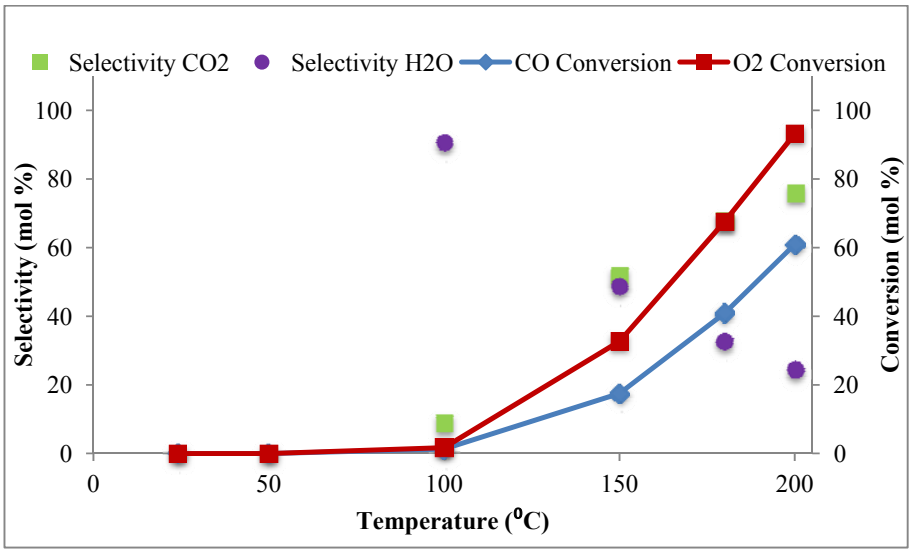

Figure 5.18: PROX reaction over the Pt-Ni-Al catalyst employing a C:O_2 ratio of 1:0.5

Figure 5.18 shows the activity of the catalyst in the PROX reaction and similarly to the Pt-Al catalyst this catalyst also shows activity from 100 °C onwards. In comparison to the mono-metallic catalysts, this catalyst shows much better activity towards the oxidation of CO in the presence of H_2. Selectivity towards CO_2 and CO conversion for this catalyst reaches a maximum at 200 °C, with a CO conversion of ± 61 % and selectivity towards CO_2 of ± 75 %.

This catalyst under PROX conditions thus favors the oxidation of CO rather than the undesired oxidation of H_2 at higher PROX temperatures.

Effects of O_2 concentration in the PROX reaction were investigated by altering the C:O_2 ratios. Figure 5.19 shows the PROX reaction using a C:O_2 ratio of 1:1 and the results obtained follow the same trend as seen in all the other reactions, where an increase in the O_2 content increased CO conversion. Maximum CO conversion for this catalyst was obtained at 200 °C, with a selectivity towards CO_2 of 68 %. However, O_2 conversion at high CO conversions was almost 100 %. This result can be correlated to the *in situ redox* reactions of the catalyst, suggesting that the catalyst is reducing to its metallic form and then consuming the O_2 present in the feed to re-oxidize itself. No other products were observed in the GC chromatograms that could explain the high O_2 conversions and the used catalyst characterization will confirm this statement (Section 5.8).

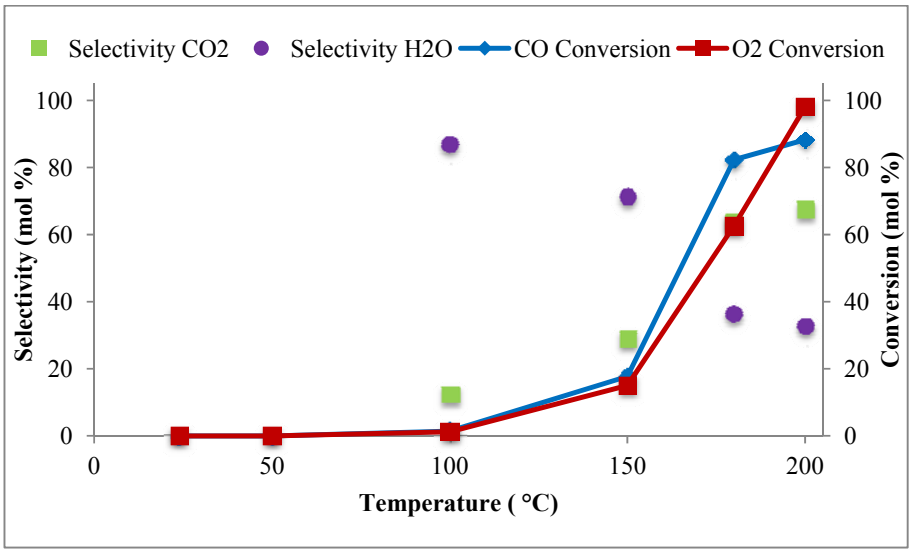

Figure 5.19: PROX reaction over the Pt-Ni-Al catalyst employing a C:O_2 ratio of 1:1

Similar trends to the previous reaction are observed using a C:O_2 ratio of 1:2. From Figure 5.20 it can be seen that the CO conversion is much higher with excess O_2 in the feed, with maximum CO conversion reaching a high of ± 99.9 % at 180 °C and this remains constant up to 200 °C. With regards to the O_2 conversion, a similar result is obtained to the previous reaction, also suggesting that the catalyst is reducing at higher temperatures and re-oxidizing *in situ* by consuming O_2 present in the feed.

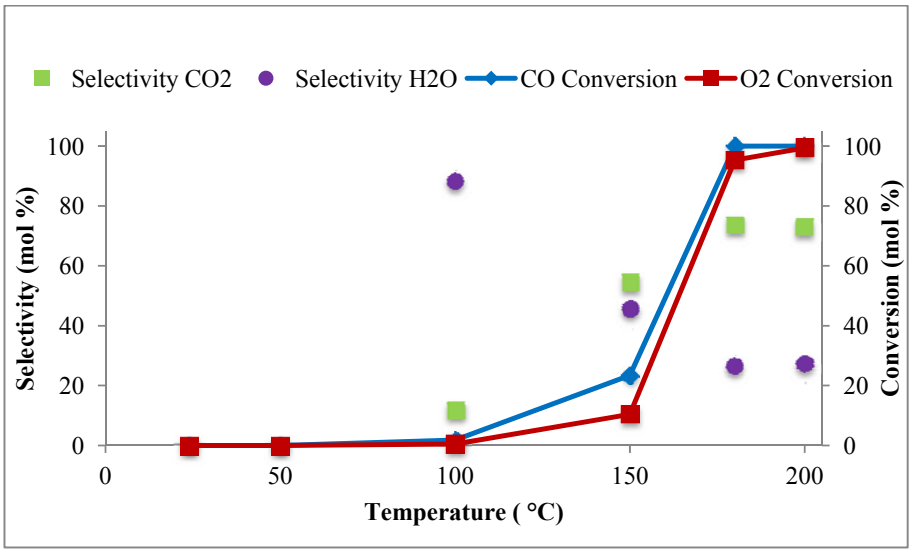

Figure 5.20: PROX reaction over the Pt-Ni-Al catalyst employing a C:O_2 ratio of 1:2

Following the reaction depicted in Figure 5.20, the catalyst was calcined *in situ* under a positive flow of air for 4 hours at 200 °C, cooled to room temperature and subjected to the

same reaction. Results obtained were similar for the catalyst in the first PROX reaction, indicating that the catalyst can be regenerated and results were reproducible following the calcination in situ. The same procedure was conducted on the Pt-Al catalyst that followed the reaction depicted in Figure 5.16 and the results obtained were again reproduced.

5.7.4 ISO-CONVERSIONS

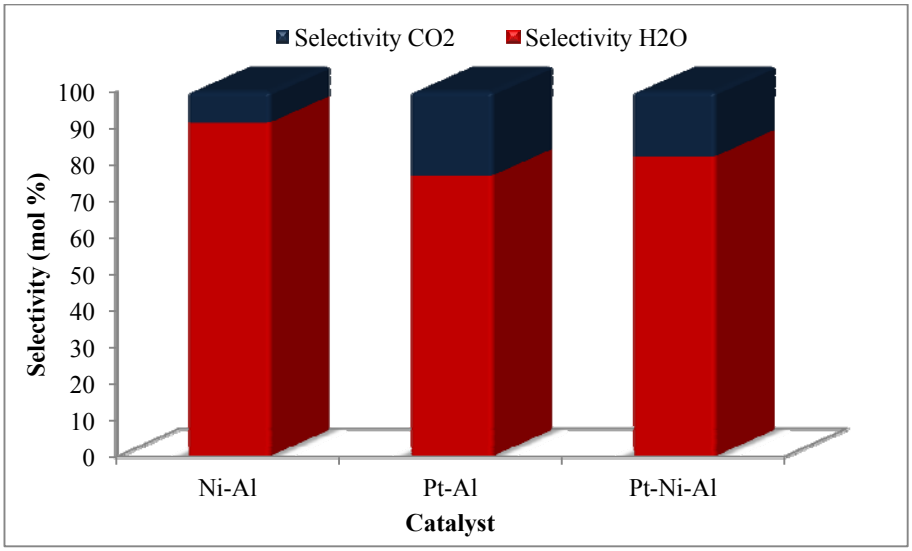

Figure 5.21: Selectivity of the products at an iso-conversion of 1.5 % (150 °C)

Figure 5.21 shows the iso-conversion of 1.5 % data of the catalysts using a $C:O_2$ ratio of 1:0.5 at a temperature of 150 °C (PROX reaction). From this it can be seen that with regards to the selectivity of CO_2 at low CO conversions, the Pt-Al catalyst is more selective than both the Ni containing catalysts. But from the results obtained from the complete study of the PROX reactions of the catalysts it is clear that within the PROX reaction temperature range the Pt-Ni-Al catalyst showed better activity towards CO conversion and selectivity towards CO_2 compared to both the monometallic catalysts. Studies reported by Jo et al. [14] showed that a 5 % Pt/Al_2O_3 catalyst exhibited maximum CO conversion at a temperature of 150 °C following various pre-treatments prior to catalytic testing. Their results and the results obtained in this study indicate that Pt/Al_2O_3 catalysts are active for the preferential oxidation reaction at this temperature which suggests its suitability in iso-conversion studies. The Ni/Al_2O_3 catalyst, however, has not been reported in literature for this reaction, but reports have been made of this catalyst being active for oxidation reactions at much higher temperatures beyond the PROX range. Also the mono-metallic Ni25 catalyst at this temperature of 150 °C, irrespective of the GHSV's employed, only gave a maximum CO

conversion of 2.5%. Therefore a higher temperature was used for determining only the selectivities of the Pt containing catalysts at iso-conversion, where these catalysts showed higher activity towards CO conversion and selectivity towards CO_2.

An iso-conversion of 20 % was investigated at 180 °C using a $C:O_2$ ratio of 1:0.5 for the catalysts. The mono-metallic Ni-Al catalysts still showed very low conversions, irrespective of the GHSV employed at this temperature and a 20 % conversion could not be obtained for this catalyst. Therefore the iso-conversion of 20 % at 180 °C relates to only the Pt containing samples.

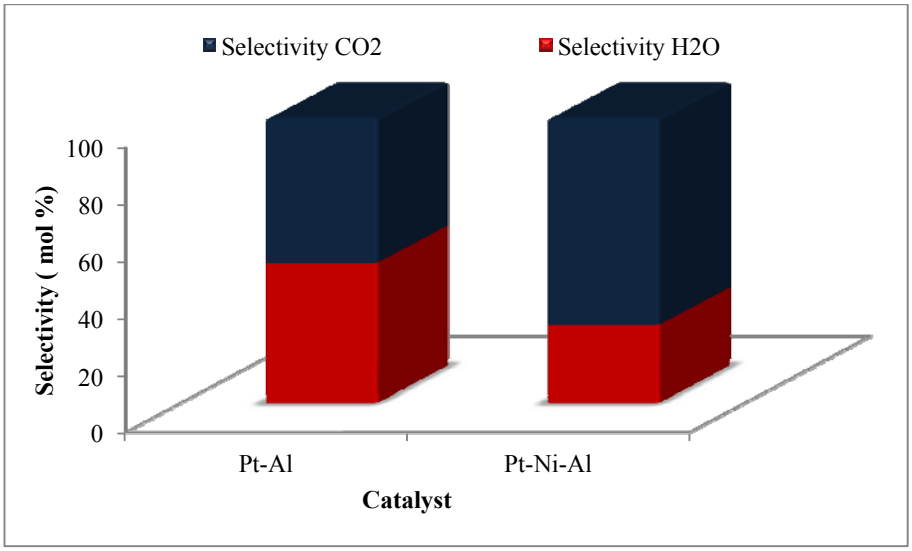

Figure 5.22: Selectivity of the products at an iso-conversion of 20 % (180 °C)

Figure 5.22 shows the selectivities to CO_2 at an iso-conversion of 20 % of the Pt catalysts using a $C:O_2$ ratio of 1:0.5 at a temperature of 180 °C. From this it can be seen that under these conditions the Pt-Ni-Al catalyst is more selective to CO_2 than both the mono-metallic catalysts. With regards to CO conversion of the catalysts, the Pt-Ni-Al catalyst also showed much better activity compared to both mono-metallic catalysts. All PROX temperature ranges screened for the catalysts gave the same result. Selectivity towards CO_2 for the Pt-Ni-Al catalyst also showed that the Pt addition to the mono-metallic Ni catalyst enhanced or promoted its activity which was even higher compared to the mono-metallic Pt catalyst.

Ko et al**.** [5] stated that, with regards to the correlation between the onset temperature of reduction in TPR traces and the catalytic activity, the alloyed catalyst that showed lower temperature reduction compared to the mono-metallic catalyst should show greater PROX

activity at lower temperatures. Results obtained in this study clearly indicate that the Pt-Ni-Al catalyst, exhibiting a lower onset reduction temperature, indeed showed better activity and selectivity towards CO_2 in the PROX reaction.

Similarly to the NiO/Al_2O_3 systems (Section 4.5), following all reactions carried out on the Pt containing catalysts, conversion and selectivity data were also collected while the reactor was cooling at two temperatures. Both the Pt-Al and Pt-Ni-Al catalysts showed similar conversions at similar temperatures to those obtained when increasing the temperatures, with an error of ± 5 %, only for the reactions where O_2 conversions did not reach 100 %. As explained previously, the catalysts that had consumed O_2 from the feed were calcined and re-tested and results obtained from the previous run were reproduced.

5.7.5 H_2 vs CO conversion during the PROX reactions

Although all the catalysts indicated higher selectivities towards H_2O than CO_2 at lower PROX temperatures where CO conversions were low, the maximum H_2 conversion did not exceed 1 %. Also at high CO conversions over the catalysts, shown in Figures 5.23 and 5.24, H_2 conversion still did not exceed 1 %. Considering the feed used, 50 % consisted of H_2 and only 1 % consisted of CO. Therefore, based on the results obtained, only a small portion of the H_2 was converted to form H_2O during the conversion of CO, which is ultimately what is desired in the PROX reaction.

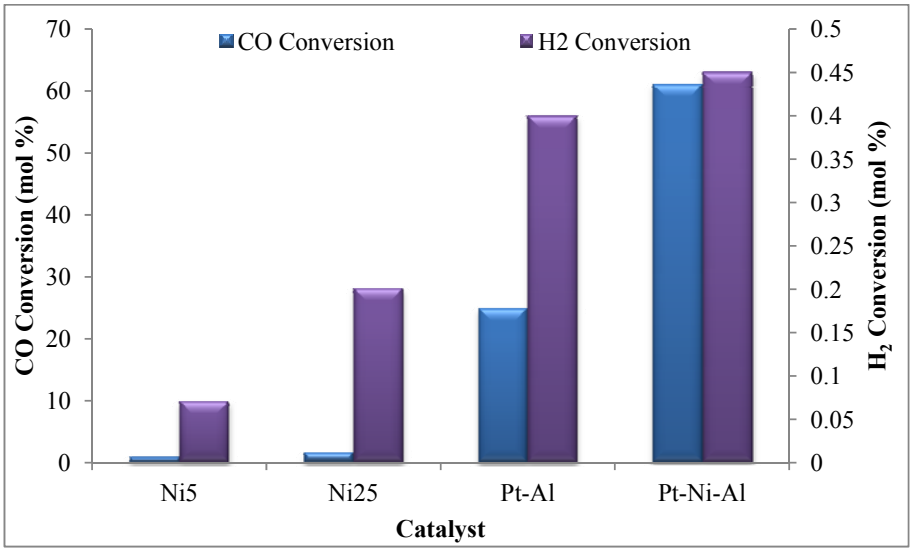

Figure 5.23: CO and H_2 conversions at 200 °C using a C:O_2 ratio of 1:0.5 of the catalysts

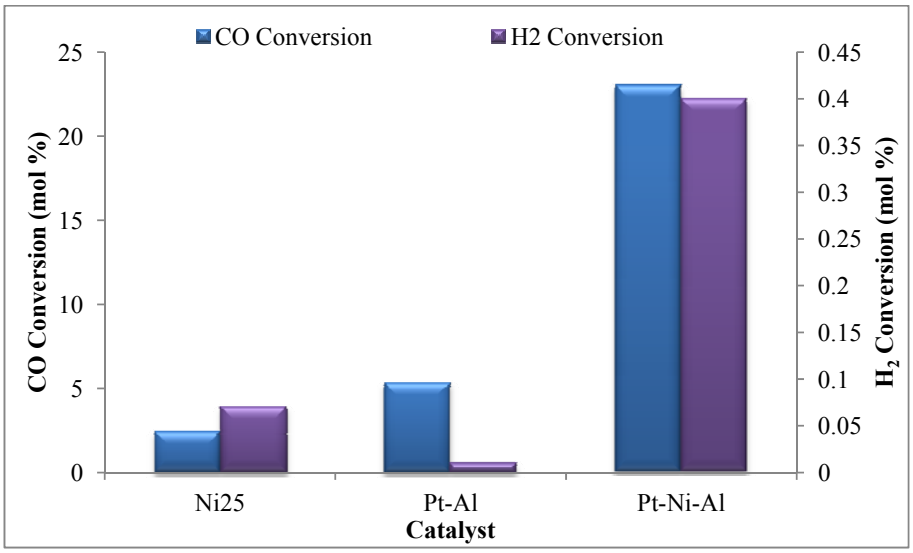

Figure 5.24: CO and H_2 conversions at 150 °C using a C:O_2 ratio of 1:2 of the catalysts

5.8 Used supported Pt catalyst characterization

From Table 5.6 it can be observed that with regards to the surface properties of the catalyst, the surface areas, pore volumes and pore diameters of the used catalysts decrease compared to those of the fresh catalysts shown in Table 5.2. Results indicated are consistent where decreases in the surface areas are accompanied by decreases in the pore volumes, and with regards to the pore diameter, these decrease when surface areas decrease [15]. This was also evident for the mono-metallic Ni25 used catalyst (Section 4.5).

Table 5.6: Surface characterization of the used supported Pt catalysts

Catalyst	Surface area (m^2/g)	Pore volume (cm^3/g)	Pore diameter (Å)
Pt-Al	163	0.30	90
Ni25	95	0.25	109

The XRD patterns of the used catalysts are depicted in Figure 5.25, where no new phases can be seen for the used catalysts compared to the fresh catalysts (Section 5.4). However, these catalysts showed signs of reduction at higher temperatures where the O_2 balances decreased (± 87-92%), but C and H balances remained constant (± 95-101 %). Also, as mentioned by Elkhalifa and Friedrich [15], this could be due to the reduction-oxidation cycles that

accompany the catalytic activity of the catalysts during the reactions. The Mars and van Krevelan mechanism also proposes that the reactant, in this case CO, extracts lattice O_2 from the surface layer of the catalysts, which was mentioned for the Ni-Al systems, thereby reducing them [16]. The lattice O_2 is then replenished by O_2 from the feed during the re-oxidation process [16]. This result is evident for the supported Pt catalysts since calcination following the reaction with air, re-oxidizes the catalyst. As evident from the XRD pattern of the used catalyst (Figure 5.25), the phases still present are attributed to the metal oxide phases. This reaction is also coupled with the Eley-Rideal mechanism, explaining that CO which does not reside on the catalyst surface long enough to define the physisorbed state, can interact with an adsorbed O_2 species to form CO_2 [16]. It is likely this mechanism could be taking place at higher temperatures where the O_2 balances start fluctuating and CO conversions increase; but no observable decrease was observed with the C balances. If CO was adsorbing too strongly to the catalyst surface at higher temperatures, desorption would require much higher temperatures and also this would be evident from the C balances of the reaction which would show a decrease. Active metal sites would also have been blocked by C deposition and results would have shown a decrease in CO conversion. Thus was not observed.

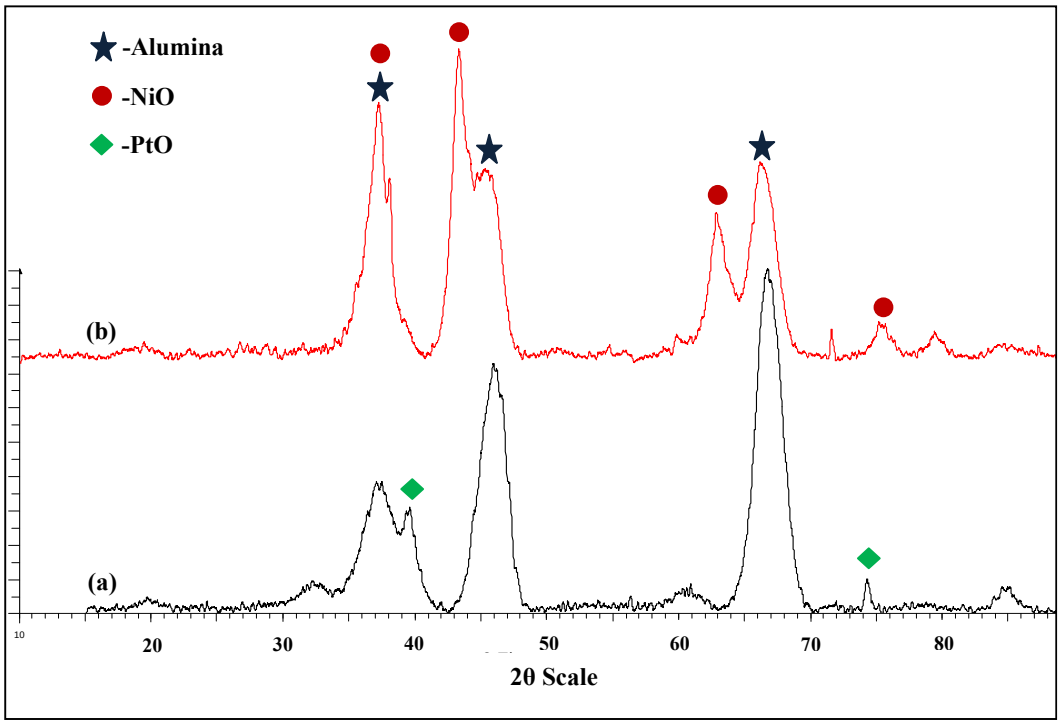

Figure 5.25: XRD diffractograms of used the (a) Pt-Al and (b) Pt-Ni-Al catalysts

References

[1] P. Salagre, J.L.G. Fierro, F. Medina, J.E. Sueiras, J. Mol. Catal. A: Chem. 106 (1996) 125-134.

[2] S.M. Morris, P.F. Fulvio, M. Jaroniec, J. Am. Chem. Soc. 130 (2008) 15210-15216.

[3] B. Li, S. Kado, Y. Mukainakano, T. Miyazawa, T. Miyao, S. Naito, K. Okumura, K. Kunimori, K. Tomishige, J. Catal. 245 (2007) 144-155.

[4] Z.-M. Liu, X.-h. Li, Z.-j. Chen, P. Ying, Z.-c. Feng, C. Li, J. Fuel Chem. Technol. 37 (2009) 205-211.

[5] E.-Y. Ko, E. Park, K. Seo, H. Lee, D. Lee, S. Kim, Catal Lett. 110 (2006) 275-279.

[6] V.P. de Souza, D. Costa, D. dos Santos, A.G. Sato, J.M.C. Bueno, Int. J. Hydrogen Energy. 37 (2012) 9985-9993.

[7] C. Li, Y.-W. Chen, Thermochimica Acta. 256 (1995) 457-465.

[8] H. Liu, L. Ma, S. Shao, Z. Li, A. Wang, Y. Huang, T. Zhang, Chin. J. Catal. 28 (2007) 1077-1082.

[9] M.M. Khader, J. Mol. Catal. A: Chem. 104 (1995) 87-94.

[10] E. Kiss, G. Bošković, M. Lazić, G. Lomić, R. Marinković-Nedučin, Scanning. 28 (2006) 236-241.

[11] M. Moreno, G.T. Baronetti, M.A. Laborde, F.J. Mariño, Int. J. Hydrogen Energy. 33 (2008) 3538-3542.

[12] E.-Y. Ko, E.D. Park, K.W. Seo, H.C. Lee, D. Lee, S. Kim, Catal. Today. 116 (2006) 377-383.

[13] O. Korotkikh, R. Farrauto, Catal. Today. 62 (2000) 249-254.

[14] M.-C. Jo, G.-H. Kwon, W. Li, A.M. Lane, J. Ind. Eng. Chem. 15 (2009) 336-341.

[15] E. Elkhalifa, H. Friedrich, Catal Lett. 141 (2011) 554-564.

[16] B.K. Hodnett, Heterogeneous catalytic oxidation: fundamental and technological aspects of the selective and total oxidation of organic compounds, John Wiley and Sons, New York, 2000.

CHAPTER 6

Summary and Conclusion

The synthesis, characterization and catalytic testing of nickel, Pt and Pt-Ni catalysts supported on alumina has allowed for a comparative study of these catalysts to be carried out.

The X-ray diffractograms of the calcined catalyst samples: Ni/Al_2O_3 and $Pt/Ni/Al_2O_3$, showed that NiO species were formed in the catalysts during calcination. The PtO phase was observed for Pt/Al_2O_3, but it was difficult to observe on the $Pt/Ni/Al_2O_3$ due to low the weight percentage of Pt compared to Ni present on the support. All the catalysts were crystalline in nature and showed the crystalline phases of the materials that were present. *In-situ* reduction and oxidation studies indicated that the catalysts had reversible phase changes and that the catalysts were stable during these phase transformations. Li et al. [1] suggested that the sequential impregnation of the catalysts generally allowed these to be reduced to their metal precursors and then to be easily re-oxidized following calcination in air.

TEM images of the catalysts showed that these catalysts had even particle distributions. The nickel particle sizes were larger than those of the Pt particles in both the mono-metallic and bi-metallic catalysts. The elemental mapping images (EDX) also showed that Ni and Pt were distributed evenly across the support in all three catalysts. All catalysts displayed lower BET surface areas than the supports, indicating the presence of metal on the surface of the support. With regards to the pore diameter, only the Ni-Al catalyst showed a decrease indicating the presence of Ni within the pores of the support. Pore diameters of the Pt catalysts, when compared to the support and the mono-metallic Ni catalyst, tended to increase and this was due to Pt atoms being more preferably located on the surface of the supports.

N_2 adsorption-desorption isotherms for all catalyst showed typical type IV isotherms with H1 hysteresis loops which were characteristic for mesoporous materials.

TPR profiles of the catalysts indicated that the addition of Pt on the Ni containing catalyst promoted reduction at lower temperatures, suggesting that the Pt alloyed with Ni particles present on the surface of the support, which correlated to a report in literature [2]. This was also evident as the metal dispersion of the alloyed sample was lower than that in both mono-

metallic catalysts, as was also mentioned in literature [3]. With regards to the correlation between the onset temperature of reduction in the TPR traces and the catalytic activity of the catalysts, the alloyed catalyst (Pt-Ni-Al) showed lower temperature reduction and a higher degree of reducibility compared to the mono-metallic catalysts. Ni and Pt therefore exhibit a synergistic effect (Figure 6.1) towards CO conversion and selectivity towards CO_2 in the PROX reaction.

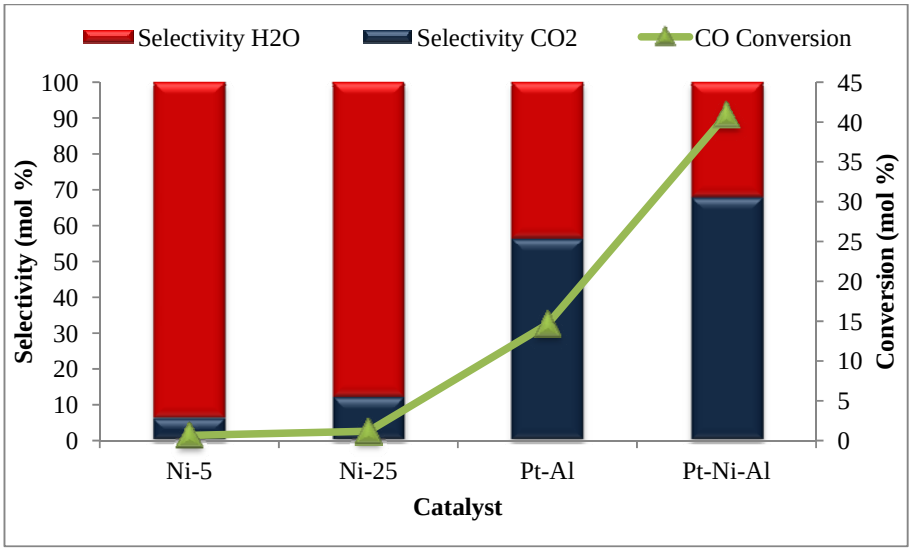

Figure 6.1: CO conversion and selectivity towards CO_2 at 180 °C for all catalysts

TPD results of the catalysts indicated the presence of weak, moderate and strong acidic sites, with the exception of the mono-metallic Ni25 catalyst which didn't display any strong acidic sites. As metal loadings increased in the Ni series the specific acidity of the catalyst also increased. For the supported Pt catalysts the bi-metallic Pt-Ni-Al catalyst showed the highest specific acidity compared to all the mono-metallic catalysts prepared.

TOS experiments for all the catalyst indicated that they were stable under PROX conditions for long periods of time, displaying constant CO conversion and selectivity towards CO_2.

H_2 conversions of the catalysts for all the PROX reactions did not exceed 1 %, even if the selectivity towards H_2O was higher than CO_2. The PROX reaction requires minimal H_2 conversion when oxidizing CO, and based on the results obtained, the amount of H_2 converted to H_2O over the catalysts presented in this dissertation was very low.

Additional remarks:

All catalytic tests for PROX activity were carried out on supported materials in their oxide phases. Literature has reported that better activity towards CO oxidation under PROX conditions at lower temperatures may be achieved by various pre-treatment steps prior to catalytic testing. Also different synthesis methods and calcination temperatures have been reported, that improve catalytic results in the PROX reaction. The effects of CO_2 and H_2O can also be determined by introducing them into the reaction mixture. Varying GHSVs can also enhance the activity of the catalysts in the PROX reaction. Other commercial supports (CeO_2, TiO_2 etc.) have also proved to enhance the activity of the supported metal oxides in the PROX reaction (Sn, Fe etc.). All of these effects should be examined in future work.

REFERNCES

[1] B. Li, S. Kado, Y. Mukainakano, T. Miyazawa, T. Miyao, S. Naito, K. Okumura, K. Kunimori, K. Tomishige, J. Catal. 245 (2007) 144-155.

[2] V.P. de Souza, D. Costa, D. dos Santos, A.G. Sato, J.M.C. Bueno, Int. J. Hydrogen Energy. 37 (2012) 9985-9993.

[3] R. Padilla, M. Benito, L. Rodríguez, A. Serrano-Lotina, L. Daza, J. Power Sources. 192 (2009) 114-119.

APPENDIX A

Reactor setup and catalyst packing

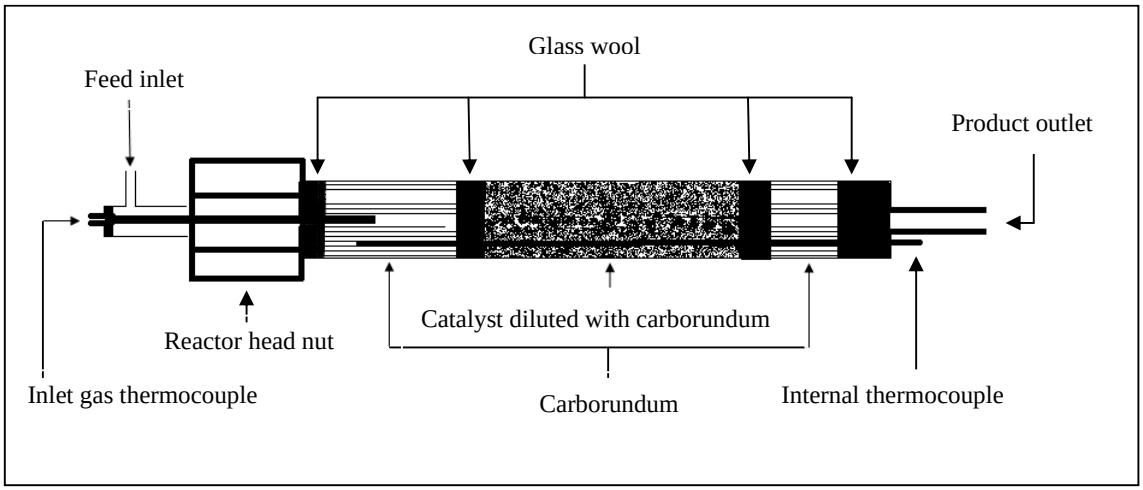

Figure A1: Schematic representation of the loaded reactor tube

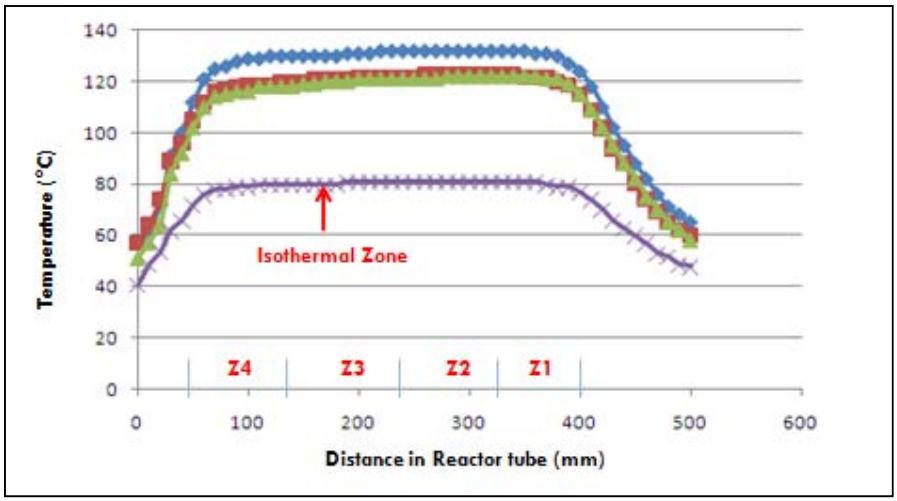

Figure A2: Temperature profile of the reactor tube showing the isothermal zone

APPENDIX B

Test units and GC chromatographs

Figure B1: The test units (Test unit on left was used for this study)

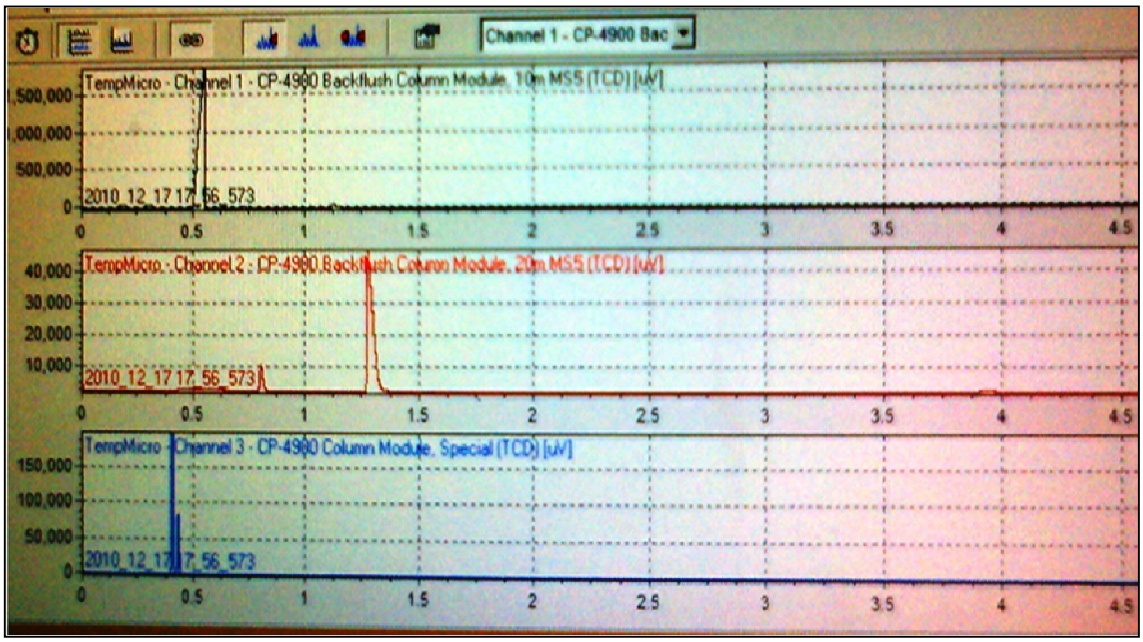

Figure B2: GC chromatographs

APPENDIX C

Characterization of catalysts

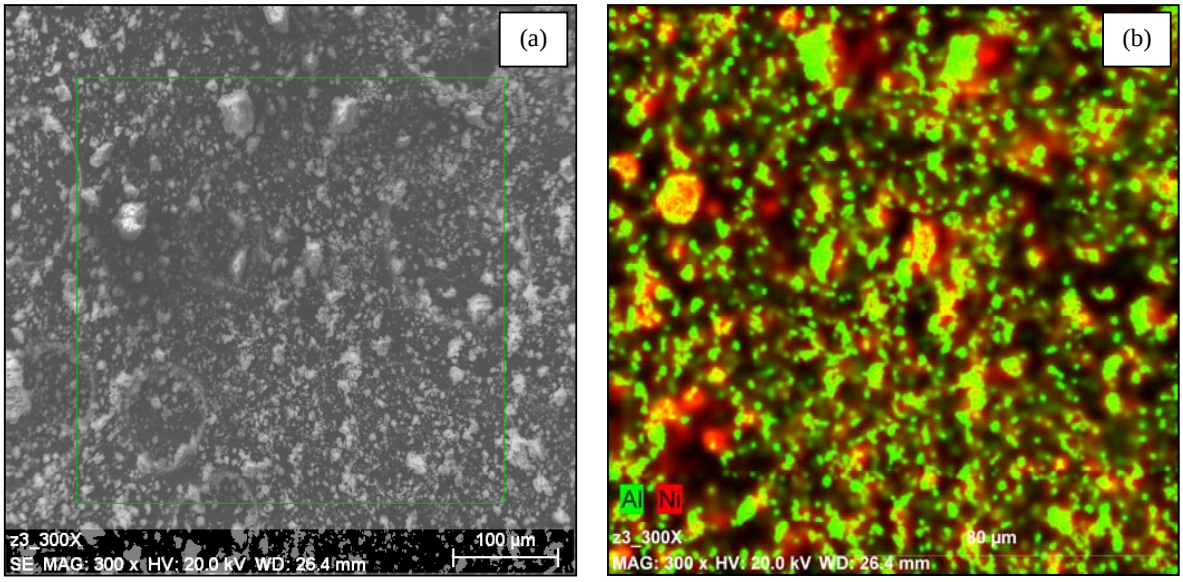

Figure C1: SEM of the Ni5 (a) Bright field and (b) Elemental mapping

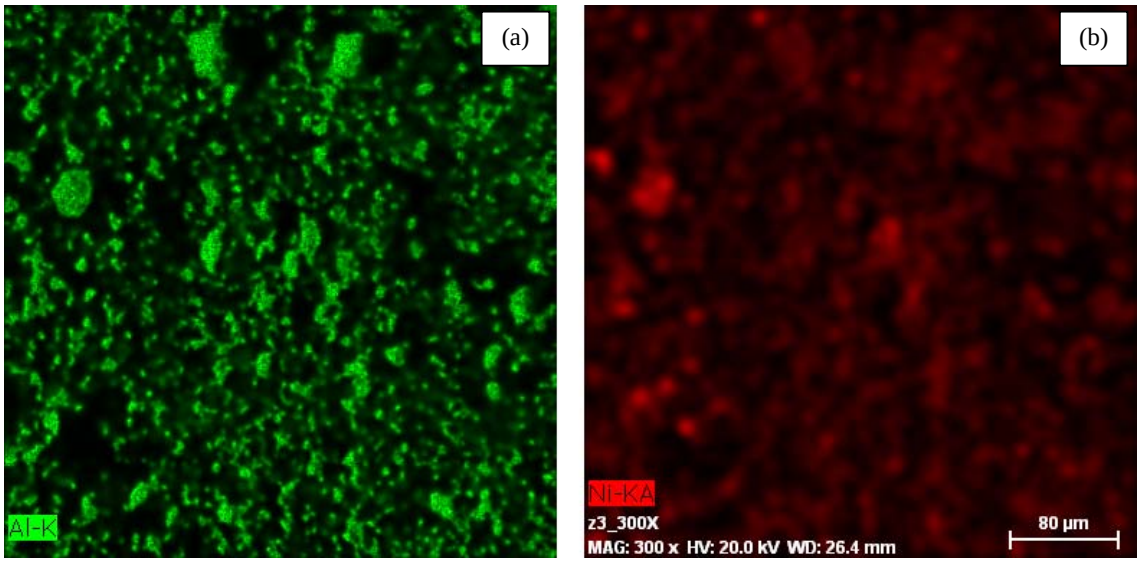

Figure C2: Electron mapping of the Ni5 catalyst showing the distribution of (a) Al and (b) Ni

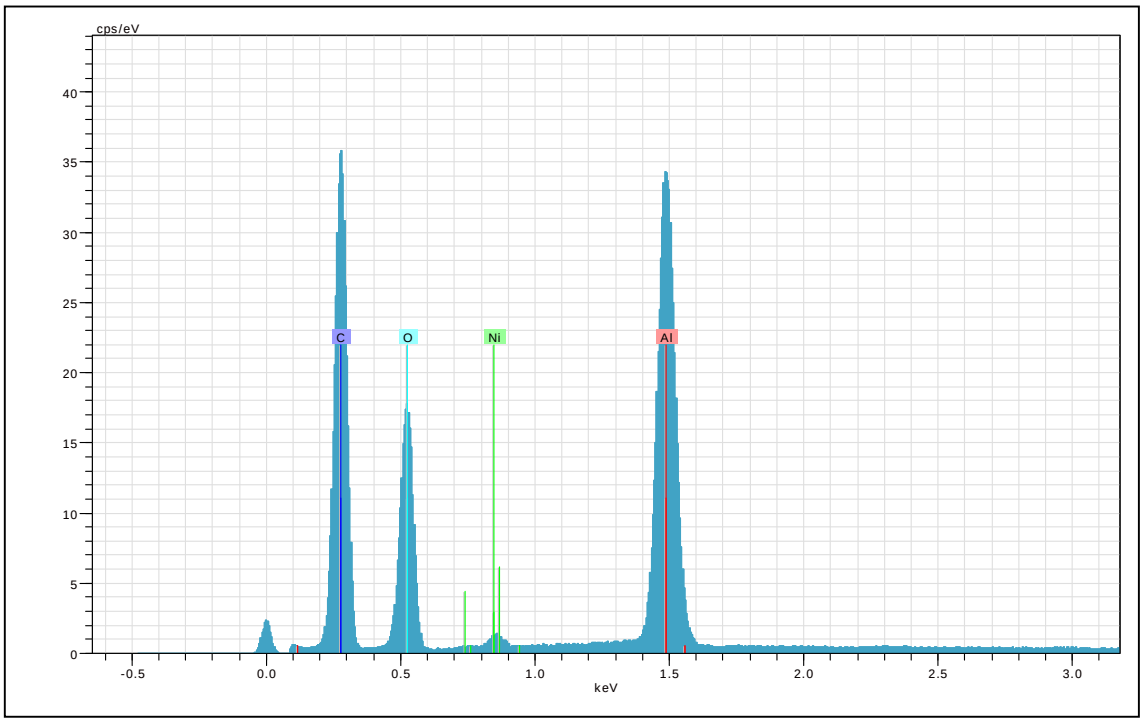

Figure C3: Electron mapping graph of Ni5

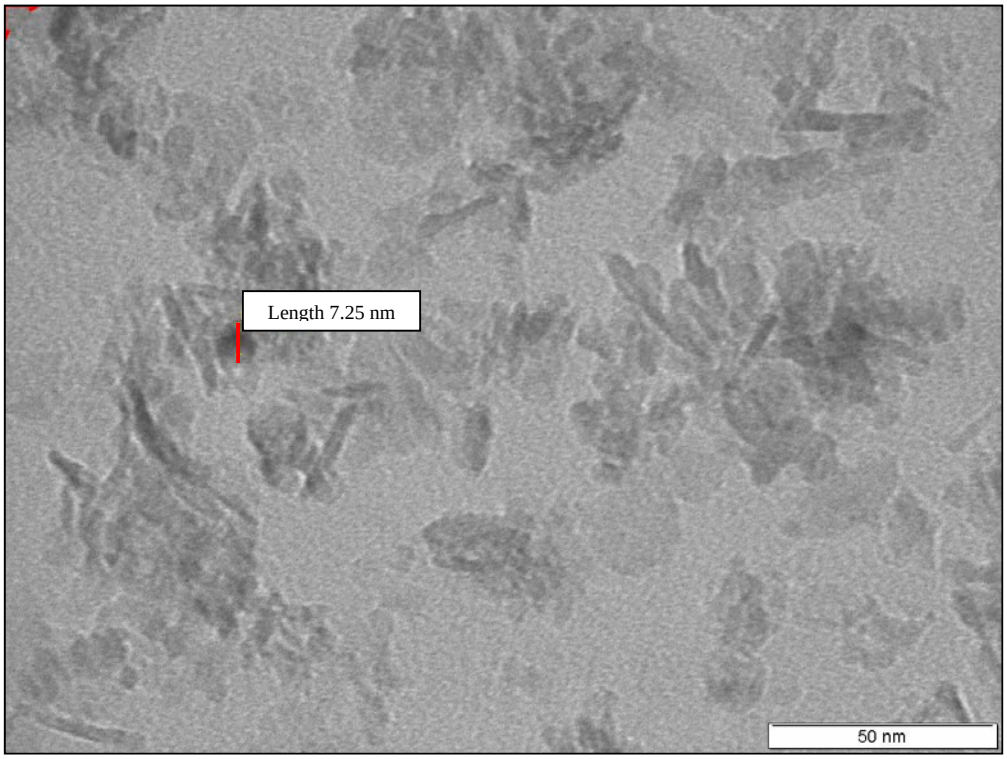

Figure C4: TEM image of Ni5 showing the estimated particle size

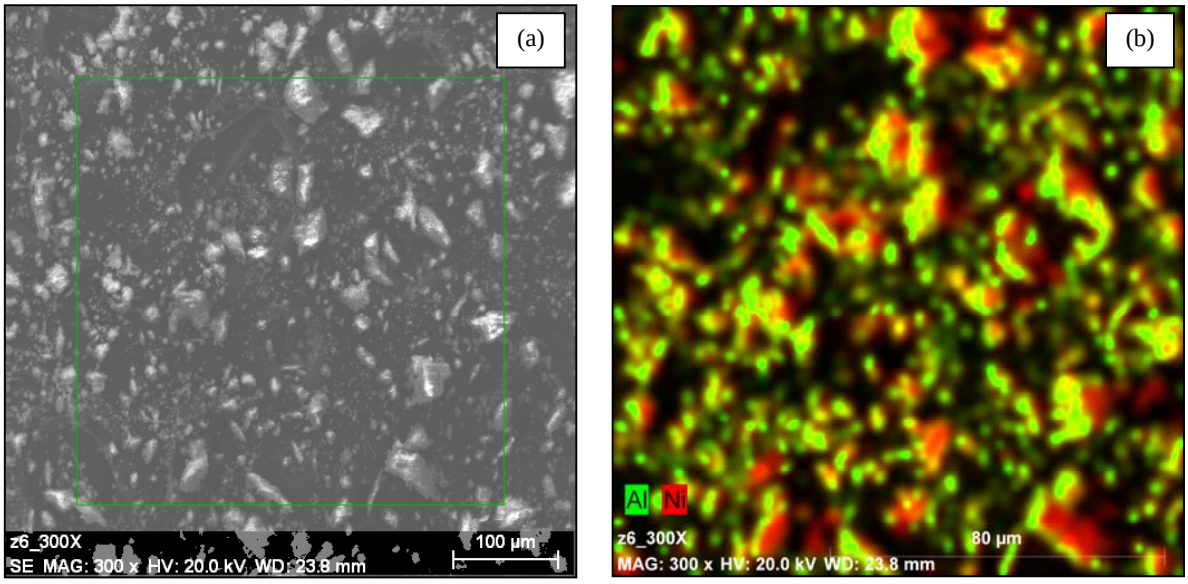

Figure C5: SEM of the Ni25 (a) Bright field and (b) Elemental mapping

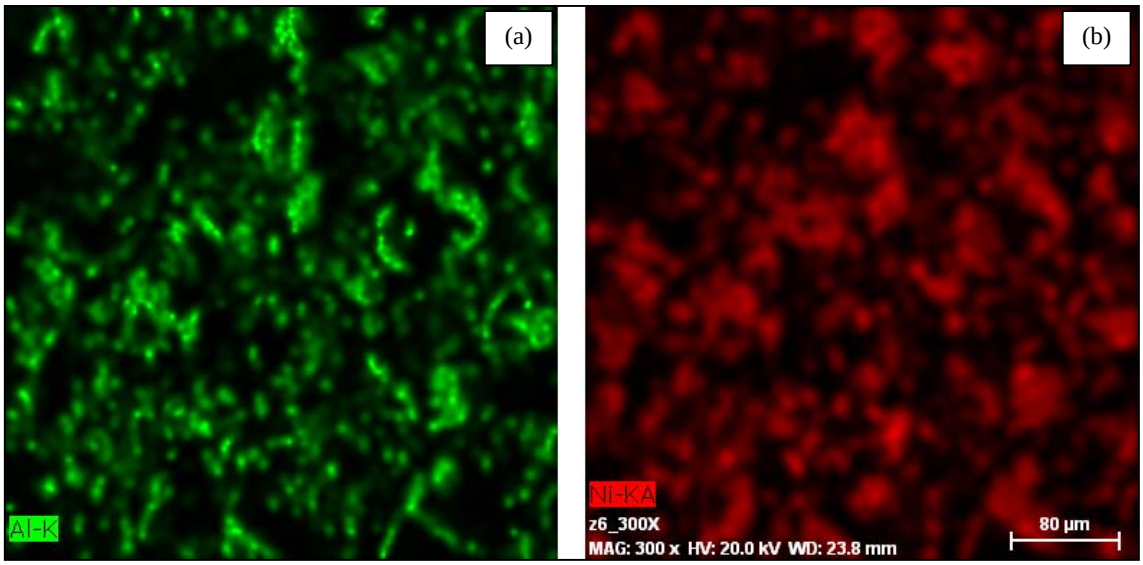

Figure C6: Electron mapping of the Ni25 catalyst showing the distribution of (a) Al and (b) Ni

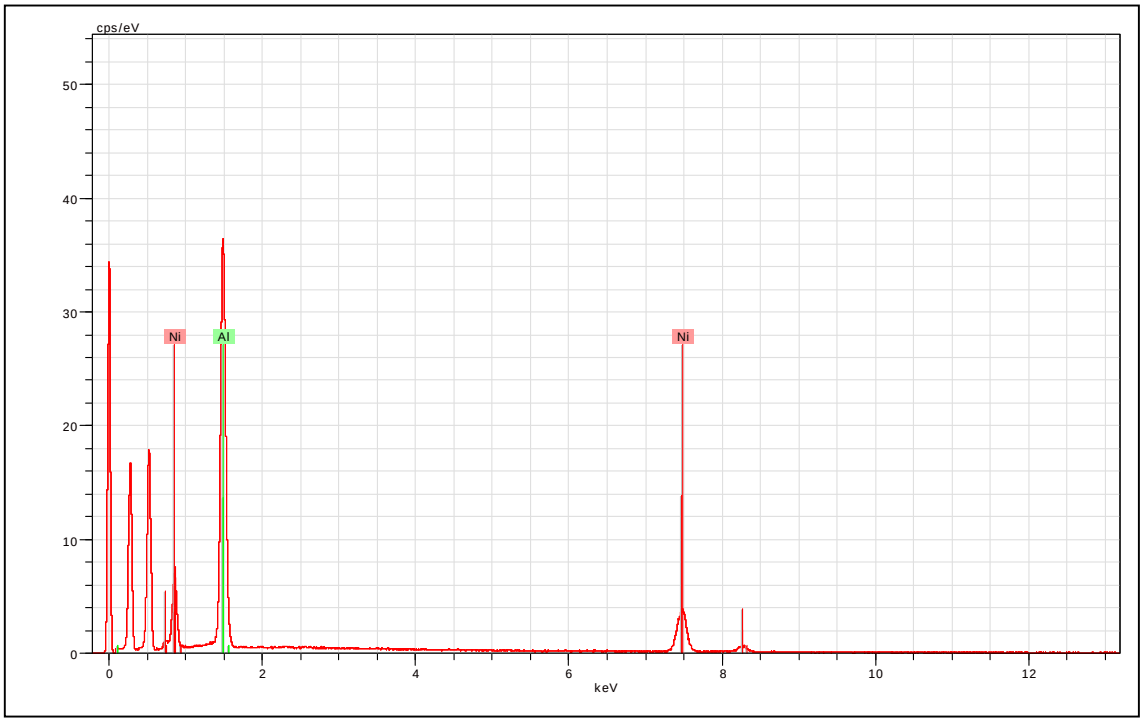

Figure C7: Electron mapping graph of Ni25

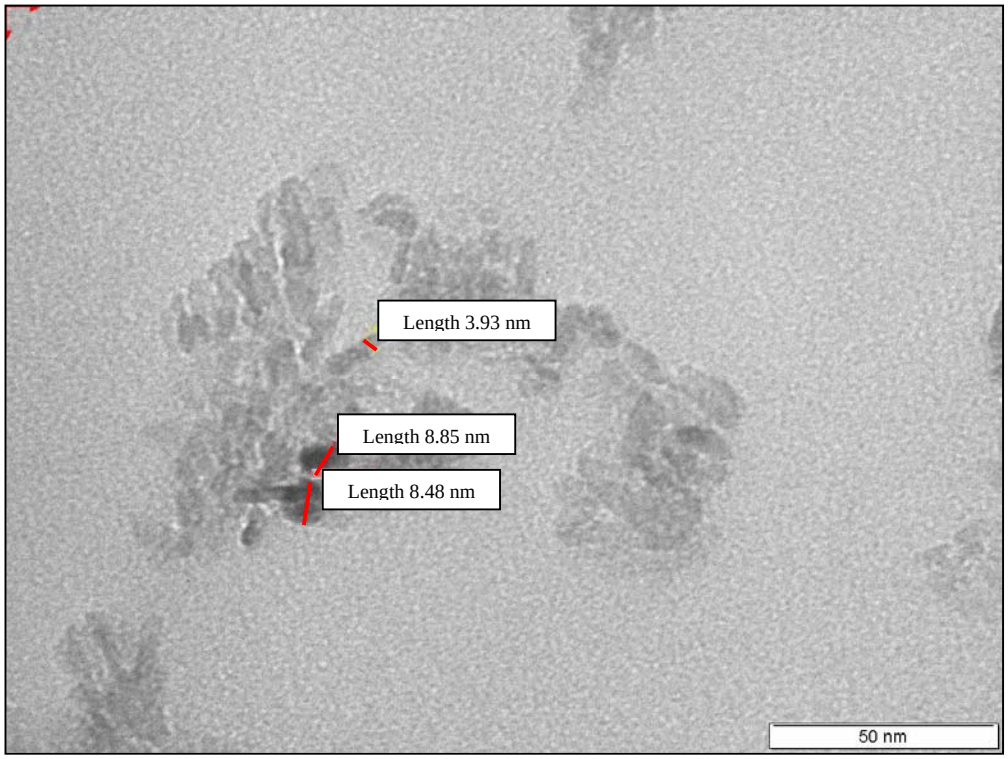

Figure C8: TEM image of Ni25 showing the estimated particle sizes

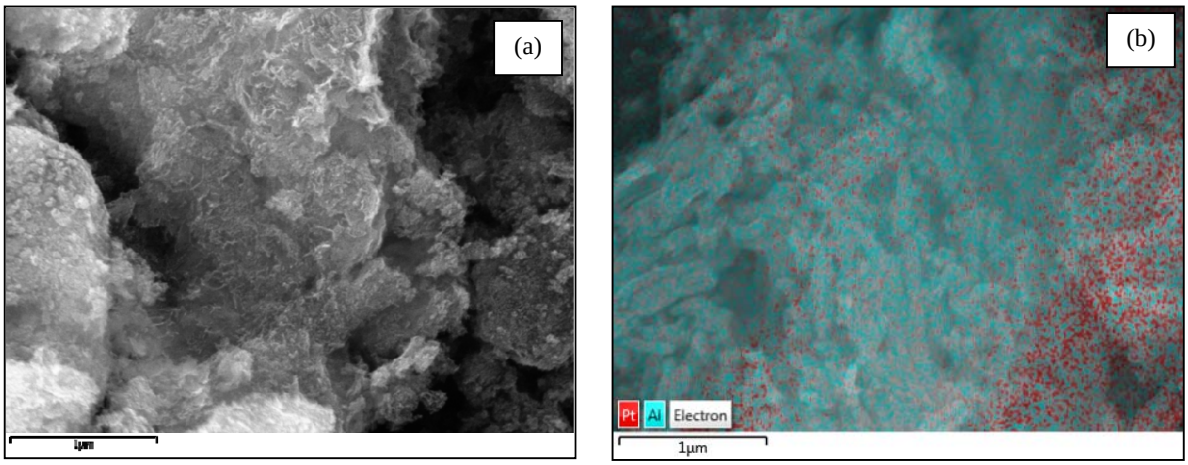

Figure C9: SEM of the Pt-Al catalyst (a) Bright field and (b) Elemental mapping

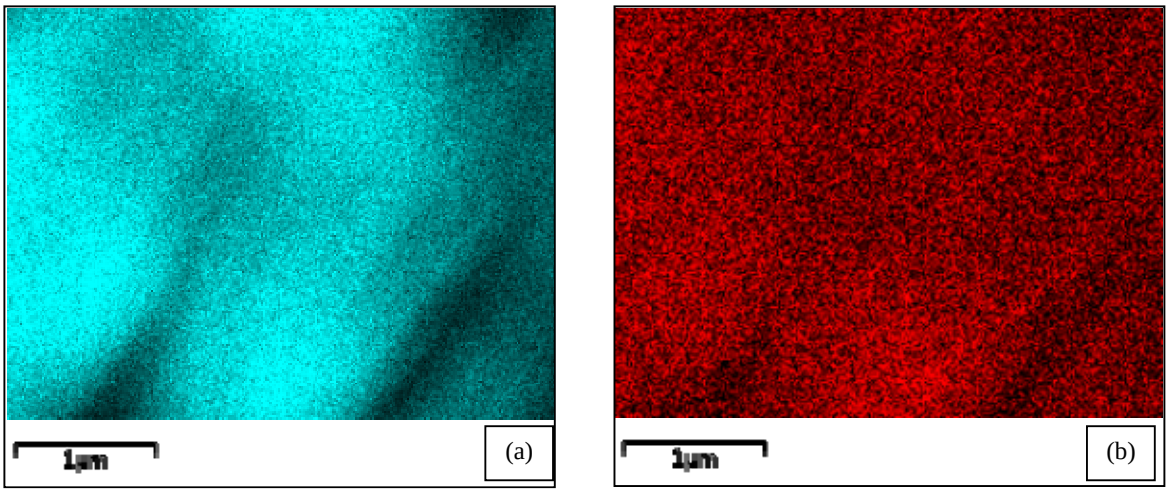

Figure C10: Electron mapping of the Pt-Al catalyst showing the distribution of (a) Al and (b) Pt

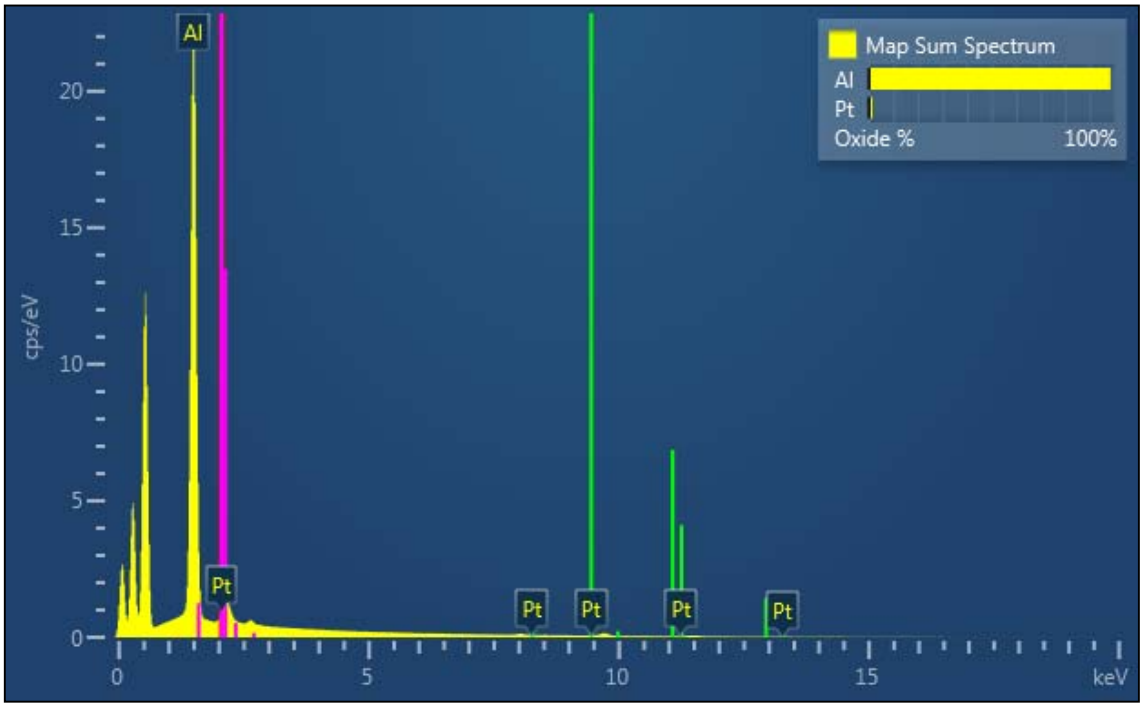

Figure C11: Electron mapping graph of Pt-Al

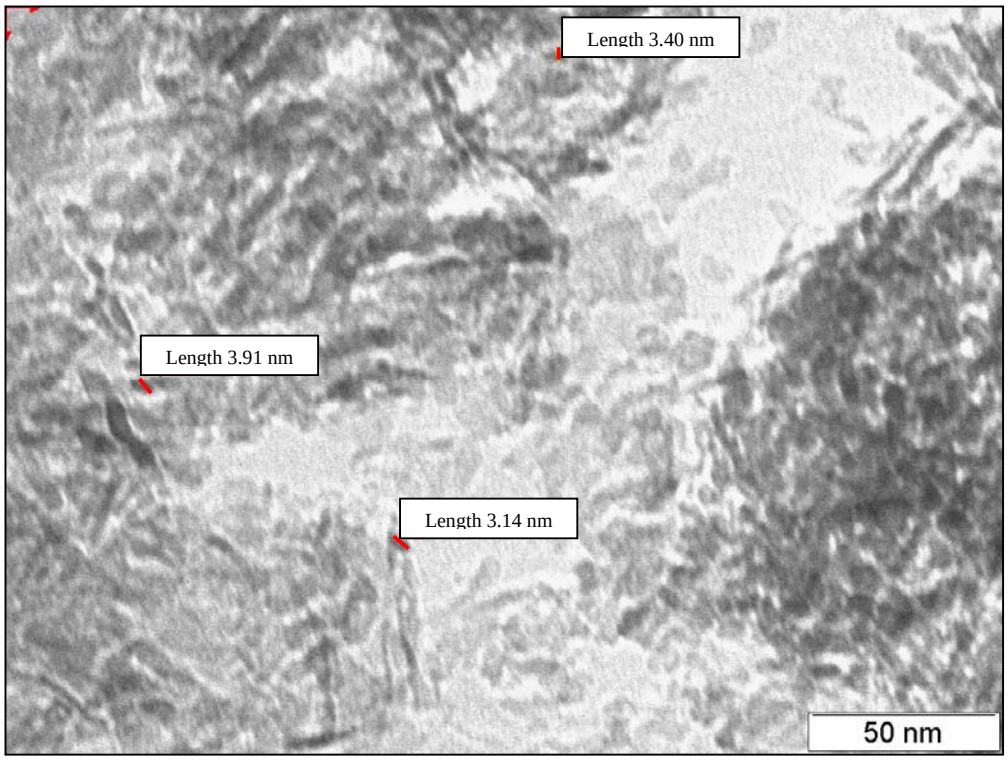

Figure C12: TEM image of Pt-Al showing the estimated particle sizes

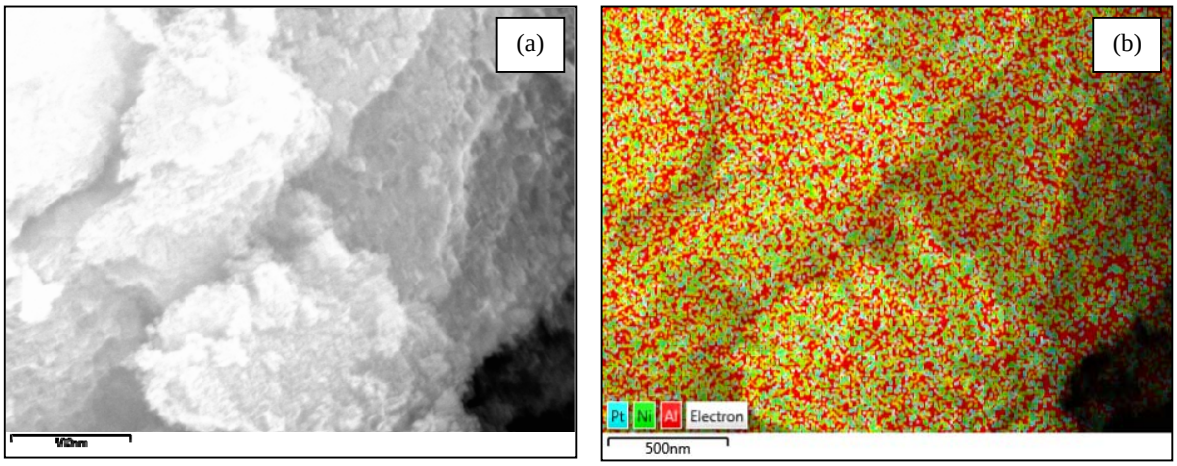

Figure C13: SEM of the Pt-Ni-Al catalyst (a) Bright field and (b) Elemental mapping

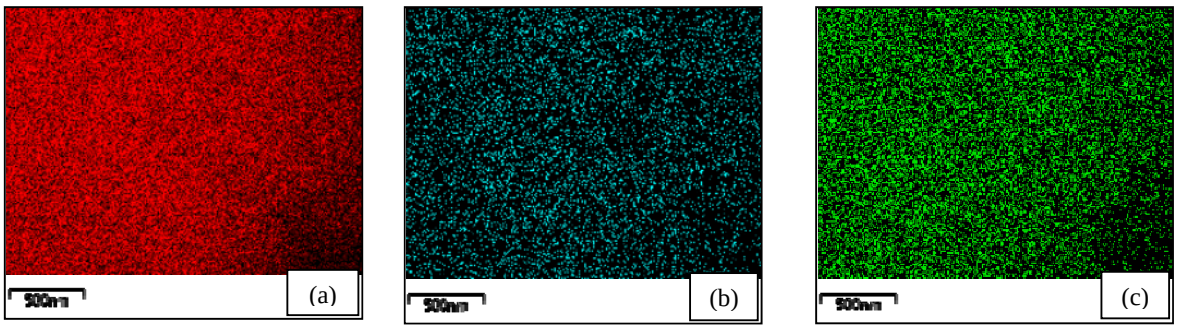

Figure C14: Electron mapping of the Pt-Ni-Al catalyst showing the distribution of (a) Al and (b) Pt and (c) Ni

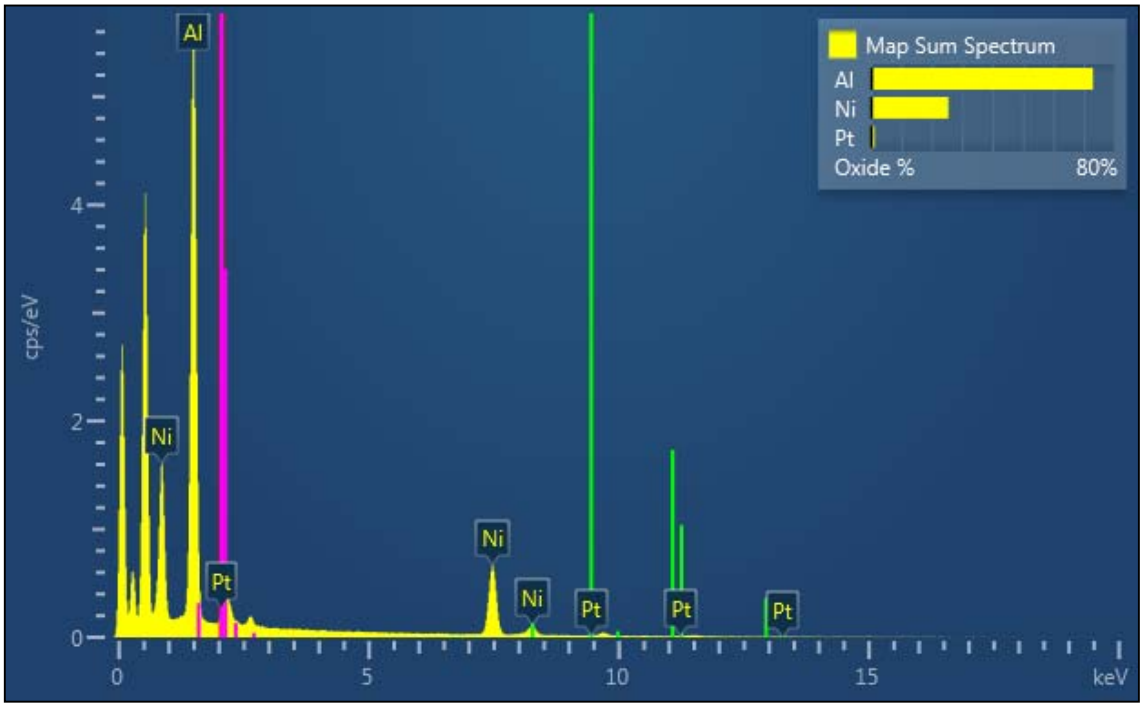

Figure C15: Electron mapping graph of Pt-Ni-Al

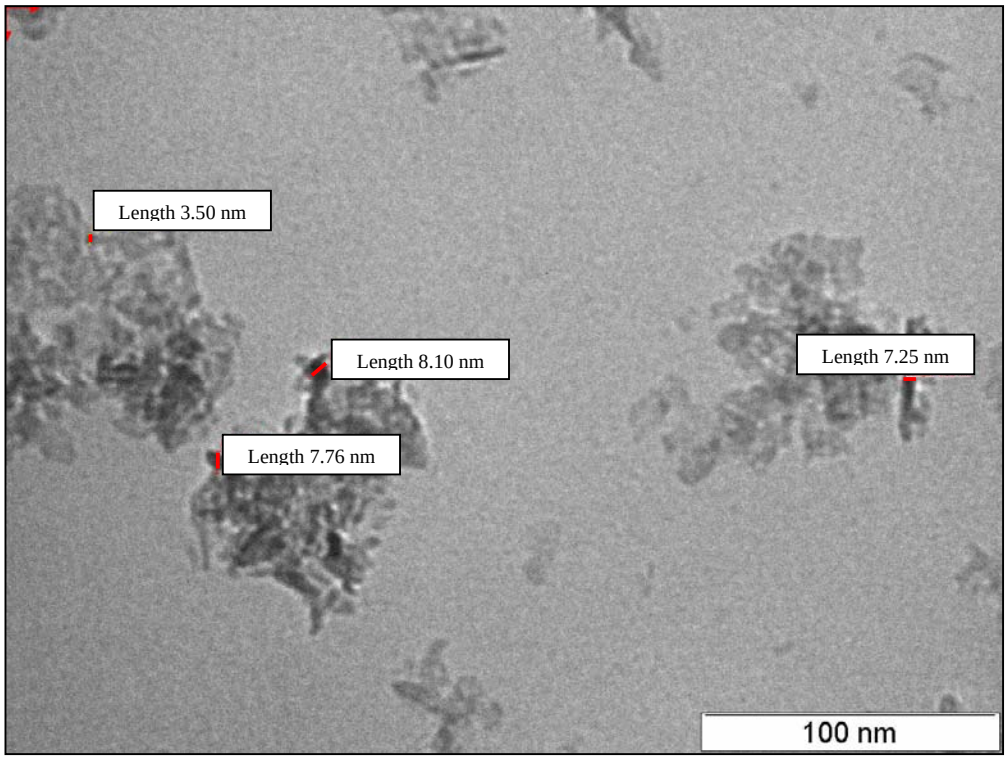

Figure C16: TEM image of Pt-Ni-Al showing the estimated particle sizes